②

AD-A251 550   FINAL REPORT

‖‖‖‖‖‖‖‖‖‖‖

S DTIC
ELECTE
JUN 10 1992
A D

RESEARCH ON SPECIALIZED COMPUTATIONAL METHODS FOR FLUID-STRUCTURE INTERACTION SIMULATIONS FOR ADVANCED SUBMARINE TECHNOLOGY

J. Tinsley Oden

Principal Investigator

The University of Texas

Texas Institute for Computational Mechanics

May, 1992

92-13778
‖‖‖‖‖‖‖‖‖‖‖

1

92 5 26 004

Contents

i

Final Report

RESEARCH ON SPECIALIZED COMPUTATIONAL METHODS FOR FLUID–STRUCTURE INTERACTION SIMULATIONS FOR ADVANCED SUBMARINE TECHNOLOGY

1 Introductory Comments

This document summarizes research done during the period November 15, 1988–February 2, 1992 on a project aimed at the development of new advanced computational methods for modeling coupled elastic scattering problems in linear acoustics. The principal feature of the research was to develop and explore the use of advanced hp-adaptive finite element methods for this class of problems, including the possible use of coupled boundary element and finite element methods.

Early in the project, the research team elected to take a fresh approach to these types of modeling problems: it was known that large scale problems in linear acoustics can represent enormous computational efforts, and that new approaches would be necessary in order to cope with the increasing complexity of acoustical analyses needed in the design of acoustical systems associated with modern submarines. Previous experience and successes by members of the research team in developing new adaptive hp finite element methods for problems in solid mechanics and fluid mechanics naturally led to the plan to develop new hp strategies for structural acoustics. But having made this decision, the important question of how these physical phenomena are to be modeled remain the next major decision in determining the direction of the research.

Certainly, the classical approaches to this problem are well documented: acoustical fluid is modeled using the Helmholtz equation, the structure is modeled using linear structural mechanics, and mechanical coupling is provided at the interface. But there are many different

1

techniques that can be used to model these types of problems. Traditionally, the problem is solved in the frequency domain with a boundary element type formulation to modeling acoustical fluid. There are, however, a number of other approaches worth considering. These include the use of finite elements to model the fluid, with appropriate boundary conditions in the far field. Also, which particular boundary element method would be best suited for this class of problems was, at the beginning of this effort, unknown. Codes exist which employ one boundary element formulation or another, but all of these were known to possess a number of serious deficiencies, and many of these precluded the use of high–order adaptive *hp* methods. Then there was also a classical approach in which linear acoustics was modeled by integrating a system of hyperbolic conservation laws. This is by no means a common approach to these problems, but it carried with it the possibility of incorporating additional physics into the formulation that may be of use later. Moreover, it was not known at the onset how these more direct methods compared in efficiency and accuracy with some of the conventional methods. Finally, mathematical and convergence properties of various boundary element methods have only begun to be established and *a posteriori* error elements, vital for the use of any adaptive scheme, were not available for boundary element methods, and in particular, were not available forcoupled finite element and boundary element methods.

After a detailed study of the literature and a number of initial calculations, two parallel approaches were attempted in which the principal effort was directed toward a coupled boundary element/finite element method formulation and a smaller pilot effort was initiated on the use of *hp*-finite element techniques for analyzing transient coupled acoustics problems. This latter approach occupied around 15 to 20 percent of the total effort and was considered from the onset as a completely exploratory, somewhat high–risk component of the work.

The prinicpal mathematical model that was selected to provide the basis of this study was that of the classical problem of elastic scattering in linear acoustics: an elastic body occupying a bounded domain Ω is submerged into an infinite acoustical fluid subjected to an incident pressure field. One wishes to determine:

- the pressure field in the fluid, in particular on the surface of the scatterer, and

- the velocity field in the elastic structure.

The time variable is eliminated using Fourier transforms and the problem reduces the solution to the Helmholtz equation in the exterior domain, coupled with the equations of linear elasticity in Ω in the frequency. The principal idea, therefore, was similar to that in the NASHUA code [2]. The boundary integral approach is used to replace the Helmholtz equation and the problem reduces to the solution of linear elasticity/linear structural mechanics equations inside Ω coupled with a boundary integral formulation on the boundary $\Gamma = \partial\Omega$.

2

In both the BEM/FEM study and in the transient acoustic study, new data structures were developed that would allow the implementation of a new class of adaptive hp finite element methods in which both the local mesh size h and the order p of the approximation were treated as free parameters. In addition, it is necessary to develop mathematically rigorous a *posteriori* error estimates to drive the hp-adaptive process. The ultimate purpose of developing such high order adaptive schemes was an effort to produce exponential rates of convergence, so that, it was hoped, highly accurate results could be obtained with relatively few degrees of freedom compared with conventional methods. This super–algebraic convergence property, which was proved earlier to hold for linear elliptic problems, if also applicable to the subject classes of problems would allow one of the principal missions of the project to be fulfilled: the treatment of very large–scale modeling problems with relatively few degrees of freedom. In summary, the principal goals of the project can be stated as follows:

- The derivation of a uniformly stable boundary element formulations in the equations valid for the whole range of wave numbers k. The formulation should be compatible with the the C^0 regularity assumption for finite element approximations of the structure.

- The development of C^0 finite element approximations for one–, two–, and three–dimensional geometries. This part of the project included such fundamental issues as the development of new hp finite element data structures and constrained approximations for coupled boundary element/finite element problems.

- The development of a coupled finite element/boundary element code and the verification of expected rates of convergence. This included first the development of a two–dimensional code and led to preliminary work on a three–dimensional code that is currently under study and further development.

- The derivation, implementation, and verification of an a *posteriori* error estimate for boundary element methods. These estimates perhaps represent a significant variance from those that have been reported for the simplest one–dimensional cases.

- The development of adaptive strategies. Having obtained a local error estimate, these strategies would provide for reducing mesh size or increasing spectral order so as to achieve a target error with a number of unknowns.

- The solution of selected problems. These are designed to demonstrate the effectiveness of the methodology on classical benchmark problems and, ultimately, on realistic scattering problems of interest in Naval research.

- The verification of the applicability of the *hp* approximation to structural mechanics, including bulky structures such as bulkheads, but also possibly shells, thin beams and plates.

- The development of a mathematical foundation for transient acoustics, including studying mathematical properties of linear hyperbolic systems associated with transient acoustics, the development of new transient *hp*-adaptive schemes, the development of high order transient solvers and associated *a posteriori* error estimates, and associated adaptive strategies.

2   State-of-the-Art at the Start

It is accurate to say that at the beginning of this project virtually no papers existed in the literature on large–scale transient acoustics calculations. The theory itself, while existing within the framework of abstract Cauchy problems in functional analysis, is not generally known in the acoustics literature nor were the investigators able to find large scale projects of any kind that used finite element methods for these types of problems. Also, it was not known whether or not these approaches would be fruitful, or, if they worked, if they would be competitive with more traditional schemes or if they would produce new insight into acoustical scattering phenomena. These questions, to an extent, remain open but considerable progress was made in developing these new methodologies.

For the boundary integral formulation and the associated boundary element methods, the following main schools of research were identified:

- The German school, represented mostly by mathematicians (Wendland, Stefan, Costubal, and others).

- The American school, represented by full–spectrum from theoretical mathematics to practical engineering calculations (Hsiao Kleinman, Prelite, Cruze, Bannerjee, Rizzo, and others).

- The British school of acoustics (Burton, Miller, Jones, Unsell and others) and BEM (Brebbia, etc.).

- The French school of FEMs (Nedelec, Hamoli, and others).

- Other works (such as the work of Johnston in Sweden, among others).

A variety of different boundary integral formulations were known at the start of this project and some mathematical basis for them have been established, but the bulk of the literature which focused on acoustics and finite element approximations employed the classical

4

collocation approach. There are papers in the literature on adaptive boundary integral formulations, and among these we mention the work of Rencis, Rauk, and Stephen but very few numerical solutions to any cases other than simple test problems were found.

3 Technical Approach at the Start

First, the initial approaches to the BEM/FEM formulation are discussed as these comprise the major portion of the initial work. Due to the complexity of the problem and many uncertain open questions it was decided that a simplified class of models would be first formulated which minimized the complexity of coping with the behavior of the elastic structure. This idea consists of replacing the effects of the structure, particular the non–local Green's operator, with a local spring–like approximation, reducing the problem to the solution of a Helmholtz equation in the exterior domain with a Robin (impedance) boundary condition on the fluid/structure interface. Three features of this approach should be noted:

1. A mathematical structure of this simplified model resembles the general problem; the same function spaces are used, natural eigenfrequencies exist, and many of the computational issues are the same.

2. Wherever a boundary integral formulation is used, the resulting formulation involves exactly the same integrals as for the general coupled problem.

3. The boundary element code being developed for the simplified model could, with some modifications, could be reconfigured to be used as a major part of the final code for the general coupled problem.

Emphasis was first placed on the two–dimensional problem. While most of the mathematical details remain the same in three dimensions, associated technical details, especially those involving hp-adaptivity are much simpler and easier to implement for the two–dimensional case. Moreover, it was unclear in the beginning of the project precisely what type of boundary formulation would be most appropriate. It was known that the traditional Helmholtz integral equation or the hypersingular integral formulation, or the more popular Burton-Miller formulation all had mathematical and technical deficiencies that had to be coped with. Initial calculations were nevertheless done with the Helmholtz formulation and with a form of the hypersingular integral formulation.

Secondly, for the work on the transient acoustics, a number of essentially one–dimensional cases were initially explored. A few of the issues were more basic. They involved a study of abstract Cauchy problems for linear acoustics, ignoring initially the effects of the elastic structure. It also involved the development of high order temporal integration schemes

to advance the solution in time with an accuracy commiserate with the order of the spatial approximation. It is natural, that some of the more classical high order schemes were first explored including, for example, higher order multistep methods such as the Adams-Bashford scheme, various types of Runge-Kutta methods, including explicit Runge-Kutta, implicit Runge-Kutta, and singly implicit Runge-Kutta methods, and some initial studies of Taylor-Galerkin schemes which heretofore had not been applied to these types of acoustics formulations.

4 Progress, Success and Failures

The first stage of this project was completed in the summer of 1990 and documented in [3]. At this point the following decisions were made and results were obtained:

- The existence of fictitious frequencies in both Helmholtz formulation and the standard hypersingular formulation were found to be major deficiencies in these techniques, even though they provide the basis of a number of commercial and laboratory codes that are in use today. The Burton-Miller formulation, while overcoming this particular deficiency, nevertheless had also a number of deficiencies which are not adequately addressed in the literature. These included complexities with evaluating hypersingular integrals, and with the overall robustness of the scheme when applied to reasonable sample problems.

- The Burton-Miller formulation was nevertheless finally selected as a basis for the FEM code. However, a Galerkin approach rather than a collocation approach was selected.

- An L^2-residual technique was developed for *a posteriori* error estimation. It was derived mathematically, verified experimentally, and proved to be asymptotically exact for a significant class of BEM formulations.

- A two-dimensional experimental hp boundary element code was developed for the model problem discussed in the previous section. This code was completed, and used to solve several trial problems including the infinite cylinder problem in two dimensions.

- Simple h-adaptive strategies and p-adaptive strategies based on the residual error estimate and on the equidistribution principle were developed. These were applied to model problems and became functional in mid–1990.

- A singly–implicit Runge-Kutta scheme was devised to be used in conjunction with an hp method and a finite difference method for temporal approximations in the transient acoustics studies. Preliminary *a posteriori* error estimates were derived, these being

6

based on residual methods for the spatial domain and a rather standard Runge-Kutta scheme for controlling the time step.

The principal difficulties encountered at this point in the project were connected with the correct implementation of the hypersingular part of the Burton-Miller formulation. In particular, initial studies showed that, contrary to previous expectations, nonexponential convergence rates were obtained. Nevertheless, the Burton-Miller formulation for the boundary integral methods and the h-p adaptive schemes for the structural approximation were regarded as viable approaches it was decided to go forward with the implementation of these methodologies for a broader class of problems. Work was then directed in three directions:

1. Development of a two–dimensional code for the full coupled problem,

2. development of a three–dimensional code for the model problem with simplified Robin boundary conditions, and

3. the exploration of new temporal schemes, in addition to Runge-Kutta methods, for handling high–order transient acoustic calculations.

All of these tasks were completed by the end of 1991 and reported in [4] and [5]. At this point in the project, a number of the major conceptual, mathematical and modeling issues were thought to be understood and the basis for modeling a considerably more general class of problems was established. In particular:

- The issue of the correct implementation of the hypersingular operators was successfully solved in [5] and in more detail later in [6]. This involved, as noted earlier, a full Galerkin approximation of the hypersingular integral formulation; we believe this was the first such formulation attempted in the literature. Fortunately, subsequent calculations showed that this led to optimal rates of convergence so that, once again, the possibility of obtaining exponentially convergent techniques for general classes of acoustics problems emerged.

- A three–dimensional h-p boundary element code for the model problem was completed and verified by solving the problem of elastic scattering on a sphere and on a finite cylinder.

- A technique for obtaining L^2 *a posteriori* error estimates was coded, implemented, and tested on a number of sample problems.

- A two–dimensional hp-adaptive coupled boundary element/finite element code for coupled scattering problems was completed. This represented the completion of a major

research tool in which a variety of computational issues could be studied. Initially this code was used to study scattering of plane waves on infinite elastic cylinders.

- The feasibility of appllying hp approximations for structural problems was tested on a cylindrical elastic shell. The effect of shell thickness on the behavior of both the structure and on scattering was explored. It was discovered that for simple geometries such as this, a two–dimensional finite element code based on hp-adaptive methods was perfectly adequate and could approximate the shell behavior for thicknesses ranging from very thin shells to very thick shells. On the other hand, some deterioration in the quality of solutions for problems with corners and discontinuities was observed. It was clear from these examples that in future calculations the ability to use h-adaptivity in the neighborhood of scatterers such as corners represents a vital and useful part of the overall strategy.

- A new class of high–order Taylor-Galerkin schemes were developed and proved to be unconditionally stable for the transient acoustics problem. This was regarded as a significant advance in existing technology. These schemes proved to be very robust and accurate and outperformed classical Runge-Kutta methods on a significant number of test problems. Some preliminary adaptive strategies for transient acoustics were studied and a research code was developed that produced a number of interesting results. Still, much work remains to be done in this area. Current results appear to be sensitive to the particular adaptive strategy used, and further work is needed in developing robust and precise error estimates for these classes of problems.

- Also, progress was made in developing adaptive techniques for the transient response of elastic structures coupled to the transient acoustic package. These results also look promising, although they are still very preliminary in nature.

It can be said that at the conclusion of this project a number of major new results have been established and a good starting point for the continuation of the work into three–dimensional simulations is in place. Further work will be augmented by studies on parallel computation, for it is believed that with the use of parallel algorithms, additional efficiencies can be obtained which enhance further those expected to be produced by the hp-adaptive algorithms.

5 Final Technical Approach and Final Goals

As a summary of some of the ideas outlined earlier, the following assumptions have been established for current and future work. The weak or variational form of the Burton-Miller

8

formulation, coupled with the residual variational formulation for the elasticity equations, will be used as a basis for further work.

- General h-p approximations of both boundary and domain variational formulations will be used.

- *A posteriori* estimates will be derived based on error residual methods for the structure and L^2 estimates for the boundary element method.

- Continued work will be done on hp-adaptive data structures and adaptive strategies which could lead to exponential rates of convergence.

- Work will continue on modeling coupling the transient behavior of the acoustical fluid to that of an elastic structure and with the high–order multistage Taylor-Galerkin methods will be the driving algorithm for the temporal approximation.

- Studies of parallel algorithms will be undertaken.

6 Problems Perceived and Future Directions

The work on the final three–dimensional code for the coupling problem initiated in November of 1991 remains to be a major task in the current research. The following tasks should be listed:

- Development of a three–dimensional FE code for the elasticity equations coupled to the boundary element method.

- A study of techniques for using hp-FEM's for treating thin flexible structures such as beams, plates, and shells.

- A geometrical CAD-like code is needed which is capable of modeling solid objects and general surfaces. This requires the development of a new preprocessor including an h-p mesh generator for nontrivial geometries.

- Development of an *a posteriori* estimate for the three–dimensional coupled problem together with some new hp-adaptive strategies.

- Extension of the transient acoustic work to fully coupled problems and then to three dimensions.

- Exploration of domain decomposition methods and coarse–grain parallel algorithms for the solution of some large scale problems on multiprocessor architectures.

9

As for difficulties yet to be resolved, on the theoretical side the integration of almost singular functions remains a critical issue. The development of inexpensive but precise integration procedures for almost singular integrands may determine the overall success of the proposed methodology. Currently rather simple adaptive procedures are used and these may prove to be quite expensive unless more simplified quadratures can be obtained. On the other hand, simplified quadrature rules may defeat all the gains obtained using adaptivity.

Research on a theory of *a posteriori* error estimation must be continued. This includes the study of more practical inexpensive implementations of residual estimates and a search for new estimates that would be more sensitive to the errors in derivatives in the solution. Most importantly, techniques for handling geometric singularities such as lines, corners and material interfaces which are known to be very important in the scattering of acoustical waves must be studied. The major issues have to do with the geometry of these classes of problems and how well that geometry is approximated. Our feeling is that the geometry questions are open, and that a considerable amount of additional work is needed before they are adequately understood or correctly factored into any reasonable acoustical analysis capability.

7. DOCUMENTATION

The research outlined above has led to the publication of a number of articles, reports and papers. Also several oral presentations of the work were made at national and international conferences and symposia. A list of these documents and lectures is given below.

1. Papers Published in Refereed Journals:

Karafiat, A., Geng, P. and Oden, J.T., "Variational Formulations and *hp*-Boundary Element Approximations for Hypersingular Integral Equations for Helmholtz Exterior Boundary-Value Problems in Two Dimensions," *Int. J. Engineering Science*, (in press).

Ainsworth, M. and Oden, J.T., "A Procedure for A Posteriori Error Estimation for *hp* Finite Element Methods," *Computer Methods in Applied Mechanics and Engineering,* (in press).

Ainsworth, M. and J.T. Oden, "A Unified Approach to A Posteriori Error Estimation Using Element Residual Methods," *Numerische Mathematik*, (in press).

Demkowicz, L., Oden, J.T., Ainsworth, M. and Geng, P., "Solution of Elastic Scattering Problems in Linear Acoustics using h-p Boundary Element Methods," *Jnl. of Computational and Applied Mathematics*, vol. 36 (1991), pp. 29-63.

Safjan, A., Demkowicz, L., and Oden, J.T., "Adaptive Finite Element Methods for Hyperbolic Systems with Application to Transient Acoustics," *International Journal for Numerical Methods in Engineering*, Vol. 32, pp. 677-707, 1991.

Oden, J.T., "The Best FEM," *Finite Elements in Analysis and Design*, Vol. 7, 1990, pp. 103-114.

Oden, J.T., and Strouboulis, T., "A Posteriori Error Estimation of Finite Elements Approximation in Fluid Mechanics," *Computer Methods in Applied Mechanics and Engineering,* Vol. 78, 1990, pp. 201-242.

Oden, J.T., L. Demkowicz, W. Rachowicz, and T.A. Westermann, "A Posteriori Error Analysis in Finite Elements: The Element Residual Method for Symmetrizable Problems with Applications to Compressible Euler and Navier-Stokes Equations," *Computer Methods in Applied Mechanics and Engineering*, Vol. 82, pp. 183-203, 1990.

Oden, J.T. and L. Demkowicz, "h-p Adaptive Finite Element Methods in Computational Fluid Dynamics," *Computer Methods in Applied Mechanics and Engineering*, Vol. 89, 1991, pp. 11-40.

Demkowicz, L., Oden, J.T., Rachowicz, W., and Hardy, O., "Toward a Universal hp Adaptive Finite Element Strategy. Part 1. Constrained Approximation & Data Structure," *Computer Methods in Applied Mechanics and Engineering*, 77, 1989, 79-112.

Demkowicz, L., Rachowicz, W., Oden, J.T., and Westermann, T., "Toward a Universal hp Adaptive Finite Element Strategy. Part 2. A Posteriori Error Estimation," *Computer Methods in Applied Mechanics and Engineering*, 77, 1989, 113-180.

Rachowicz, W., Oden, J.T., and Demkowicz, L., "Toward a Universal hp Adaptive Finite Element Strategy, Part 3. Design of *hp* Meshes," *Computer Methods in Applied Mechanics and Engineering*, 77, 1989, pp. 181-212.

Oden, J.T., "Theory and Implementation of High-Order Adaptive h-p Methods for the Analysis of Incompressible Viscous Flows," *Computational Nonlinear Mechanics in Aerospace Engineering*, AIAA Progress in Aeronautics and Astronautics Series, S.N. Atluri, ed. (in press).

Edwards, M.G., Oden, J.T. and Demkowicz, L., "An h-r Adaptive Second Order Approximate Riemann Solver for the Euler Equtions in Two Dimensions," *Journal of Statistical and Scientific Computing*, SIAM Publishers, (in press).

2. Books (and sections thereof) Published:

Oden, J.T. and J.M. Bass, "New Developments in Adaptive Methods for Computational Fluid Dynamics," *Computing Methods in Applied Sciences and Engineering*, ed. R. Glowinski and A. Lichnewsky, SIAM Publications, Philadelphia, pp. 180-210, 1990.

3. Technical Reports, Non-Refereed Papers

Karafiat, A., Geng, P. and Oden, J.T., "Variational Formulations and *hp*-Boundary Element Approximations for Hypersingular Integral Equations for Helmholtz Exterior Boundary-Value Problems in Two Dimensions," TICOM Report 92-01, April, 1992.

Demkowicz, L., Karafiat, A. and Oden, J.T., "Variational (Weak) Form of the Hypersingular Formulation for the Helmholtz Exterior Boundary-Value Problems," TICOM Report 91-05, June, 1991.

Safjan, A. and Oden, J.T., "h-p Adaptive Finite Element Methods in Transient Acoustics," ASME, NCA - Vol. 12, *Structural Acoustics*, Eds. R.F. Keltie et al., Book No. H00718, 1991, pp. 93-99

Oden, J.T., Demkowicz, L., and Bennighof, J., "Fluid Structure Interaction in Underwater Acoustics," *Applied Mechanics Review*, 43(5), May 1990.

Oden, J.T., "New Developments in Adaptive Finite Element Methods in Computational Fluid Dynamics," *Proceedings*, MSC Users' Conference, 1990.

Ainsworth, M. and J.T. Oden, "A Unified Approach to A Posteriori Error Estimation Using Element Residual Methods," TICOM Report 91-03, Austin, 1991.

4. Presentations:

Safjan, A., and Oden, J.T., "h-p Adaptive FInite Element Methods in Transient Acoustics," presented at Winter Annual Meeting of ASME, December 1-6, 1992, Atlanta, Georgia.

Ainsworth, M. and Oden, J.T., "A Procedure for A Posteriori Error Estimation for *hp* Finite Element Methods," presented at Second Workshop on Reliability in Comptuational Mechanics, Cracow, Poland, October 14-16, 1991.

Oden, J.T., Demkowicz, L. and Bennighof, J., "Fluid-Structure Interaction in Underwater Acoustics," presented at 11th National Congress on Applied Mechanics, Tucson, AZ, May 1990.

Oden, J.T., "Adaptive Finite Elementds in Computational Fluid Mehcanics," ONR Structural Acoustics Program Review Meeting, Palo Alto, CA, July 12-13, 1990.

Oden, J.T., "Progress in Acoustical Modeling," Structural Acoustics Program Review, Boston, MA, January 28-31, 1990.

Oden, J.T., "A General hp-Adaptive Finite Element Method for Broad Classes of Problems in Engineering," Fourth International Conference on Computing in Civil and Building Engineering, Tokyo, Japan, July 29-31, 1991.

Oden, J.T., "Progress on Adaptive High-Order hp-Finite Element Methods in Computational Fluid Dynamics," First U.S. National Congress, Chicago, IL, July 22-24, 1991.

Oden, J.T., "Smart Algorithms and Adaptive Finite Element Methods in CFD: Their Status and Potential," Second SA CFD Symposium, Stellenbosch, South Africa, June 24-27, 1991.

Oden, J.T., "Toward Optimal Control in Computational Fluid Dynamics: Smart Algorithms and Adaptive Methods," 27th Annual Meeting of the Society of Engineering Science, Santa Fe, New Mexico, October 21-25, 1990.

Oden, J.T., "h-p Adaptive Finite Element Methods for Compressible and Incompressible Flows," Symposium on Computational Technology for Flight Vehicles, NASA Langley Research Center, Hampton, VA, November 5-7, 1990.

Oden, J.T, "New Developments in Adaptive Finite Element Methods in Computational Fluid Dynamics," Sixth Chautauqua Meeting, White Plains, NY, September 9-11, 1990.

Oden, J.T., "Smart Algorithms and Adaptive Methods for Compressible and Incompressible Flow: Optimization of the Computational Process," presented at Boston, MA, October 1-3, 1990. Conference entitled, "Large-Scale Computing in the 21st Century."

Oden, J.T., "Progress in Fluid Structure Interaction: The Texas Group," ONR Fluid Structure Interaction Program Review Meeting, Austin, TX, January 24-25, 1991.

Oden, J.T., "Progress in Fluid Structure Interaction: The Texas Group," ONR Fluid Structure Interaction Program Review Meeting, Boston, MA, July 13-14, 1991.

13

Appendix A

Variational Formulations and *hp*-Boundary Element Approximations for Hypersingular Integral Equations for Helmholtz Exterior Boundary–Value Problems in Two Dimensions

Abstract

In this paper, a weak hypersingular formulation of the Helmholtz exterior bound-ary–value problem in two dimensions is presented. The weak formulation derived here is implemented into an *h-p*-adaptive boundary element approximation and the elementwise L^2-residual is used as the error estimation in the adaptive scheme. A series of numerical experiments on the convergence of the solution and the properties of L^2-residual is given. The work is an extension of methods and results contained in [2] and [3].

1   Introduction

The aim of this paper is to formulate weak hypersingular boundary integral equations for the exterior boundary–value problems for the Helmholtz equations in two dimensions. The presented work is an extension of methods and results of earlier work [2]. Additional details concerning formulation of the boundary–value problem, its physical meaning and related mathematical concepts can be found in [2] and [3].

The priority in the development of variational formulations of hypersingular integral equa-tions for the Helmholtz exterior boundary–value problem belongs to M. A. Hamdi [5]. The

---

*On leave from the Section of Applied Mathematics of Technical University of Cracow, 31-55 Kraków, ul. Warszawska 24, Poland.

1

classical Helmholtz exterior boundary-value problem is the following: For a given bounded domain Ω with a smooth boundary Γ and completion Ω^e (Fig. 1), find a function $u: \Omega^e \to C$ which satisfies

- the Helmholtz differential equation

$$- \Delta u - k^2 u = 0 \qquad \text{in } \Omega^e, \tag{1.1}$$

- the Sommerfeld boundary condition at infinity

$$\left| \frac{\partial u}{\partial r} - iku \right| = o\left(r^{-\frac{1}{2}}\right) \tag{1.2}$$

- a boundary condition on Γ,

where k is the wave number.

In a mathematical description of acoustic scattering, a scattered pressure p^s is assumed to fulfill equations (1.1) and (1.2). The incident pressure p^{inc} fulfills equation (1.1) in the whole space $\mathbb{R}^2$ and the total pressure

$$p = p^{inc} + p^s \tag{1.3}$$

fulfills one of the typical boundary conditions on Γ:

$$p = 0 \text{ or} \tag{1.4}$$

$$\frac{\partial p}{\partial n_e} = 0 \text{ or} \tag{1.5}$$

$$\frac{\partial p}{\partial n_e} = \varepsilon p. \tag{1.6}$$

In (1.6), ε is a positive constant. If $\varepsilon = 0$, we obtain the formulation for rigid scattering; for $\varepsilon > 0$, a formulation of a compliant boundary with spring stiffness $\frac{1}{\varepsilon}$ is obtained

2 Classical Integral Formulations

It is well known that the fundamental solution of (1.1) in two dimensions has a form (cf. [1])

$$\phi(\boldsymbol{x}, \boldsymbol{y}) = \frac{i}{4} H_0(kr) \tag{2.1}$$

2
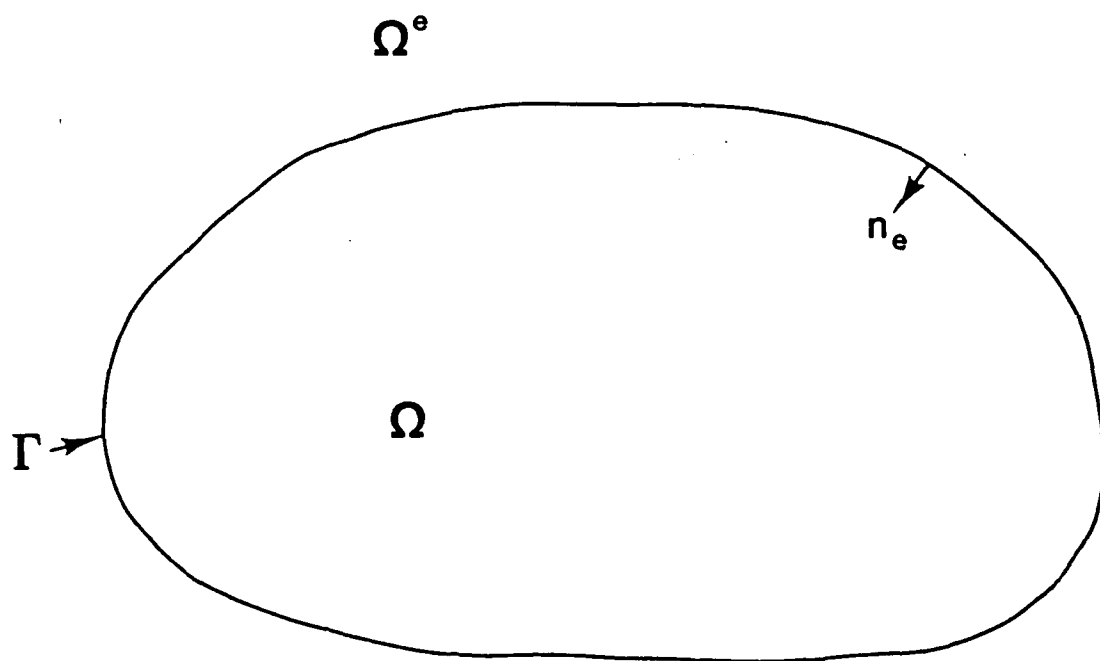
Figure 1: Exterior boundary-value problem.

where $i^2 = -1$, $r = x - y$, $r = |r|$, and H_0 is the Hankel function of the first kind and zeroth order. The function ϕ may also be written as

$$\phi(x, y) = \frac{1}{2\pi} \log\left(\frac{1}{r}\right) + \phi_0(r) \tag{2.2}$$

where $\phi_0(r) \in C^\infty(0, \infty)$ and ϕ_0 with its derivative are bounded in the neighborhood of 0.

We assume next that

$$u \in C^2(\Omega^e) \cap C^{1,\alpha}(\overline{\Omega}^e) \tag{2.3}$$

where $C^{1,\alpha}$ is the space of functions the first derivatives of which fulfill a Hölder condition with exponent α.

From the Green formula, taking into account (1.1) and (1.2) we may obtain the Helmholtz Integral Formulation on the boundary Γ ([3]):

$$\frac{1}{2}u(x) = \fint_\Gamma \left[u(y)\frac{\partial\phi}{\partial n_y}(x, y) - \frac{\partial u}{\partial n_y}(y)\phi(x, y) \right] ds(y), \quad x \in \Gamma \tag{2.4}$$

where the integral is understood as a Cauchy Principal Value Integral, however it has been proven [3] that it is in fact a Lebesgue integral.

For the pressure, the Helmholtz Integral Formulation becomes

$$\frac{1}{2}p(x) = \int_\Gamma \left[\frac{\partial\phi}{\partial n_y}(x, y)p(y) - \phi(x, y)\frac{\partial p}{\partial n_y}(y) \right] ds(y) + p^{inc}(x) \tag{2.5}$$

because p^{inc} multiplied by ϕ satisfies the second Green identity inside Ω:

$$\int_\Gamma \frac{\partial\phi}{\partial n_y}(x, y)p^{inc}(y)ds(y) - \int_\Gamma \phi(x, y)\frac{\partial p^{inc}}{\partial n_y}(y)ds(y) = 0 \tag{2.6}$$

Using a similar technique, the hypersingular integral formulation may be obtained [3]

$$\frac{1}{2}\frac{\partial u}{\partial n_x}(x) = \fint_\Gamma u(y)\frac{\partial^2\phi}{\partial n_x \partial n_y}(x, y)ds(y) - \fint_\Gamma \frac{\partial u}{\partial n_y}(y)\frac{\partial\phi}{\partial n_x}(x, y)ds(y), \quad x \in \Gamma \tag{2.7}$$

which, for the pressure, becomes

$$\frac{1}{2}\frac{\partial p}{\partial n_x}(x) = \fint_\Gamma p(y)\frac{\partial^2\phi}{\partial n_x \partial n_y}(x, y)ds(y) - \fint_\Gamma \frac{\partial p}{\partial n_y}(y)\frac{\partial\phi}{\partial n_x}(x, y)ds(y) + \frac{\partial p^{inc}}{\partial n_x}(x), \quad x \in \Gamma \tag{2.8}$$

The first integrals in both equations should be considered as Hadamard Finite Part Integrals:

$$\fint_\Gamma u(y)\frac{\partial^2\phi}{\partial n_x \partial n_y}(x, y)ds(y) \overset{def}{=} \lim_{\varepsilon \to 0} \left\{ \int_{\Gamma \backslash B_\varepsilon} u(y)\frac{\partial^2\phi}{\partial n_x \partial n_y}(x, y)ds(y) - \frac{u(x)}{\pi\varepsilon} \right\} \tag{2.9}$$

4

Equations (2.4) and (2.7) may be obtained as limit cases of corresponding equations taken for $x_m \in \Omega^e$:

$$u(x_m) = \int_\Gamma \left[u(y) \frac{\partial \phi}{\partial n_y}(x_m, y) - \frac{\partial u}{\partial n_y}(y) \phi(x_m, y) \right] ds(y) \qquad (2.10)$$

and

$$\frac{\partial u}{\partial n_x}(x_m) = \int_\Gamma u(y) \frac{\partial^2 \phi}{\partial n_x \partial n_y}(x_m, y) ds(y) - \int_\Gamma \frac{\partial u}{\partial n_y}(y) \frac{\partial \phi}{\partial n_x}(x_m, y) ds(y) \qquad (2.11)$$

using appropriate limit theorems for potentials. Here n_x denotes an outward normal vector to the boundary Γ at $x = \lim_{m \to \infty} x_m \in \Gamma$. For the total pressure p, equations (2.10) and (2.11) become

$$p(x_m) = \int_\Gamma \left[p(y) \frac{\partial \phi}{\partial n_y}(x_m, y) - \frac{\partial p}{\partial n_y}(y) \phi(x_m, y) \right] ds(y) + p^{inc}(x_m) \qquad (2.12)$$

$$\frac{\partial p}{\partial n_x}(x_m) = \int_\Gamma \left[p(y) \frac{\partial^2 \phi}{\partial n_x \partial n_y}(x_m, y) - \frac{\partial p}{\partial n_y}(y) \frac{\partial \phi}{\partial n_x}(x_m, y) \right] ds(y) + \frac{\partial p^{inc}}{\partial n_x}(x_m) \qquad (2.13)$$

The integrals (2.10)–(2.13) are usual Lebesgue integrals of bounded functions.

3 Propositions and Lemmas

Lemma 1. If $\phi(x, y)$ is the fundamental solution of (1.1) defined by (2.1), then the following equality holds:

$$k^2 \int_\Omega \phi(x, y) dy + \int_\Gamma \frac{\partial \phi}{\partial n_y}(x, y) ds(y) + \frac{1}{2} = 0, \quad \forall \, x \in \Gamma \qquad (3.1)$$

Proof: Let us define a ball

$$B_\epsilon(x) = \left\{ y \in I\!\!R^2 \colon \|x - y\| \le \epsilon \right\} \qquad (3.2)$$

with its boundary (circle)

$$S_\epsilon(x) = \left\{ y \in I\!\!R^2 \colon \|x - y\| = \epsilon \right\} \qquad (3.3)$$

(see Fig. 2). Applying the first Green identity to $u(x) \equiv 1$ and ϕ we obtain

$$- \int_{\Omega^e \setminus B_\epsilon} \Delta_y \phi(x, y) dy + \int_{\Gamma \setminus B_\epsilon} \frac{\partial \phi}{\partial n_y}(x, y) ds(y) + \int_{S_\epsilon \cap \Omega^e} \frac{\partial \phi}{\partial n_y}(x, y) ds(y) = 0 \qquad (3.4)$$

ϕ fulfills (1.1), then

$$- \int_{\Omega^e \setminus B_\epsilon} \Delta_y \phi(x, y) dy = k^2 \int_{\Omega^e \setminus B_\epsilon} \phi(x, y) dy \to k^2 \int_{\Omega^e} \phi(x, y) dy \qquad (3.5)$$

5

Figure 2: Directions in a circle.

On the circle S_ϵ the relation

$$\frac{\partial \phi}{\partial n_y}(x, y) = -\phi'(r)$$

is valid (Fig. 2). Then for the smooth boundary

$$\int_{S_\epsilon \cap \Omega^\epsilon} \left(-\phi'(\epsilon)\right) ds(y) = \left[\frac{1}{2\pi\epsilon} + \phi'(\epsilon)\right] \int_{S_\epsilon \cap \Omega^\epsilon} ds(y) \to \frac{1}{2} + 0 = \frac{1}{2} \qquad (3.6)$$

The second integral tends to

$$\int_\Gamma \frac{\partial \phi}{\partial n_y}(x, y) ds(y) \qquad (3.7)$$

which, with (3.6), gives (3.1). ∎

Proposition 1. For a piecewise smooth boundary Γ, any $p \in C^1(\Gamma)$ and any $\varphi(x, y) = \varphi(r) \in C^2(0, \infty)$, we have

$$\int_\Gamma \frac{\partial}{\partial \tau_y}\left(\frac{\partial \varphi}{\partial \tau_x}\right)(x, y) p(y) ds(y) + \int_\Gamma \frac{\partial \varphi}{\partial \tau_x}(x, y)\frac{\partial p}{\partial \tau_y}(y) ds(y) = 0 \qquad (3.8)$$

where $\tau y = (y)$ is the tangent vector at y.

Proof: It is well known that for each closed, piecewise smooth curve $\Gamma \subset \mathbb{E}^2$ and for any function $u \in C^1(\Gamma)$

$$\int_\Gamma \nabla u(y) \cdot \tau(y) ds(y) = 0 \qquad (3.9)$$

If we substitute now

$$u(y) = \frac{\partial \varphi}{\partial \tau_x}(x, y) p(y) \qquad (3.10)$$

we obtain (3.8). ∎

Proposition 2. For any function $\varphi \in C^2(\Omega)$ the following equality holds:

$$\frac{\partial^2 \varphi}{\partial n_x \partial n_y}(x, y) = -\frac{\partial}{\partial \tau_y}\left(\frac{\partial \varphi}{\partial \tau_x}(x, y)\right) - \tau_x \tau_y \Delta_y \varphi(x, y) \qquad (3.11)$$

Proof: We use formulas (see Fig. 3)

$$\begin{aligned} \tau_1 &= n_2 \\ \tau_2 &= -n_1 \end{aligned} \qquad (3.12)$$

7

$$\frac{\partial^2 \varphi}{\partial n_x \partial n_y} + \tau_x \tau_y \Delta_y \varphi = \frac{\partial^2 \varphi}{\partial x_1 \partial y_1} n_1(x) n_1(y) + \frac{\partial^2 \varphi}{\partial x_1 \partial y_2} n_1(x) n_2(y)$$

$$+ \frac{\partial^2 \varphi}{\partial x_2 \partial y_1} n_2(x) n_1(y) + \frac{\partial^2 \varphi}{\partial x_2 \partial y_2} n_2(x) n_2(y) + \frac{\partial^2 \varphi}{\partial y_1^2} \tau_1(x) \tau_1(y) + \frac{\partial^2 \varphi}{\partial y_2^2} \tau_1(x) \tau_1(y)$$

$$+ \frac{\partial^2 \varphi}{\partial y_1^2} \tau_2(x) \tau_2(y) + \frac{\partial^2 \varphi}{\partial y_2^2} \tau_2(x) \tau_2(y)$$

$$= \tau_1(x) \tau_1(y) \frac{\partial^2 \varphi}{\partial y_1^2} + \tau_1(x) \tau_2(y) \frac{\partial^2 \varphi}{\partial y_1 \partial y_2} + \tau_2(x) \tau_1(y) \frac{\partial^2 \varphi}{\partial y_2 \partial y_1} + \tau_2(x) \tau_2(y) \frac{\partial^2 \varphi}{\partial y_2^2}$$

$$= \tau_i(y) \left[\nabla_x \frac{\partial \varphi}{\partial y_i} \cdot \tau(x) \right] = -\tau_i \frac{\partial}{\partial y_i} \left(\frac{\partial \varphi}{\partial \tau_x} \right) = -\frac{\partial}{\partial \tau_y} \left(\frac{\partial \varphi}{\partial \tau_x} \right)$$

∎

Let us fix any point $x \in \Gamma$ and introduce there a local tangential-normal coordinate system (ξ_1, ξ_2) (Fig. 3). In this system, the boundary Γ will be given by a function f

$$(\xi_1, \xi_2) \in \Gamma \iff \xi_2 = f(\xi_1), \quad \forall \xi_1 \in (\delta_2, \delta_2) \quad \delta_1 < 0 < \delta_2 \tag{3.13}$$

Lemma 2. Let $x_m \in \Omega^e$, $x_m \to x \in \Gamma$. Let the function f given by (3.13) belong to $C^{1,\alpha}(\delta_1, \delta_2)$ and p be bounded on Γ. Then

$$\int_\Gamma \phi(x_m, y) p(y) ds(y) \longrightarrow \int_\Gamma \phi(x, y) p(y) ds(y) \tag{3.14}$$

as $m \to \infty$.

Proof: We introduce regularizing functions

$$
\begin{aligned}
v(x) &= \int_\Gamma \phi(x, y) p(y) ds(y) \\
v_\varepsilon(x) &= \int_{\Gamma \setminus B_\varepsilon} \phi(x, y) p(y) ds(y) + \int_{\Gamma \cap B_\varepsilon} \phi_\varepsilon(x, y) p(y) ds(y)
\end{aligned}
\tag{3.15}
$$

where (cf. (2.2))

$$\phi_\varepsilon(x, y) = \phi_\varepsilon(r) = \frac{1}{4\pi} \left(1 - 2 \log \varepsilon - \frac{r^2}{\varepsilon^2} \right) + \phi_0(r) \tag{3.16}$$

It can be easily verified that the function

$$\Psi_\varepsilon(x, y) = \Psi_\varepsilon(r) = \begin{cases} \phi(r) &, \varepsilon < r \\ \phi_\varepsilon(r) &, 0 \le r \le \varepsilon \end{cases} \tag{3.17}$$

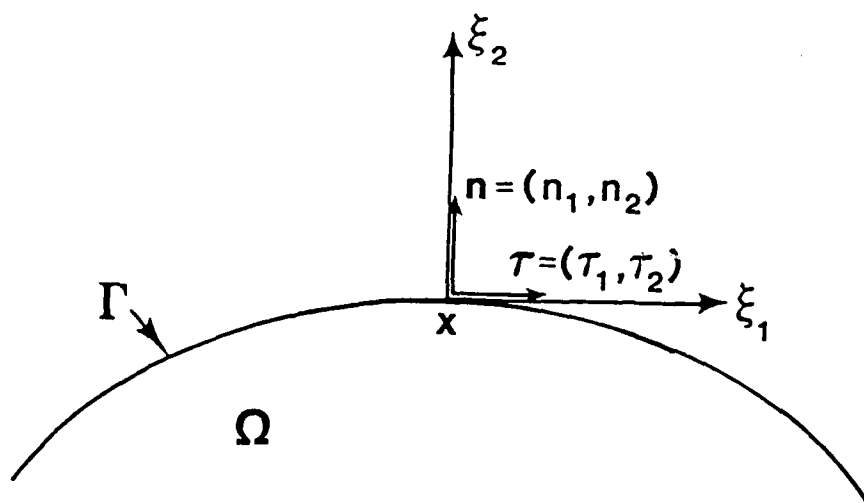as a function of x, y is a C^1 function in $\mathbb{R}^2$.

8

Figure 3: Tangential–normal local coordinate system.

Assuming that $|p(\boldsymbol{y})| \leq M$ we have now, for $\varepsilon \leq \delta$,

$$|v(\boldsymbol{x}) - v_\varepsilon(\boldsymbol{x})| \leq \int_{\Gamma \cap B_\varepsilon} \left| -\frac{\log r}{2\pi} - \frac{1}{4\pi}\left(1 - 2\log\varepsilon - \frac{r^2}{\varepsilon^2}\right)\right| |p(\boldsymbol{y})| ds(\boldsymbol{y})$$

$$\leq \frac{M}{4\pi} \int_{\Gamma \cap B_\varepsilon} \left| 2(\log\varepsilon - \log r) + \frac{r^2}{\varepsilon^2} - 1\right| ds(\boldsymbol{y})$$

$$\leq \frac{M}{4\pi} \int_{-\varepsilon}^{\varepsilon} \left| 2\log\frac{\varepsilon}{r} + \frac{r^2}{\varepsilon^2} - 1\right| \sqrt{1 + (f'(y))^2}\, d\xi_1 \qquad (3.18)$$

$$\leq \frac{M}{4\pi} \int_{-\varepsilon}^{\varepsilon} \left| 2\log\frac{\varepsilon}{r} + \frac{r^2}{\varepsilon^2} - 1\right| |1 + r^\alpha|\, d\xi_1 \leq C\varepsilon\log\varepsilon \to 0$$

as $\varepsilon \to 0$. Then v is the limit of the uniformly convergent sequence of continuous functions ν_ε and therefore is continuous. ∎

Lemma 3. Let us suppose all assumptions of Lemma 2 hold and, moreover, the Hölder condition on p over Γ is fulfilled. We have then

$$\int_\Gamma \frac{\partial\phi}{\partial n_{\boldsymbol{y}}}(\boldsymbol{x}_m, \boldsymbol{y})p(\boldsymbol{y})ds(\boldsymbol{y}) \longrightarrow \int_\Gamma \frac{\partial\phi}{\partial n_{\boldsymbol{y}}}(\boldsymbol{x}, \boldsymbol{y})p(\boldsymbol{y})ds(\boldsymbol{y}) + \frac{1}{2}p(\boldsymbol{x}) \qquad (3.19)$$

Proof:

$$\int_\Gamma \frac{\partial\phi}{\partial n_{\boldsymbol{y}}}(\boldsymbol{x}_m, \boldsymbol{y})p(\boldsymbol{y})ds(\boldsymbol{y}) = \int_\Gamma \frac{\partial\phi}{\partial n_{\boldsymbol{y}}}(\boldsymbol{x}_m, \boldsymbol{y})[p(\boldsymbol{y}) - p(\boldsymbol{x})]ds(\boldsymbol{y}) + p(\boldsymbol{x})\int_\Gamma \frac{\partial\phi}{\partial n_{\boldsymbol{y}}}(\boldsymbol{x}_m, \boldsymbol{y})ds(\boldsymbol{y})$$

$$= \int_\Gamma \frac{\partial\phi}{\partial n_{\boldsymbol{y}}}(\boldsymbol{x}_m, \boldsymbol{y})[p(\boldsymbol{y}) - p(\boldsymbol{x})]ds(\boldsymbol{y}) + p(\boldsymbol{x})\int_\Omega \Delta_{\boldsymbol{y}}\phi(\boldsymbol{x}_m, \boldsymbol{y})ds(\boldsymbol{y}) \qquad (3.20)$$

$$= \int_\Gamma \frac{\partial\phi}{\partial n_{\boldsymbol{y}}}(\boldsymbol{x}_m, \boldsymbol{y})[p(\boldsymbol{y}) - p(\boldsymbol{x})]ds(\boldsymbol{y}) - p(\boldsymbol{x})k^2\int_\Omega \phi(\boldsymbol{x}_m, \boldsymbol{y})ds(\boldsymbol{y})$$

Next we take functions similar to those in Lemma 2:

$$\omega(\boldsymbol{x}) = \int_\Gamma \frac{\partial\phi}{\partial n_{\boldsymbol{y}}}(\boldsymbol{x}, \boldsymbol{y})[p(\boldsymbol{y}) - p(\boldsymbol{x})]ds(\boldsymbol{y})$$

$$\omega_\varepsilon(\boldsymbol{x}) = \int_{\Gamma \setminus B_\varepsilon} \frac{\partial\phi}{\partial n_{\boldsymbol{y}}}(\boldsymbol{x}, \boldsymbol{y})[p(\boldsymbol{y}) - p(\boldsymbol{x})]ds(\boldsymbol{y}) \qquad (3.21)$$

$$+ \int_{\Gamma \cap B_\varepsilon} \frac{\partial\phi_\varepsilon}{\partial n_{\boldsymbol{y}}}(\boldsymbol{x}, \boldsymbol{y})[p(\boldsymbol{y}) - p(\boldsymbol{x})]ds(\boldsymbol{y})$$

10

where $\phi_\varepsilon(\boldsymbol{x}, \boldsymbol{y})$ is defined by (3.16).

$$|\omega(\boldsymbol{x}) - \omega_\varepsilon(\boldsymbol{x})| = \int_{\Gamma \cap B_\varepsilon} \left| \frac{\partial \phi}{\partial n_{\boldsymbol{y}}}(\boldsymbol{x}, \boldsymbol{y}) - \frac{\partial \phi_\varepsilon}{\partial n_{\boldsymbol{y}}}(\boldsymbol{x}, \boldsymbol{y}) \right| |p(\boldsymbol{y}) - p(\boldsymbol{x})| ds(\boldsymbol{y})$$

$$= \int_{\Gamma \cap B_\varepsilon} \left| \frac{-1}{2\pi r} + \phi_0'(r) + \frac{r}{2\pi\varepsilon^2} - \phi_0'(r) \right| \frac{|\boldsymbol{n}(\boldsymbol{y}) \cdot \boldsymbol{r}|}{r} |p(\boldsymbol{y}) - p(\boldsymbol{x})| ds(\boldsymbol{y}) \qquad (3.22)$$

$$\leq \frac{C}{2\pi} \int_{-\varepsilon}^{\varepsilon} \left| \frac{r}{\varepsilon^2} - \frac{1}{r} \right| |\cos\beta(\boldsymbol{y})| r^\alpha d\xi_1 \leq C\varepsilon^\alpha$$

where $\beta(\boldsymbol{y})$ is the angle between $\boldsymbol{n}(\boldsymbol{y})$ and $\boldsymbol{r}$ (see Fig. 4) and C denotes different constants. Then ω is the uniform limit of ω_ε and is continuous. We have obtained then

$$\int_\Gamma \frac{\partial \phi}{\partial n_{\boldsymbol{y}}}(\boldsymbol{x}_m, \boldsymbol{y})[p(\boldsymbol{y}) - p(\boldsymbol{x})] ds(\boldsymbol{y}) \longrightarrow \int_\Gamma \frac{\partial \phi}{\partial n_{\boldsymbol{y}}}(\boldsymbol{x}, \boldsymbol{y})[p(\boldsymbol{y}) - p(\boldsymbol{x})] ds(\boldsymbol{y}) \qquad (3.23)$$

In turn, by Lemma 1,

$$k^2 p(\boldsymbol{x}) \int_\Omega \phi(\boldsymbol{x}_m, \boldsymbol{y}) d\boldsymbol{y} \longrightarrow k^2 p(\boldsymbol{x}) \int_\Omega \phi(\boldsymbol{x}, \boldsymbol{y}) d\boldsymbol{y}$$

$$= -p(\boldsymbol{x}) \int_\Gamma \frac{\partial \phi}{\partial n_{\boldsymbol{y}}}(\boldsymbol{x}, \boldsymbol{y}) ds(\boldsymbol{y}) - \frac{1}{2} p(\boldsymbol{x}) \qquad (3.24)$$

Finally, (3.20), (3.23), and (3.24) imply (3.19). ∎

Remark. The proof of inequality (3.22) does not depend upon the assumption that $\boldsymbol{x} \in \Gamma$. It does not use even the fact that $|\cos\beta(y)| \leq Cr^\alpha$ for $\boldsymbol{x} \in \Gamma$ (Proposition 3). For this reason estimation (3.22) does not depend upon $\boldsymbol{x}$ and convergence of ω_ε is uniform.

Proposition 3. If the first derivative of the function f which describes the boundary Γ (3.13) fulfills in a given interval (δ_1, δ_2) the Hölder condition with exponent α, then there is a constant $C > 0$ such that

$$|\cos\beta(\boldsymbol{x})| \leq Cr^\alpha, \ |\cos\beta(\boldsymbol{y})| \leq Cr^\alpha, \ |\boldsymbol{n}_x - \boldsymbol{n}_y| \leq Cr^\alpha \qquad (3.25)$$

in this interval.

Proof: We establish the tangential–normal coordinate system as in Lemma 2 (Fig. 5). We have the following relations

$$|\cos\beta(\boldsymbol{x})| = \left| \sin\left(\beta(\boldsymbol{x}) - \frac{\pi}{2}\right) \right| = \frac{h}{r} = \frac{|f(\xi(\boldsymbol{y}))|}{r} = \frac{|\xi(\boldsymbol{y}) f'(\bar{\xi})|}{r} \leq Cr^\alpha \qquad (3.26)$$
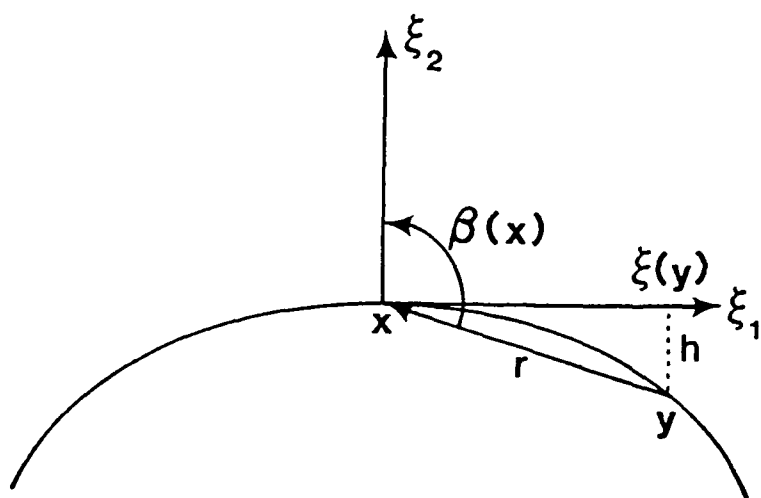
The proof for $\cos\beta(\boldsymbol{y})$ is analogous.

11

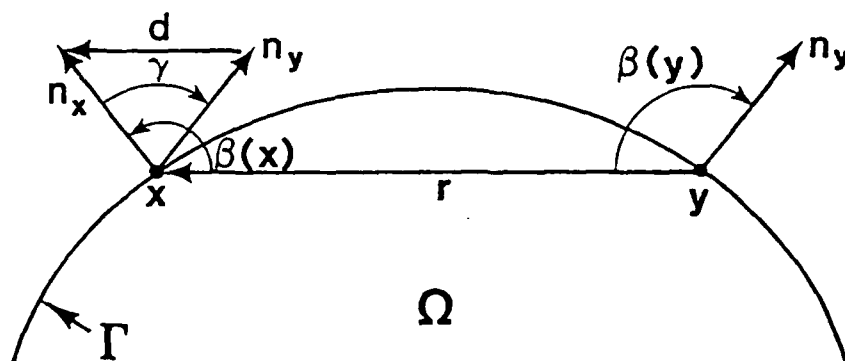Figure 4: Dependence of $\beta(\mathbf{x})$ upon $\mathbf{r}$.

Figure 5: Vectors n_x, n_y, r and angles between them.

The vector $\boldsymbol{d} = \boldsymbol{n}_x - \boldsymbol{n}_y$ is presented in Fig. 5.

$$|\boldsymbol{d}| = 2\left|\sin\frac{\gamma}{2}\right| = 2\left|\sin\left(\frac{1}{2}\left[\beta(\boldsymbol{x}) + \beta(\boldsymbol{y}) - \pi\right]\right)\right| = 2\left|\cos\left(\frac{1}{2}\left[\beta(\boldsymbol{x}) + \beta(\boldsymbol{y})\right]\right)\right|$$

$$= \sqrt{2}\sqrt{\cos\left(\beta(\boldsymbol{x}) + \beta(\boldsymbol{y})\right) + 1} = \sqrt{2}\sqrt{\cos\beta(\boldsymbol{x})\cos\beta(\boldsymbol{y}) - \sin\beta(\boldsymbol{x})\sin\beta(\boldsymbol{y}) + 1} \leq Cr^{\alpha}$$

because of (3.26).

Lemma 4. By the assumptions of Lemma 3

$$\int_{\Gamma}\frac{\partial\phi}{\partial n_{\boldsymbol{x}}}(\boldsymbol{x}_m, \boldsymbol{y})\, p(\boldsymbol{y})ds(\boldsymbol{y}) \longrightarrow \int_{\Gamma}\frac{\partial\phi}{\partial n_{\boldsymbol{x}}}(\boldsymbol{x}, \boldsymbol{y})p(\boldsymbol{y})ds(\boldsymbol{y}) - \frac{1}{2}p(\boldsymbol{x}) \tag{3.27}$$

where $\boldsymbol{n}_x$ is the outward normal vector at $\boldsymbol{x} \in \Gamma$.

Proof:

$$\int_{\Gamma}\frac{\partial\phi}{\partial n_{\boldsymbol{x}}}(\boldsymbol{x}_m, \boldsymbol{y})p(\boldsymbol{y})ds(\boldsymbol{y}) = \int_{\Gamma}\left[\frac{\partial\phi}{\partial n_{\boldsymbol{x}}}(\boldsymbol{x}_m, \boldsymbol{y}) + \frac{\partial\phi}{\partial n_{\boldsymbol{y}}}(\boldsymbol{x}_m, \boldsymbol{y})\right]p(\boldsymbol{y})ds(\boldsymbol{y})$$

$$- \int_{\Gamma}\frac{\partial\phi}{\partial n_{\boldsymbol{y}}}(\boldsymbol{x}_m, \boldsymbol{y})p(\boldsymbol{y})ds(\boldsymbol{y}) \tag{3.28}$$

The definition of ϕ implies

$$\frac{\partial\phi}{\partial x_i}(\boldsymbol{x}_m, \boldsymbol{y}) = \phi'(r)\frac{\partial r}{\partial x_i} = -\phi'(r)\frac{\partial r}{\partial y_i} = -\frac{\partial\phi}{\partial y_i}(\boldsymbol{x}_m, \boldsymbol{y})$$

from which follows

$$\frac{\partial\phi}{\partial n_{\boldsymbol{x}}}(\boldsymbol{x}_m, \boldsymbol{y}) + \frac{\partial\phi}{\partial n_{\boldsymbol{y}}}(\boldsymbol{x}_m, \boldsymbol{y}) = \sum_{i=1}^{2}\left[\frac{\partial\phi}{\partial x_i}n_i(\boldsymbol{x}) + \frac{\partial\phi}{\partial y_i}n_i(\boldsymbol{y})\right] = \sum_{i=1}^{2}\frac{\partial\phi}{\partial x_i}\left[n_i(\boldsymbol{x}) - n_i(\boldsymbol{y})\right] \tag{3.29}$$

Quite analogously to the proof of (3.23), with the use of (3.29) and Proposition 3, the convergence

$$\int_{\Gamma}\left[\frac{\partial\phi}{\partial n_{\boldsymbol{x}}}(\boldsymbol{x}_m, \boldsymbol{y}) + \frac{\partial\phi}{\partial n_{\boldsymbol{y}}}(\boldsymbol{x}_m, \boldsymbol{y})\right]p(\boldsymbol{y})ds(\boldsymbol{y}) \to \int_{\Gamma}\left[\frac{\partial\phi}{\partial n_{\boldsymbol{x}}}(\boldsymbol{x}, \boldsymbol{y}) + \frac{\partial\phi}{\partial n_{\boldsymbol{y}}}(\boldsymbol{x}, \boldsymbol{y})\right]p(\boldsymbol{y})ds(\boldsymbol{y}) \tag{3.30}$$

may be established. This with Lemma 3 gives (3.27).

Lemma 5. By the assumptions of Lemma 3

$$\fint_{\Gamma}\frac{\partial\phi}{\partial\tau_{\boldsymbol{x}}}(\boldsymbol{x}_m, \boldsymbol{y})p(\boldsymbol{y})ds(\boldsymbol{y}) \longrightarrow \fint_{\Gamma}\frac{\partial\phi}{\partial\tau_{\boldsymbol{x}}}(\boldsymbol{x}, \boldsymbol{y})p(\boldsymbol{y})ds(\boldsymbol{y}) \tag{3.31}$$

and

$$\frac{\partial}{\partial\tau_{\boldsymbol{x}}}\int_{\Gamma}\phi(\boldsymbol{x}, \boldsymbol{y})p(\boldsymbol{y})ds(\boldsymbol{y}) = \fint_{\Gamma}\frac{\partial\phi}{\partial\tau_{\boldsymbol{x}}}(\boldsymbol{x}, \boldsymbol{y})p(\boldsymbol{y})ds(\boldsymbol{y}) \tag{3.32}$$

14

Proof: For the beginning let us consider the following Cauchy Principal Value integral:

$$\fint_{-a}^{a} \frac{\partial \phi}{\partial x}(x,y)p(x)dy = \int_{-a}^{a} \frac{\partial \phi_0}{\partial x}(x,y)p(x)dy + \frac{p(x)}{2\pi}\int_{-a}^{a}\frac{\partial}{\partial x}\left(\log\frac{1}{r}\right)dy \qquad (3.33)$$

$$\fint_{-a}^{a}\frac{\partial}{\partial x}\left(\log\left(\frac{1}{r}\right)\right)dy \overset{\text{def}}{=} \lim_{\varepsilon\to 0}\left[\int_{-a}^{-\varepsilon}\frac{\partial}{\partial x}\left(\log\left(\frac{1}{r}\right)\right)dy + \int_{\varepsilon}^{a}\frac{\partial}{\partial x}\left(\log\frac{1}{r}\right)dy\right]$$

$$= \lim_{\varepsilon\to 0}\left[-\int_{-a}^{-\varepsilon}\frac{1}{r}\frac{\partial r}{\partial x}dy - \int_{\varepsilon}^{a}\frac{1}{r}\frac{\partial r}{\partial x}dy\right] = \lim_{\varepsilon\to 0}\left[\int^{-\varepsilon}-a\frac{dr}{r} + \int_{\varepsilon}^{a}\frac{dr}{r}\right] = 0 \qquad (3.34)$$

(3.33) and (3.34) imply

$$\fint_{-a}^{a}\frac{\partial \phi}{\partial x}(x,y)p(x)dy = \int_{-a}^{a}\frac{\partial \phi_0}{\partial x}(x,y)p(x)dy \qquad (3.35)$$

The same result can be obtained when we replace ϕ by Ψ_ε (cf. (3.17)):

$$\int_{-a}^{a}\frac{\partial \Psi_\varepsilon}{\partial x}(x,y)p(x)dy \fint_{-a}^{a}\frac{\partial \Phi_0}{\partial x}(x,y)p(x)dy \qquad (3.36)$$

We define once more the "regularizing" functions

$$t(\widehat{x}) = \int_{\Gamma}\frac{\partial \phi}{\partial \tau_x}(\widehat{x},y)\,p(y)ds(y)$$

$$\qquad (3.37)$$

$$t_\varepsilon(\widehat{x}) = \int_{\Gamma\backslash B_\varepsilon}\frac{\partial \phi}{\partial \tau_x}(\widehat{x},y)\,p(y)ds(y) + \int_{\Gamma\cap B_\varepsilon}\frac{\partial \phi_\varepsilon}{\partial \tau_x}(\widehat{x},y)\,p(y)ds(y)$$

where τ_x is a tangent vector at x (fixed), and assume that boundary Γ is defined by function f (cf. (3.13)). Then

$$|t(\widehat{x}) - t_\varepsilon(\widehat{x})| = \left|\int_{\Gamma\cap B_\varepsilon}\left[\frac{\partial \phi}{\partial \tau_x}(\widehat{x},y) - \frac{\partial \phi_\varepsilon}{\partial \tau_x}(\widehat{x},y)\right]p(y)ds(y)\right|$$

$$\leq \left|\int_{\Gamma\cap B_\varepsilon}\left[\frac{\partial \phi}{\partial \tau_x}(\widehat{x},y) - \frac{\partial \phi_\varepsilon}{\partial \tau_x}(\widehat{x},y)\right][p(y) - p(\widehat{x})]\,ds(y)\right|$$

$$+ \left|\int_{\Gamma\cap B_\varepsilon}\left[\frac{\partial \phi}{\partial \tau_x}(\widehat{x},y) - \frac{\partial \phi_\varepsilon}{\partial \tau_x}(\widehat{x},y)\right]p(\widehat{x})\,ds(y)\right|$$

$$\qquad (3.38)$$

$$\leq \left|\int_{-\varepsilon}^{+\varepsilon}\left[\frac{\partial \phi}{\partial \tau_x}(\widehat{x},\widehat{y}) - \frac{\partial \phi_\varepsilon}{\partial \tau_x}(\widehat{x},\widehat{y})\right]\sqrt{1 + (f'(\widehat{y}))^2}\,[p(\widehat{y}) - p(\widehat{x})]\,d\widehat{y}\right.$$

$$+ \int_{-\varepsilon}^{+\varepsilon}\left\{\left[\frac{\partial \phi}{\partial \tau_x}(\widehat{x},\widehat{y}) - \frac{\partial \phi_\varepsilon}{\partial \tau_x}(\widehat{x},\widehat{y})\right]\sqrt{1 + (f'(\widehat{y}))^2} - \left[\frac{\partial \phi}{\partial \tau_x}(\widehat{x},\widehat{y}) - \frac{\partial \phi_\varepsilon}{\partial \tau_x}(\widehat{x},\widehat{y})\right]\right\}p(\widehat{x})\,d\widehat{y}$$

$$\left.+ \int_{-\varepsilon}^{\varepsilon}\left[\frac{\partial \phi}{\partial \tau_x}(\widehat{x},\widehat{y}) - \frac{\partial \phi_\varepsilon}{\partial \tau_x}(\widehat{x},\widehat{y})\right]p(\widehat{x})\,d\widehat{y}\right|$$

15

The last integral is equal to zero, because of (3.35) and (3.36), and the remaining terms are

$$\leq 2 \int_0^\varepsilon \left| \frac{r}{2\pi\varepsilon^2} - \frac{1}{2\pi r} \right| (1 + Cr^\alpha) Cr^\alpha dr + 2M \int_0^\varepsilon \left| \frac{r}{2\pi\varepsilon^2} - \frac{1}{2\pi r} \right| (1 + Cr^\alpha - 1) dr \leq C\varepsilon^\alpha$$

(3.39)

This inequality proves the uniform convergence of $\bar{t}_\varepsilon$ to t, then t is a continuous function and (3.31) holds.

In the next step we shall prove the existence of the Cauchy Principal Value Integral on the right side of (3.32). Let us denote by S a tangent line at $x(\xi_1 - \text{axis})$ and by B_{ε_1}, B_{ε_2}—two balls with radii $\varepsilon_1, \varepsilon_2$, centered at x.

According to (3.35),

$$\int_{S\cap(B_{\varepsilon_1}\backslash B_{\varepsilon_2})} \frac{\partial\phi}{\partial\tau_x}(x,\hat{y}) p(x) d\hat{y} = 0$$

(3.40)

By definition of the Cauchy Principal Value Integral,

$$\fint_\Gamma \frac{\partial\phi}{\partial\tau_x}(x,y)p(y)ds(y) = \int_{\Gamma\backslash B_{\varepsilon_1}} \frac{\partial\phi}{\partial\tau_x}(x,y)p(y)ds(y)$$

$$+ \lim_{\varepsilon_2\to 0} \int_{\Gamma\backslash(B_{\varepsilon_1}\backslash B_{\varepsilon_2})} \frac{\partial\phi}{\partial\tau_x}(x,y)p(y)ds(y)$$

(3.41)

$$\left| \int_{\Gamma\cap(B_{\varepsilon_1}\backslash B_{\varepsilon_2})} \frac{\partial\phi}{\partial\tau_x}(x,y)p(y)ds(y) \right| = \left| \int_{\Gamma\cap(B_{\varepsilon_1}\backslash B_{\varepsilon_2})} \frac{\partial\phi}{\partial\tau_x}(x,y)[p(y) - p(x)]ds(y) \right.$$

$$+ \int_{\Gamma\cap(B_{\varepsilon_1}\backslash B_{\varepsilon_2})} \frac{\partial\phi}{\partial\tau_x}(x,y)p(x)ds(y) - \int_{S\cap(B_{\varepsilon_1}\backslash B_{\varepsilon_2})} \frac{\partial\phi}{\partial\tau_x}(x,\hat{y}) p(x)d\hat{y}$$

$$+ \left. \int_{S\cap(B_{\varepsilon_1}\backslash B_{\varepsilon_2})} \frac{\partial\phi}{\partial\tau_x}(x,\hat{y}) p(x)d\hat{y} \right| \leq \int_{S\cap(B_{\varepsilon_1}\backslash B_{\varepsilon_2})} \frac{1}{2\pi r} \left| \frac{\partial r}{\partial\tau_x} \right| Cr^\alpha \sqrt{1 + (f'(\hat{y}))^2} d\hat{y} \quad (3.42)$$

$$+ \int_{S\cap(B_{\varepsilon_1}\backslash B_{\varepsilon_2})} \frac{1}{2\pi r} \left| \frac{\partial r}{\partial\tau_x} \right| |p(\hat{x})| \left(\sqrt{1 + (f'(\hat{y}))^2} - 1 \right) d\hat{y} \leq C \int_{\varepsilon_2}^{\varepsilon_1} r^{1-\alpha} d\alpha$$

$$\leq C \left(\varepsilon_1^\alpha - \varepsilon_2^\alpha \right)$$

(3.42) proves the existence of the integral (3.41) in the Cauchy Principal Value sense.

Functions t_ε and v_ε (cf. (3.37) and (3.15)) are bounded and continuous, moreover

$$t_\varepsilon(\hat{x}) = \frac{\partial}{\partial\tau_x} v_\varepsilon(\hat{x})$$

(3.43)

16

We have proven in (3.39) that they are uniformly convergent to $t(\hat{x})$ and $\frac{\partial}{\partial \tau_x}v(\hat{x})$ $\forall\ \hat{x} \in I\!\!R^2$. Then

$$t(\hat{x}) = \frac{\partial}{\partial \tau_x}v(\hat{x}) \qquad \forall\ \hat{x} \in I\!\!R^2$$

and (3.32) holds. ∎

4   Hypersingular Formulation

Let us begin with (2.12). If we apply to it Proposition 2, we obtain

$$\frac{\partial p}{\partial n_x(x_m)}(x_m) = - \int_\Gamma \frac{\partial}{\partial \tau_y}\left(\frac{\partial \phi}{\partial \tau_x}(x_m,y)\right)p(y)ds(y) + k^2 \int_\Gamma \tau_x \tau_y \phi(x_m,y)p(y)ds(y)$$
$$- \int_\Gamma \frac{\partial \phi}{\partial n_x}(x_m,y)\frac{\partial p}{\partial n_y}(y)ds(y) + \frac{\partial p^{inc}}{\partial n_x}(x_m) \tag{4.1}$$

Proposition 1 implies

$$\frac{\partial p}{\partial n_x}(x_m) = \int_\Gamma \frac{\partial \phi}{\partial \tau_x}(x_m,y)\frac{\partial p}{\partial \tau_x}(y)ds(y) + k^2 \int_\Gamma \tau_x \tau_y \phi(x_m,y)p(y)ds(y)$$
$$- \int_\Gamma \frac{\partial \phi}{\partial n_x}(x_m,y)\frac{\partial p}{\partial n_y}(y)ds(y) + \frac{\partial p^{inc}}{\partial n_x}(x_m) \tag{4.2}$$

Now we may pass to the limit with $x_m \to x \in \Gamma$, deriving the advantage of Lemmas 2–5:

$$\frac{\partial p}{\partial n_x}(x) = \int_\Gamma \frac{\partial \phi}{\partial \tau_x}(x,y)\frac{\partial p}{\partial \tau_y}(y)ds(y) + k^2 \int_\Gamma \tau_x \tau_y \phi(x,y)p(y)ds(y)$$
$$- \int_\Gamma \frac{\partial \phi}{\partial n_x}(x,y)\frac{\partial p}{\partial n_y}(y)ds(y) + \frac{1}{2}\frac{\partial p}{\partial n_x}(x) + \frac{\partial p^{inc}}{\partial n_x}(x) \tag{4.3}$$

The product differentiation rule implies

$$\frac{\partial}{\partial \tau_x}\left[\phi(x,y)\frac{\partial p}{\partial \tau_y}(y)\right] = \frac{\partial \phi}{\partial \tau_x}(x,y)\frac{\partial p}{\partial \tau_y}(y) + \phi(x,y)\frac{\partial^2 p}{\partial \tau_x \partial \tau_y}(y) = \frac{\partial \phi}{\partial \tau_x}(x,y)\frac{\partial p}{\partial \tau_y}(y) \tag{4.4}$$

and this allows (4.3) to convert into

$$\frac{1}{2}\frac{\partial p}{\partial n_x}(x) = \int_\Gamma \frac{\partial}{\partial \tau_x}\left[\phi(x,y)\frac{\partial p}{\partial \tau_y}(y)\right]ds(y) + k^2 \int_\Gamma \tau_x \tau_y \phi(x,y)p(y)ds(y)$$
$$- \int_\Gamma \frac{\partial \phi}{\partial n_x}(x,y)\frac{\partial p}{\partial n_y}(y)ds(y) + \frac{\partial p^{inc}}{\partial n_x}(x)$$

17

and making use of Lemma 5

$$
\frac{1}{2}\frac{\partial p}{\partial n_x}(x) = \frac{\partial}{\partial \tau_x}\int_\Gamma \phi(x,y)\frac{\partial p}{\partial \tau_y}(y)ds(y) + k^2\int_\Gamma \tau_x\tau_y\phi(x,y)p(y)ds(y)
$$

$$
- \int_\Gamma \frac{\partial \phi}{\partial n_x}(x,y)\frac{\partial p}{\partial n_y}(y)ds(y) + \frac{\partial p^{inc}}{\partial n_x}(x) \qquad \forall\, x \in \Gamma
$$

(4.5)

This is the final form of the hypersingular formulation of (1.1)–(1.3).

To obtain the *variational formulation* of (4.5) let us multiply both sides by a test function q and integrate over Γ, using simultaneously (3.8):

$$
\frac{1}{2}\int_\Gamma \frac{\partial p}{\partial n_x}(x)q(x)ds(x) = -\int_\Gamma\int_\Gamma \phi(x,y)\frac{\partial p}{\partial \tau_y}(y)\frac{\partial q}{\partial \tau_x}(x)ds(y)ds(x)
$$

$$
+ k^2\int_\Gamma\int_\Gamma \tau_x\tau_y\phi(x,y)p(y)q(x)ds(y)ds(x)
$$

(4.6)

$$
- \int_\Gamma\int_\Gamma \frac{\partial \phi}{\partial n_x}(x,y)\frac{\partial p}{\partial n_y}(y,x)ds(y)ds(x)
$$

$$
+ \int_\Gamma \frac{\partial p^{inc}}{\partial n_x}(x)q(x)ds(x)
$$

for all admissible test functions q.

If we take a linear combination of (2.5) and (4.5) with real and imaginary coefficients, we obtain the Burton-Miller formulation of the Helmholtz exterior boundary–value problem:

$$
\frac{\alpha}{2}p(x) + \frac{(1-\alpha)i}{2k}\frac{\partial p}{\partial n_x}(x) = \alpha\int_\Gamma\left[\frac{\partial \phi}{\partial n_y}(x,y)p(y) - \phi(x,y)\frac{\partial p}{\partial n_y}(y)\right]ds(y)
$$

$$
+ \frac{(1-\alpha)i}{k}\left\{\frac{\partial}{\partial \tau_x}\int_\Gamma \phi(x,y)\frac{\partial p}{\partial \tau_y}(y)ds(y) + k^2\int_\Gamma \tau_x\tau_y\phi(x,y)p(y)ds(y)\right.
$$

(4.7)

$$
\left. - \int_\Gamma \frac{\partial \phi}{\partial n_x}(x,y)\frac{\partial p}{\partial n_y}(y)ds(y)\right\} + \alpha p^{inc}(x) + \frac{(1-\alpha)i}{k}\frac{\partial p^{inc}}{\partial n_x}(x)
$$

for $\alpha \in [0,1]$.

Multiplying both sides of Eq. (4.7) by a sufficiently smooth test function $q(x)$ defined on the boundary Γ and integrating it over Γ will result in a variational formulation:

Find p and $\frac{\partial p}{\partial n} \in H(\Gamma)$ such that

$$
\frac{\alpha}{2}\int_\Gamma p(x)q(x)dx + \frac{(1-\alpha)i}{2k}\int_\Gamma \frac{\partial p}{\partial n_x}(x)q(x)dx
$$

$$
= \alpha \int_\Gamma\int_\Gamma\left[\frac{\partial\phi}{\partial n_y}(x,y)p(y)q(x) - \phi(x,y)\frac{\partial p}{\partial n_y}(y)q(x)\right]ds(y)\,ds(x)
$$

$$
+ \frac{(1-\alpha)i}{k}\left\{-\int_\Gamma\int_\Gamma\phi(x,y)\frac{\partial p}{\partial\tau_y}(y)\frac{\partial q}{\partial\tau_x}(x)ds(y)ds(x)\right.
$$

$$
\left. + k^2\int_\Gamma\int_\Gamma\phi(x,y)p(y)q(x)\tau_x\tau_y ds(y)ds(x)\right. \tag{4.8}
$$

$$
\left. -\int_\Gamma\int_\Gamma\frac{\partial\phi}{\partial n_x}(x,y)\frac{\partial p}{\partial n_y}(y)q(x)ds(y)ds(x)\right\}
$$

$$
+\alpha\int_\Gamma p^{inc}(x)q(x)ds(x) + \frac{(1-\alpha)i}{k}\int_\Gamma \frac{\partial p^{inc}}{\partial n_x}(x)q(x)ds(x)
$$

and
$$
\frac{\partial p}{\partial n} = \varepsilon\, p
$$

for all $q \in H(\Gamma)$ where $H(\Gamma)$ is a Hilbert space on Γ.

If the boundary Γ is smooth then it is also known from the weak form of the boundary value problem that the appropriate space for Helmholtz differential equation is that $p \in H^{\frac{1}{2}}(\Gamma)$ and $\frac{\partial p}{\partial n} \in H^{-\frac{1}{2}}(\Gamma)$, but for this special problem, we require that p and $\frac{\partial p}{\partial n}$ are in the same space. Thus, we here assume that $H(\Gamma) = H^{\frac{1}{2}}(\Gamma)$ in the variational formulation (4.8).

5 Numerical Implementation

In what follows, only the Burton-Miller approach is considered. The classical integral formulation and the hypersingular integral formulation can be obtained by simply selecting $\alpha = 1$ and $\alpha = 0$.

Galerkin Approximation

Approximating $p, \frac{\partial p}{\partial n}$ and q in (4.9) with linear combinations of the same basis functions

$$
p(x) = \sum_{k=1}^N p^k e_k(x), \quad \frac{\partial p}{\partial n}(x) = \sum_{k=1}^N \left(\frac{\partial p}{\partial n}\right)^k e_k(x), \quad q(x) = \sum_{k=1}^N q^k e_k(x), \tag{5.1}
$$

19

where $e_k = e_k(x)$ are real–valued basis functions and $p^k, \left(\frac{\partial p}{\partial n}\right)^k$ and q^k are complex coefficients, leads to a system of (complex) linear equations for p^k and $\left(\frac{\partial p}{\partial n}\right)^k$. $\varepsilon = $ constant allows us to eliminate $\frac{\partial p}{\partial n}$ by setting $\left(\frac{\partial p}{\partial n}\right)^k = \varepsilon p^k$ from the calculations and leads to a final system of equations of the form

$$\sum_{k=1}^{N} a_{kl} p^k = b_l, \quad l = 1, \ldots, N, \tag{5.2}$$

where the load vector is given by

$$b_l = \int_{\Gamma} \left[\alpha p^{inc}(x) + \frac{(1-\alpha)i}{k} \frac{\partial p^{inc}}{\partial n(x)}(x) \right] e_l(x) ds(x) \tag{5.3}$$

and the stiffness matrix is defined by

$$
\begin{aligned}
a_{kl} = \alpha &\left\{ \frac{1}{2} \int_{\Gamma} e_k(y) e_l(x) ds(x) - \int_{\Gamma} \int_{\Gamma} e_k(y) \frac{\partial \Phi}{\partial n(y)}(x,y) ds(y) e_l(x) ds(x) \right. \\
&\left. + \varepsilon \int_{\Gamma} \int_{\Gamma} e_k(y) \Phi(x,y) ds(y) e_l(x) ds(x) \right\} \\
&+ \frac{(1-\alpha)i}{k} \left\{ \frac{1}{2}\varepsilon \int_{\Gamma} e_k(y) e_l(x) ds(x) + \int_{\Gamma} \int_{\Gamma} e_k(y) \frac{\partial^2 \Phi}{\partial n(x) \partial n(y)} \right. \\
&\left. \times (x,y) ds(y) e_l(x) ds(x) + \varepsilon \int_{\Gamma} \int_{\Gamma} e_k(y) \frac{\partial \Phi}{\partial n(x)}(x,y) ds(y) e_l(x) ds(x) \right\}.
\end{aligned}
\tag{5.4}
$$

h-p Approximation

A one–dimensional version of the h-p approximation discussed in [4] has been implemented. The principal features of the method are as follows:

- each element has at most three nodes, two endpoints starting with linear approximation and a middle node for orders of approximation $p \geq 2$ (this spectral order p should not be confused with the pressure),

- hierarchical shape functions discussed in [7] are implemented,

- the approximation is continuous. The linear degrees of freedom are common for neighboring elements, and

- instead of quadratic elements used in the previous research (see [3]), cubic spline elements are used for the approximation of geometry. As shown in Fig. 6, the cubic
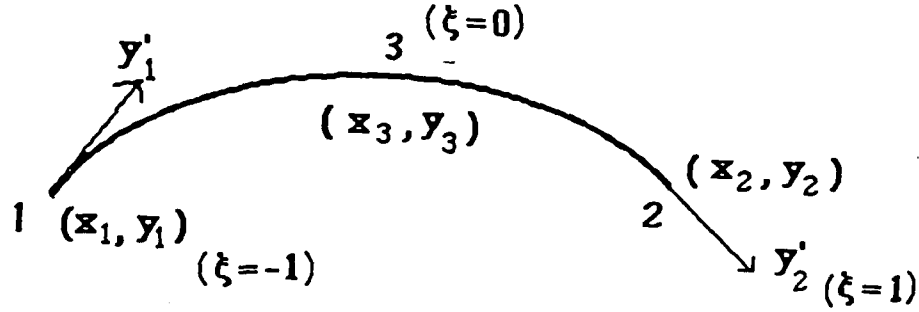
20

Figure 6: Cubic spline interpolation.

spline interpolation is defined by the map:

$$x(\xi) = x_1\phi_1(\xi) + x_2\phi_2(\xi) + a_1\Psi_1(\xi) + a_2\Psi_2(\xi)$$
$$y(\xi) = y_1\phi_1(\xi) + y_2\phi_2(\xi) + b_1\Psi_1(\xi) + b_2\Psi_2(\xi)$$

(5.5)

where $x(\xi)$ and $y(\ )$ are curvilinear coordinates with the master coordinate $\xi \in [-1,1]$, $(x_1, y_1$ and $x_2, y_2)$ are the coordinates of the two end points, and ϕ_1, ϕ_2, Ψ_1, and Ψ_2 are the cubic shape functions of cubic spline, i.e.,

$$\phi_1(\xi) = \frac{(\xi+1)^2(2-\xi)}{4} \qquad \phi_2(\xi) = \frac{(\xi-1)^2(2+\xi)}{4}$$

$$\Psi_1(\xi) = \frac{(\xi-1)^2(\xi+1)}{4} \qquad \Psi_2(\xi) = \frac{(\xi+1)^2(\xi-1)}{4}$$

(5.6)

The map is C^1-continuous whenever a_1, a_2, b_1 and b_2 in (5.5) satisfy

$$y_1' = \frac{a_1}{b_1} \qquad \text{and} \qquad y_2' = \frac{a_2}{b_2}$$

(5.7)

where y_1' and y_2' represent tangential derivative $\frac{dy}{dx}$ at end points 1 and 2, respectively. The curve defined in (5.5) will pass through the center point (x_3, y_3) at $\xi = 0$, if a_1, a_2, b_1 and b_2 in (5.6) further satisfy

$$\frac{1}{2}x_1 + \frac{1}{2}x_2 + \frac{1}{4}a_1 - \frac{1}{4}a_2 = x_3$$

(5.8)

$$\frac{1}{2}y_1 + \frac{1}{2}y_2 + \frac{1}{4}b_1 - \frac{1}{4}b_2 = y_3$$

(5.9)

21

Now, a_1, a_2, b_1 and b_2 can be determined by solving (5.7)–(5.9) and we have

$$a_1 = \frac{1}{y_1' - y_2'} \left[(4y_3 - 2y_1 - 2y_2) - y_2' (4x_3 - 2x_1 - 2x_2) \right] \qquad (5.10)$$

$$a_2 = \frac{1}{y_1' - y_2'} \left[(4y_3 - 2y_1 - 2y_2) - y_1' (4x_3 - 2x_1 - 2x_2) \right] \qquad (5.11)$$

$$b_1 = \frac{y_1'}{y_1' - y_2'} \left[(4y_3 - 2y_1 - 2y_2) - y_2' (4x_3 - 2x_1 - 2x_2) \right] \qquad (5.12)$$

$$b_2 = \frac{1}{y_1' - y_2'} \left[(4y_3 - 2y_1 - 2y_2) - y_1' (4x_3 - 2x_1 - 2x_2) \right] \qquad (5.13)$$

The cubic spline defined in (5.5) with a_1, a_2, b_1 and b_2 determined by (5.10)–(5.13) can fit three points at each element exactly and provide C^1-continuity over the whole boundary.

Singular Integration

The only singular integral involved in (4.9) is a weakly singular (logarithmic) integral. Let K_1 and K_2 be two elements. A typical contribution to the element stiffness matrix corresponding to K_1 and K_2 is of the form

$$\int_{K_1} \left[\int_{K_2} \chi_k^2(\boldsymbol{y}) \phi(\boldsymbol{x}, \boldsymbol{y}) ds(\boldsymbol{y}) \right] \chi_l^1(\boldsymbol{x}) ds(\boldsymbol{x}) \qquad (5.14)$$

where χ_k^j are shape functions for element $K_j, j = 1, 2$. Only when $K_1 = K_2$, the kernel function $\phi(x, y)$ is singular. Thus, in case of $K_1 \neq K_2$, both outer and inner integrals are evaluated using Gaussian integration with the number of integration points $N_1 = p + 1$. In the case $K_1 = K_2$, the outer integral is again evaluated using Gaussian quadrature with $N_1 = p + 1$ integration points. Integration of the inner integral with logatrithmic singular type of $\phi(x, y)$ in (5.14) is illustrated in Fig. 7. For every Gaussian integration point used to evaluate the outer integral, the element is divided into two parts: integrate from one endpoint to the singular point and from the singularity to the other endpoint and the integration is performed separately on each part. Each of the two subintegrals is converted into an integral from 0 to $d_j, j = 1, 2$, with respect to the distance between an integration point and the singular point. A special integration rule for logarithmic kernels of Gaussian type is then used with the number of integration points $N_1 = p + 1$. An additional complication arises due to the lack of an explicit relationship between the integration variable (distance s) and the master element coordinate, say η. This solved in practice by starting with an initial value for η corresponding to a linear element and performing Newton-Raphson iterations. In practical calculations, the number of iterations seldom exceeds 3.

6 Numerical Experiment 1

The classical scattering problem (see Fig. 8) for a plane wave impinging on a massless cylindrical body with radically elastic response, i.e.,

$$\frac{\partial p}{\partial n} = \varepsilon p \ (0 \leq \varepsilon < \infty: \text{ a constant}) \qquad \text{on } \Gamma \tag{6.1}$$

is used to test the method and code. Using the polar coordinates (r, θ), the exact solution to the test problem is of the form

$$p = p^{inc} + p^s \tag{6.2}$$

where the incident pressure

$$p^{inc} = P_{inc} \exp(ikr\cos\theta) = P_{inc} \exp(ikx_1) \tag{6.3}$$

with a constant P_{inc}, and the scttered pressure p^s is evaluated by the series

$$p^s(r, q) = \sum_{m=0}^{\infty} B_m H_m(kr) \cos(m\theta) \tag{6.4}$$

with H_m-Hankel functions of the first kind of order m, and coefficients B_m are given by

$$B_m = -P_{inc} b_m i^m \frac{\dfrac{dJ_m(ka)}{d(kr)} - \dfrac{\varepsilon}{k} J_m(ka)}{\dfrac{dH_m(ka)}{d(kr)} - \dfrac{\varepsilon}{k} H_m(ka)} \tag{6.5}$$

where J_m is Bessel function of the first kind of order m, a is the radius of the cylinder, and

$$b_o = 1 \text{ and } b_m = 2 \ (m = 1, 2, 3, \ldots) \tag{6.6}$$

k is the wave number. In the case $\varepsilon = 0$ the problem reduces to the classical rigid scattering problem.

In practice, we can only calculate a finite number of terms of the form (6.5) in (6.4) to obtain a solution for the test problem. The calculation of the Hankel and Bessel function also introduces some errors. Based on numerical experience, a reasonable estimation of the L^2-error of the solution calculated by using (6.1)–(6.5) is between 10^{-5} to 10^{-6}.

Forbidden Frequencies of the Test Problem

The solutions of the Helmholtz formulation and the hypersingular formulation for exterior acoustic wave problems is nonunique at certain forbidden frequencies or wavenumbers. The

forbidden wavenumbers are found to coincide with the "resonant" wavenumbers for a related interior problem. In the two-dimensional case of a circle of radius a (the test problem), for example, the forbidden wavenumbers of the Helmholtz formulation consist of values of k such that $J_n(ka) = 0$ and the forbidden wavenumbers of the hypersingular formulation consist of values of k such that $J_n'(ka) = 0$, where $J_n(ka)$ is a Bessel function of the first kind and order n and n is integer.

Example 1. Comparison of solutions for two kinds of hypersingular formulations.

In this example, we compare results solved by the Helmholtz formulation (2.5), the current hypersingular formulation (4.6), and the classical hypersingular formulation (2.7). The test problem is solved using uniform meshes of 8, 16, 32, and 64 elements with order of approximation $p = 1, 2, \ldots, 6$. The following data are chosen in the test problem:

$$\varepsilon = 0 \ (\text{rigid scattering})$$
$$P_{inc} = 1$$
$$a = 1$$
$$k = 4$$

The comparisons of the L^2-errors of the test problem solved by three different formulations for $p = 2$ and $p = 3$ are presented in Figs. 9 and 10. The results for other orders of approximation are similar and are not illustrated. Figures 9 and 10 indicate that the hypersingular formulation (4.6) can give a much better solution than the classical formulation (2.7). In Figs. 9 and 10, the solution of the Helmholtz formulation is slightly better than the solution of the hypersingular formulation (4.6), but there is no substantial difference between the solutions solved by two formulations.

It seems that the classical hypersingular formulation (2.7) results are not completely satisfactory in practical computation. In most cases, the accuracy is much lower than that of the Helmholtz formulation. The low accuracy in the hypersingular formulation deteriorates the corresponding solution of the Burton-Miller formulation. A major purpose of this research is to improve the accuracy of hypersingular formulation solution and we have arrived at this purpose.

Example 2. Illustration of the forbidden frequencies for the rigid scattering problem.

The purpose of this example is to show the effects of forbidden frequencies on formulations. Theoretically, as long as the wave number k does not coincide exactly with a forbidden frequency, the corresponding stiffness matrix is nonsingular and the approximate problem has a unique solution. In practice, for wave numbers k close to the forbidden frequencies, the condition of the matrix deteriorates and the quality of the solution drastically decreases. The situation is illustrated in Figs. 11 and 12 showing the variation of the approximate and

exact solutions at field point $(-3, 0)$ as a function of wave number k. The following data have been chosen:

$$\varepsilon = 0 \text{ (rigid scattering)}$$

$$P_{inc} = 1$$

$$a = 1$$

$$\Delta k = 0.001$$

$$k_{\min} = 1, \text{ and } k_{\max} = 9$$

For each k, the test problem was solved by the Helmholtz formulation (shown in Fig. 11) and the hypersingular formulation (shown in Fig. 12) on the same uniform mesh of 8 quadratic elements. Both formulations lose stabilities at certain frequencies. Figure 13 shows calculations of the Burton-Miller approach (based on the current hypersingular formulation (4.6)). The formulation delivers consistently stable results for the whole range of wave numbers k.

The solution produced by the current hypersingular formulation (4.6) proves very stable. With $\Delta k = 0.001$, the numerical solution in Fig. 11 only loses stability at 3 forbidden frequencies. With $\Delta k = 0.002$, $k_{\min} = 1$, and $k_{\max} = 8$, the same experiment in [3] showed that the numerical solution based on (2.7) lost stability at 9 forbidden frequencies (see Fig. 14). This simply implies that the condition of the stiffness matrix formed by the current hypersingular formulation is better than the condition of the matrix formed by the classical formulation when near a forbidden frequency.

7 Convergent Rate and *A Posteriori* Error Estimation

Convergence of the Galerkin method for boundary integral equations has been carefully analyzed in a series of works by Wendland [10] and p- and hp-versions of boundary elements are discussed by Rank [7] and Stephan and Suri [8,9] and a brief discussion was given in [6]. Here, we follow the same approach in [3] together with *a posteriori* estimates and use L^2-norm of error to measure convergent rates of the formulations, (2.5), (4.6), and (4.7).

The error estimates used in this research are based on the L^2-norm residual. For any approximation solution p_h, we define

$$r(x) = p_h(x) - 2 \int_\Gamma \left[p(y) \frac{\partial \phi(x, y)}{\partial n_y} - \frac{\partial p_h(y)}{\partial n_y} \phi(x, y) \right] ds - 2p^{inc}(x) \tag{7.1}$$

as the residual for the Helmholtz formulation and then the L^2-norm of residual is calculated

25

by

$$\|r\|^2 = \int_\Gamma (r(s))^2 \, ds = \sum_{e=1}^{N} \int_{\Gamma_e} (r(s))^2 \, ds \approx \sum_{e=1}^{N} \sum_{l=1}^{Ge} w_l^e r^2 (s_l^e) \qquad (7.2)$$

where N is the number of elements, Ge is the number of Gauss points, w_l^e represents the weight of the Gauss integral, and s_l^e represent the coordinate of the Gauss points. We use $Ge = p + 1$ in (7.2) for each element, p being the order of approximation in each element.

Based on the analysis in [3], we have the following theorem for the residual defined in (5.1).

Theorem:

Let $e = p - p_h$ denote the approximation error inherent in p_h. Then, for the rigid scattering problem, if k is not a forbidden frequency of (2.5), there exist positive constants C_1 and C_2 such that for the residual r defined in (7.1) and error e there holds

$$C_1\|r\| \leq \|e\| \leq C_2\|r\| \qquad (7.3)$$

where $\| \cdot \|$ represents the L^2-norm on Γ and p is the exact solution. In (7.3), e can be the error from the solution of the Helmholtz formulation, the hypersingular formulation, or the Burton-Miller formulation. Furthermore, if e is the error from the solution of the Helmholtz formulation, then

$$\lim_{h \to 0, p \to \infty} \frac{\|r\|}{\|e\|} = 1 \qquad (7.4)$$

where h is the maximum size of the mesh and p is the order of approximation.

In case k is a forbidden frequency, there still exists a positive constant C such that

$$\|\Pi e\| \leq C\|r\| \qquad (7.5)$$

where Π is the L^2-orthogonal projection of p onto the orthogonal complement of $N(A)$, A is defined as the integral operator A

$$Ap = \frac{1}{2}p(\boldsymbol{x}) - \int_\Gamma p(\boldsymbol{y}) \frac{\partial \phi(\boldsymbol{x}, \boldsymbol{y})}{\partial \boldsymbol{n}_h} ds \qquad (7.6)$$

and $N(A)$ is the null space of A. ∎

Compared with other forms of error estimates proposed in the boundary element method (see, e.g. [6,7]), the L^2-norm of the residual derived here is simple to calculate and the computed results agree with the theory quite well in [3].

8 Numerical Experiment 2

Example 3. Rates of convergence for the Helmholtz formulation.

Selecting

$$\varepsilon = 0 \text{ (rigid scattering)}$$
$$P_{inc} = 1$$
$$a = 1$$
$$k = 15$$

The test problem was solved using uniform meshes of 8, 16, 32, and 64 elements with order of approximation $p = 1, 2, \ldots, 6$. The corresponding rates of convergence for h-refinements at $k = 15$ are summarized in Figs. 15 and 16 and for p-refinement in Fig. 17. The rates of convergence for the h-method are very close to the theoretical rate $p + 1$, increasing in particular with the order of approximation p. The rates of convergence for the p-extensions seem to deliver the superlinear (exponential) rate of convergence.

Example 4. Rates of convergence for the hypersingular formulation.

With the same data and the same h-p meshes as in the first example, the problem was solved once again using the hypersingular formulation given in (4.6). The results, summarized in Figs. 18, 19, and 20, are slightly less satisfactory than those in the first example. The observed rates of convergence for the h-method are almost not changed for $p > 3$. The p-method shows no signs of exponential convergence. The reason for these suboptimal rates of convergence is still not clear at this writing, supposedly because of the domination of the error due to the geometry approximation. The results produced by the hypersingular formulation are more sensitive to the geometry approximation than those obtained by using the Helmholtz formulation; thus, the cubic spline interpolation in geometry may not be accurate enough for $p > 3$.

Example 5. Global effectivity of the L^2-residual estimate.

We begin with a simple comparison of the L^2-error and L^2-residual for the test problem with data and meshes discussed in Examples 1 and 2. The effectivity of the L^2-residual estimate is measured by an effectivity index which is defined by

$$\text{effectivity index} = \frac{\|r\|}{\|e\|} \tag{8.1}$$

Here, $\| \cdot \|$ is the norm of $L^2(\Gamma)$, r is the residual defined in (7.1), and $e = p_e - p_h$ where p_h is the numerical solution of the test problem and p_e is the solution solved by (6.1)–(6.6). Figure 21 summarizes results for the Helmholtz formulation, Fig. 22 for the hypersingular formulation, and Fig. 23 for the Burton-Miller formulation. The following conclusions can be drawn.

- For the Helmholtz formulation the L^2-residual seems to give an asymptotically exact error estimate for h-refinements, as predicted by the Theorem in (7.4).

- For large p and small size elements, the Helmholtz formulation effectivity index decreases, supposedly because of the domination of the error due to the geometry approximation or due to the error in calculating the exact solution by (6.1)–(6.6).

- For the hypersingular formulation, the global effectivity index stays bounded (between 1 and 2 for the test problem) but, as expected, does not converge to 1.

- The effectivity index of the Burton-Miller formulation also stays bounded and is very close to 1.

Example 6. Global effectivity of the L^2-residual estimate for a forbidden frequency.

Figure 24 presents the results of the error estimation for the test problem at a forbidden frequency of Helmholtz formulation ($k = 5.1356$) obtained by using the solution of the Burton-Miller formulation. The displayed values of the global effectivity indices stay consistently in the same range as in Fig. 23 (close to 1), indicating that the L^2-residual corresponding to the Helmholtz formulation can be used for the entire range of frequencies, provided the $N(A)$-component of the error is eliminated by an appropriate formulation (in this case, the Burton-Miller formulation).

For large p and small size elements, the decrease of the effectivity index is observed in Fig. 24. This is believed to be the domination of the error due to the geometry approximation or due to the error in calculating the exact solution by (6.1)–(6.6).

Example 7. Local effectivity of the L^2-residual estimate.

The efficiency of the adaptive method is directly determined by the local property of the error estimate. With the same data as in Examples 5 and 6, the local L^2-error and L^2-residual is also compared. The local effectivity index in each element is very close to the global effectivity index. As an example, Table 1 presents a comparison of local L^2-error and L^2-residual is also compared. The local effectivity index in each element is very close to the global effectivity index. As an example, Table 1 presents a comparison of local L^2-error and L^2-residual for a mesh of 16 quadratic elements and Burton-Miller formulation at $k = 15$ and $k = 5.1356$ (a forbidden frequency for Helmholtz formulation).

9 References

1. Colton, D., and Kress, R., Integral Equation Methods in Scattering Theory, John Wiley and Sons, NY, 1983.

2. Demkowicz, L., Karafiat, A., and Oden, J. T., "Variational (Weak) Form of the Hyper-singular Formulation for the Helmholtz Exterior Boundary–Value Problems," TICOM Report 91-05.

3. Demkowicz, L., Oden, J. T., Ainsworth, M., and Geng, P., "Solution of Elastic Scattering Problems in Linear Acoustics Using h-p Boundary Element Methods," *Journal of Computational and Applied Mathematics*, **36**, pp. 29–63, 1991.

4. Demkowicz, L., Oden, J. T., Rachowicz, W., and Hardy, O., "Toward a Universal h-p Adaptive Finite Element Strategy, Part 1: Constrained Approximation and Data Structure," *Comp. Meths. Appl. Mech. Engrg.*, **77** (1-2), pp. 79–112, 1989.

5. Hamdi, M. A., "Une formulation variationelle par équations intégrales pour la résolution de l'équation de Helmholtz avec des conditions aux limites mixtes," *C. R. Acad. Sci. Paris, 292*, (5 janvier 1981), Série II, pp. 17–20.

6. Hsiao, G. C., Kleinman, R. E., Li, R. X., and Berg, P. M. van den, "Residual Error—A Simple and Sufficient Estimate of Actual Error in Solutions of Boundary Integral Equations," in **Computational Engineering with Boundary Elements, Proceedings of the Fifth International Conference on Boundary Element Technology,** Vol. 1 (S. Grilli, C. A. Brebbia, and A. H-D Cheng, eds), Computational Mechanics Publication, Southampton, Boston, pp. 74–83, 1990.

7. Rank, E., "Adaptive h-, p-, and hp-Version for Boundary Integral Element Methods," *Int. J. for Num Meths. in Engrg.*, Vol. 28, pp. 1335–1349, 1989.

8. Stephan, E. P., and Suri, M., "On the Convergence of the p-Version of the Boundary Element Galerkin Method," *Math. Comp.*, **52**, pp. 31–48, 1989.

9. Stephan, E. P., and Suri, M., "An h-p Method with Quasiuniform Mesh for Integral Equations on Polygons," preprint 1989.
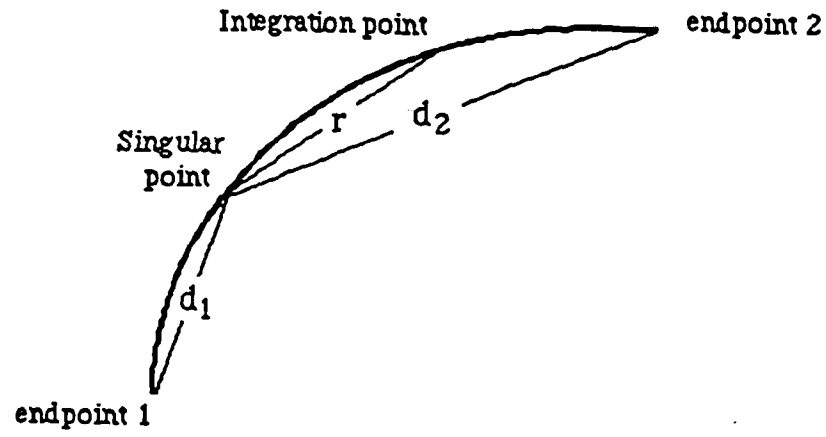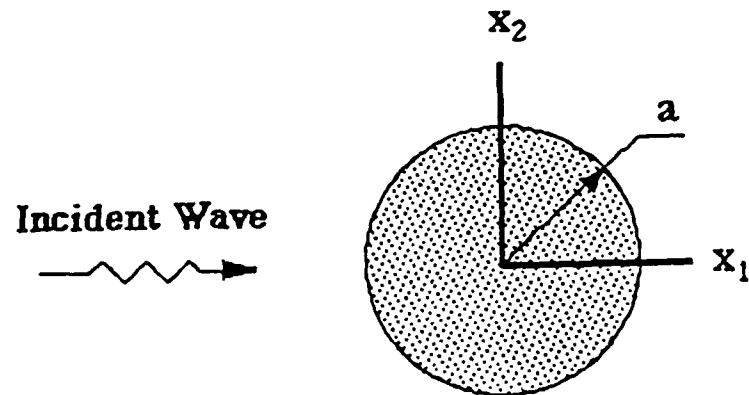
Figure 7: Evaluation of singular integrals.
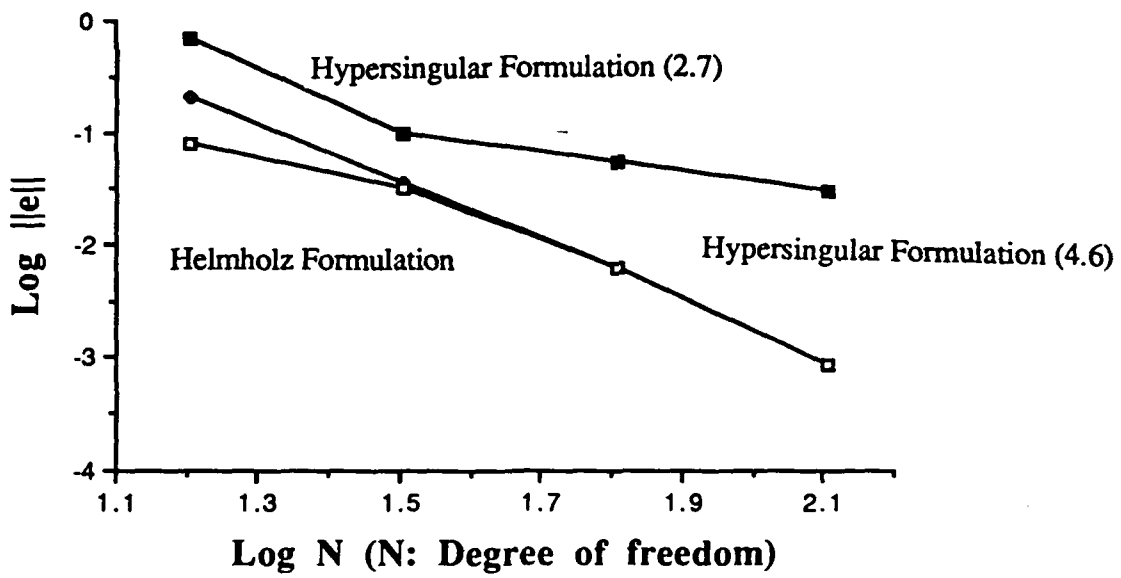

Figure 8: The test problem.

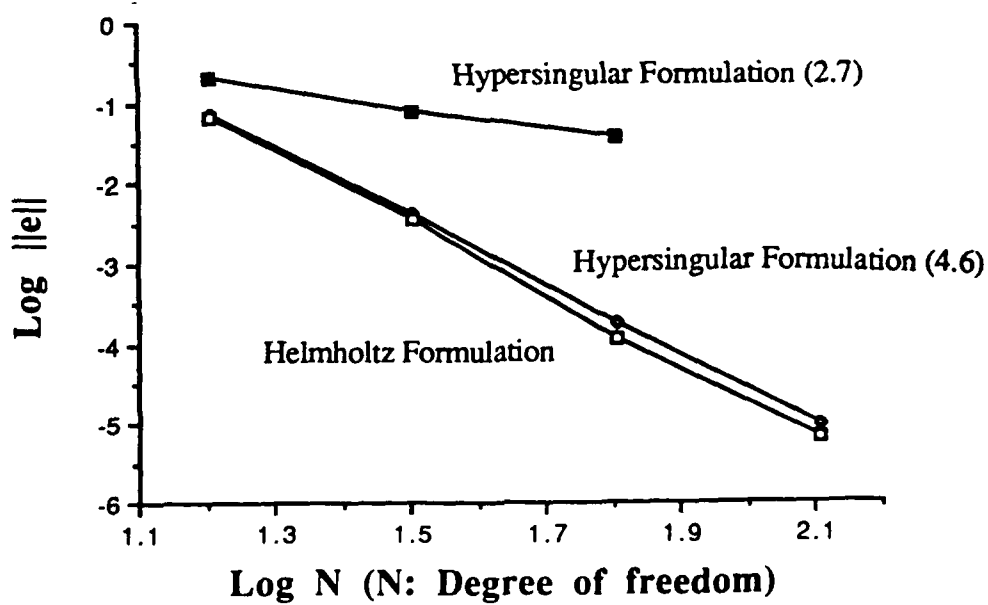Figure 9: Example 1. Comparison of L^2-errors of solutions among three formulations for $p = 2$.

Figure 10: Example 1. Comparison of L^2-errors of solutions among three formulations for $p = 3$.
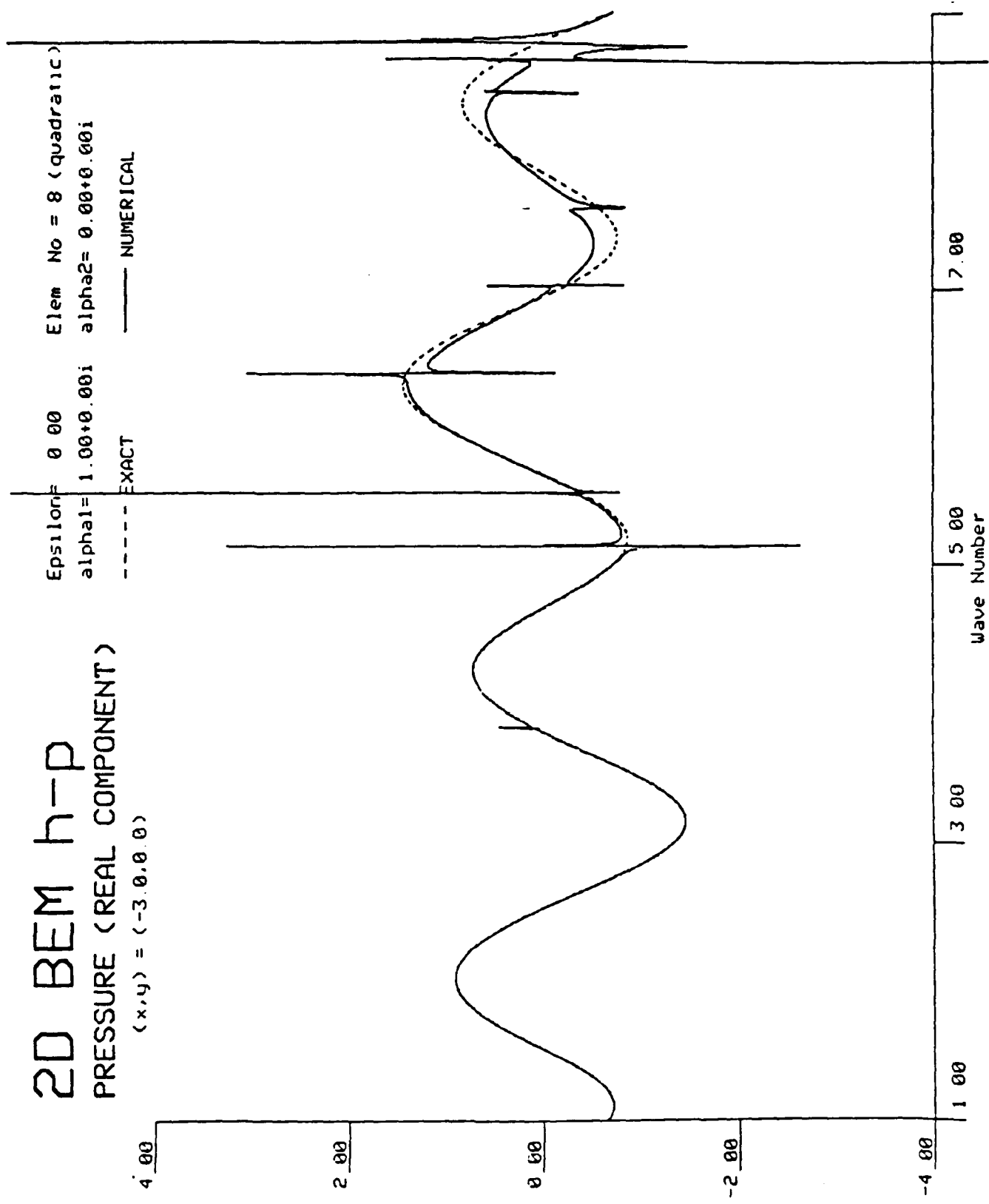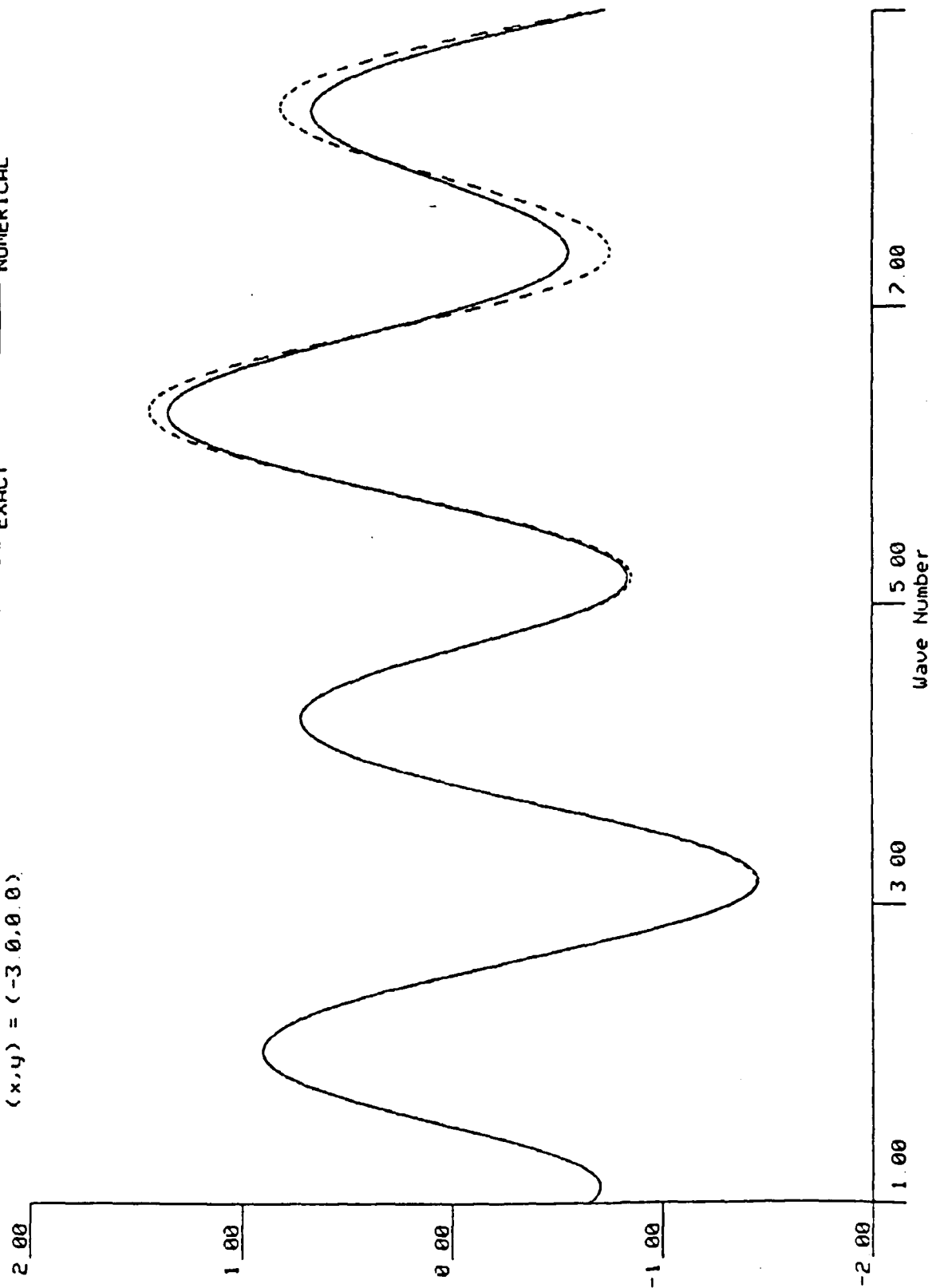
Figure 11: Example 2. Solution at a field point as a function of wave number for the Helmholtz formulation.

32
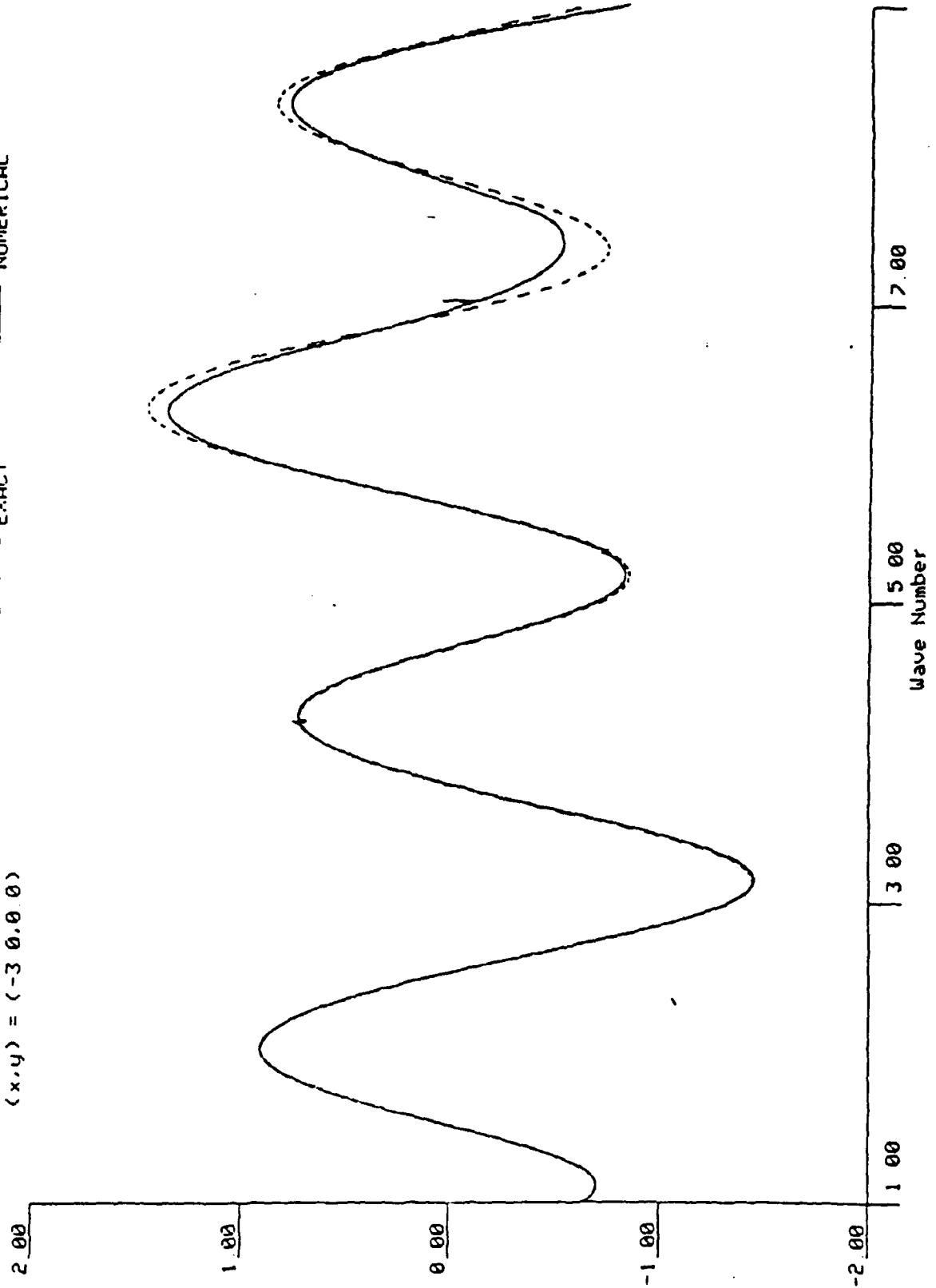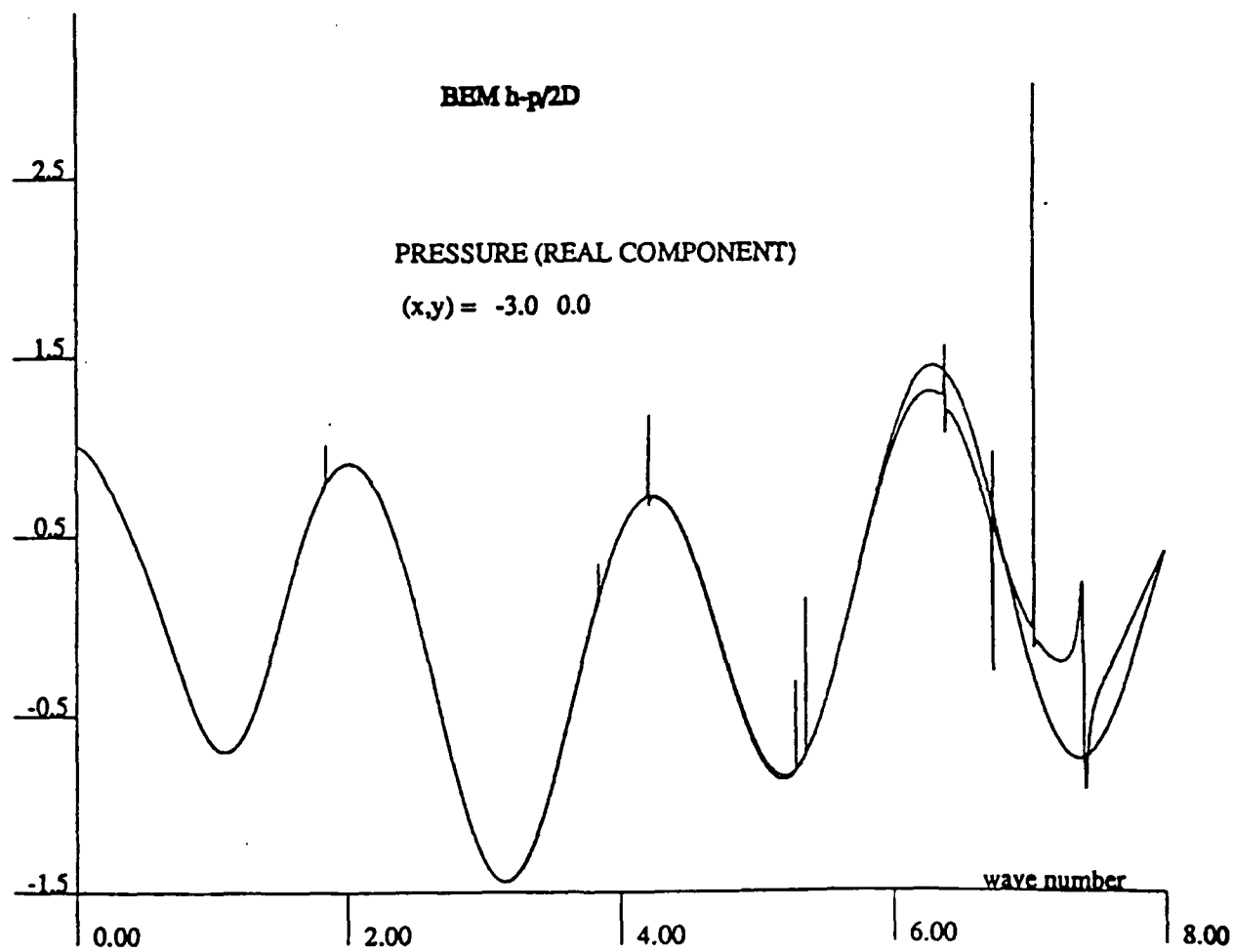
Figure 12: Example 2. Solution at a field point as a function of wave number for the hypersingular formulation (4.5).

33

Figure 13: Example 2. Solution at a field point as a function of wave number for Burton-Miller formulation.

Figure 14: Example 2. Solution at a field point as a function of wave number for the classical hypersingular formulation (2.5).
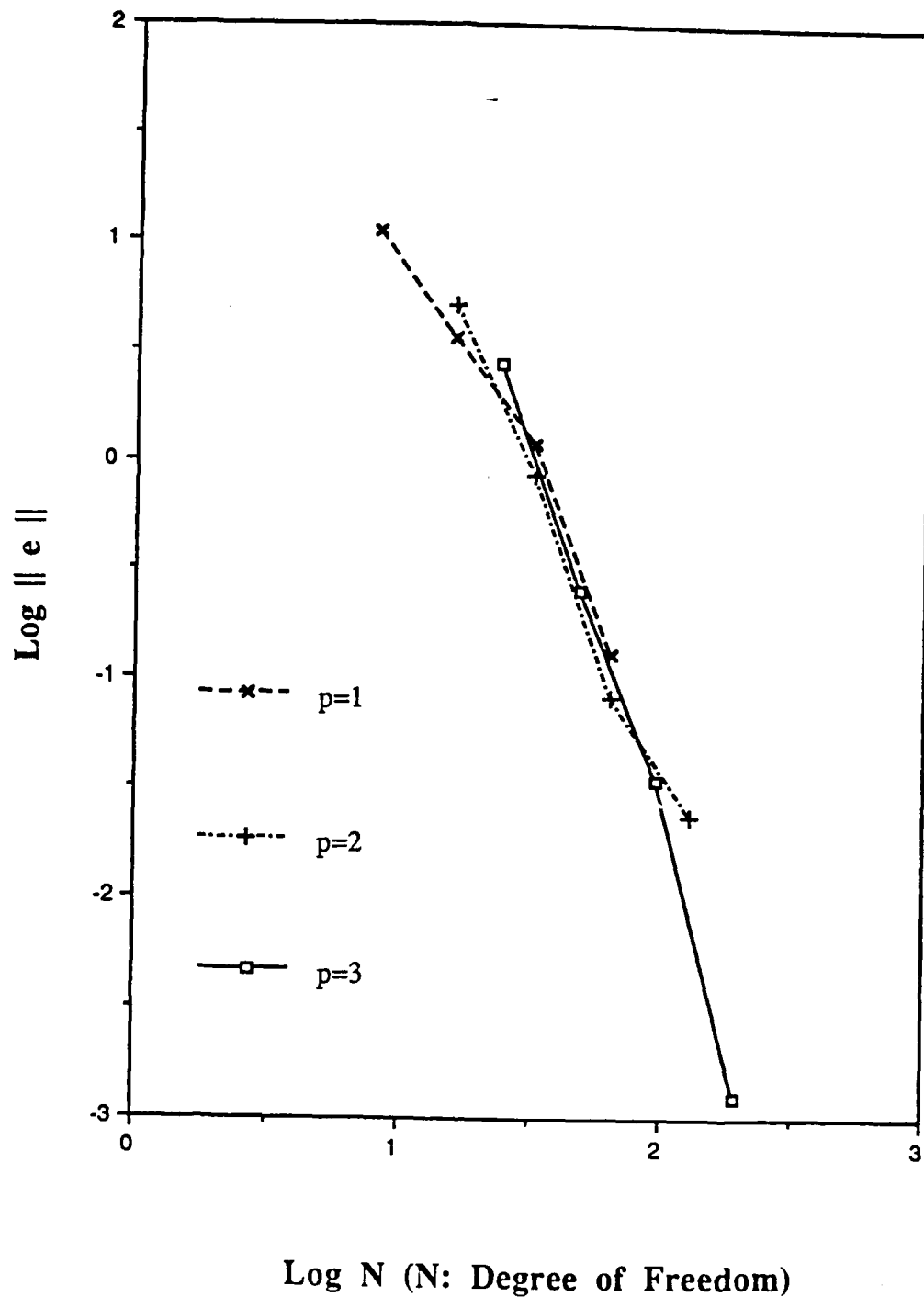
Log N (N: Degree of Freedom)

Figure 15: Example 3. Experimental rates of convergence for uniform h-refinement ($p = 1$, 2. and 3).
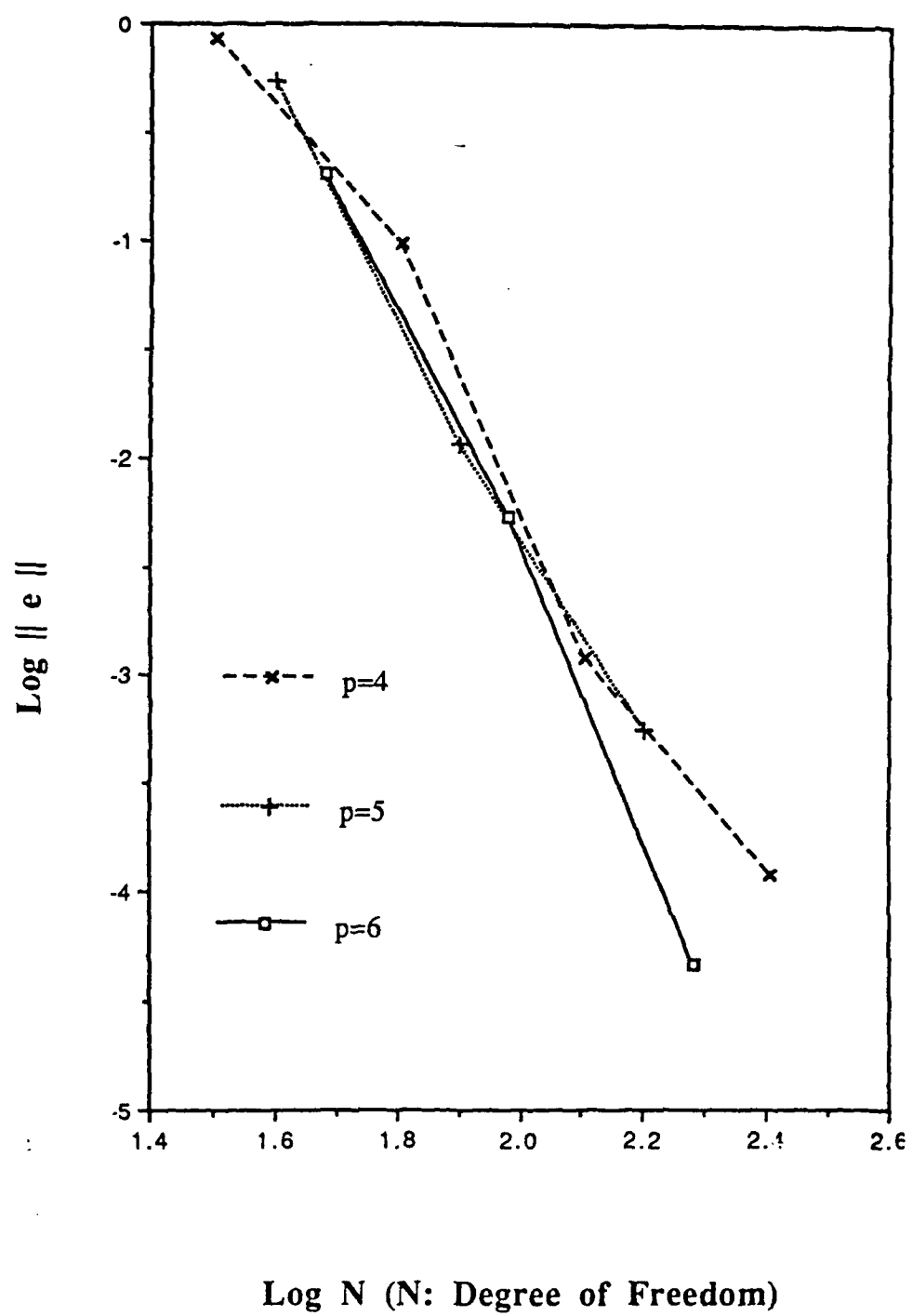
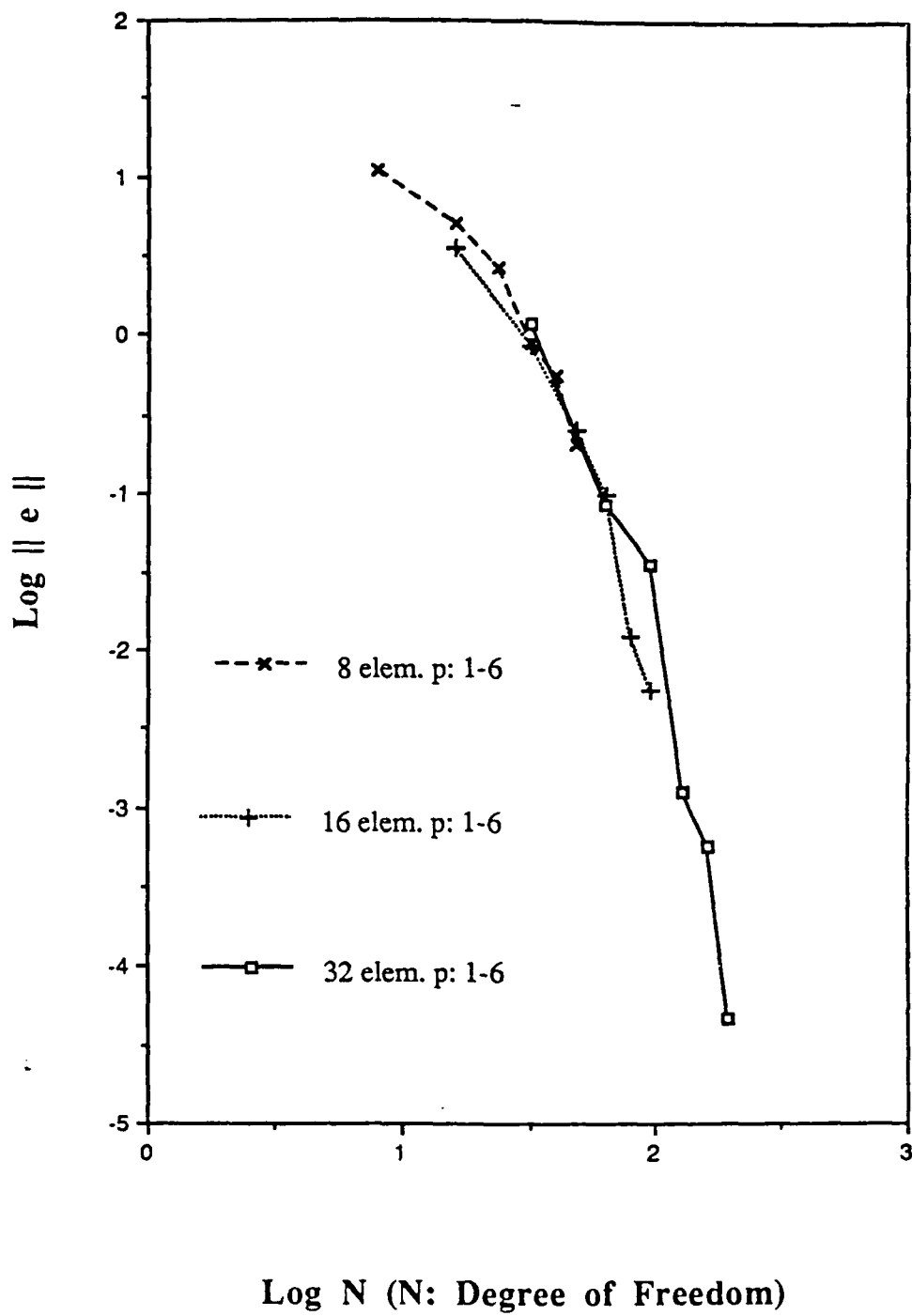Figure 16: Example 3. Experimental rates of convergence for uniform h-refinement ($p = 4$, 5, and 6).

Figure 17: Example 3. Experimental rates of convergence for uniform p-refinement.
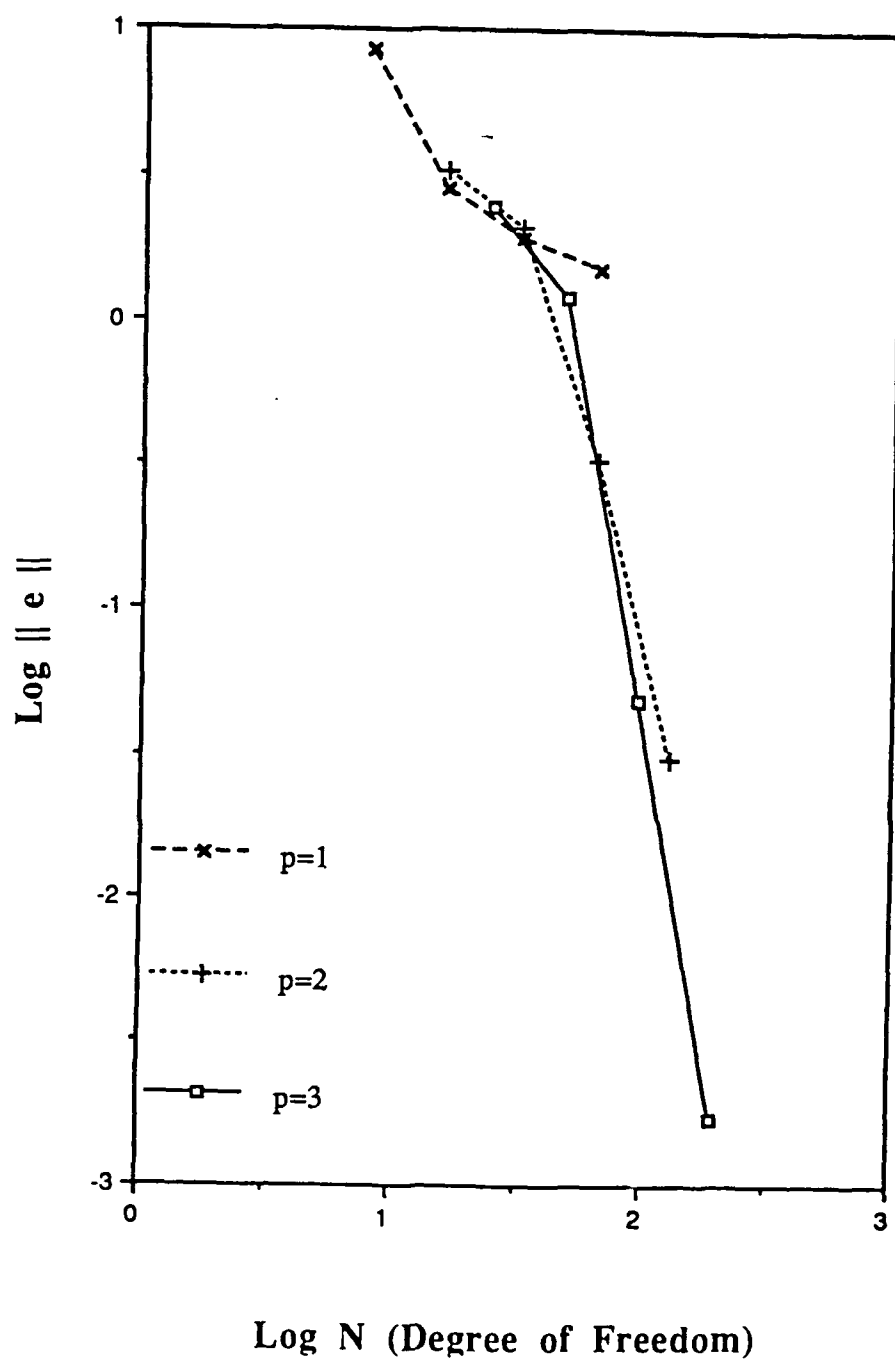
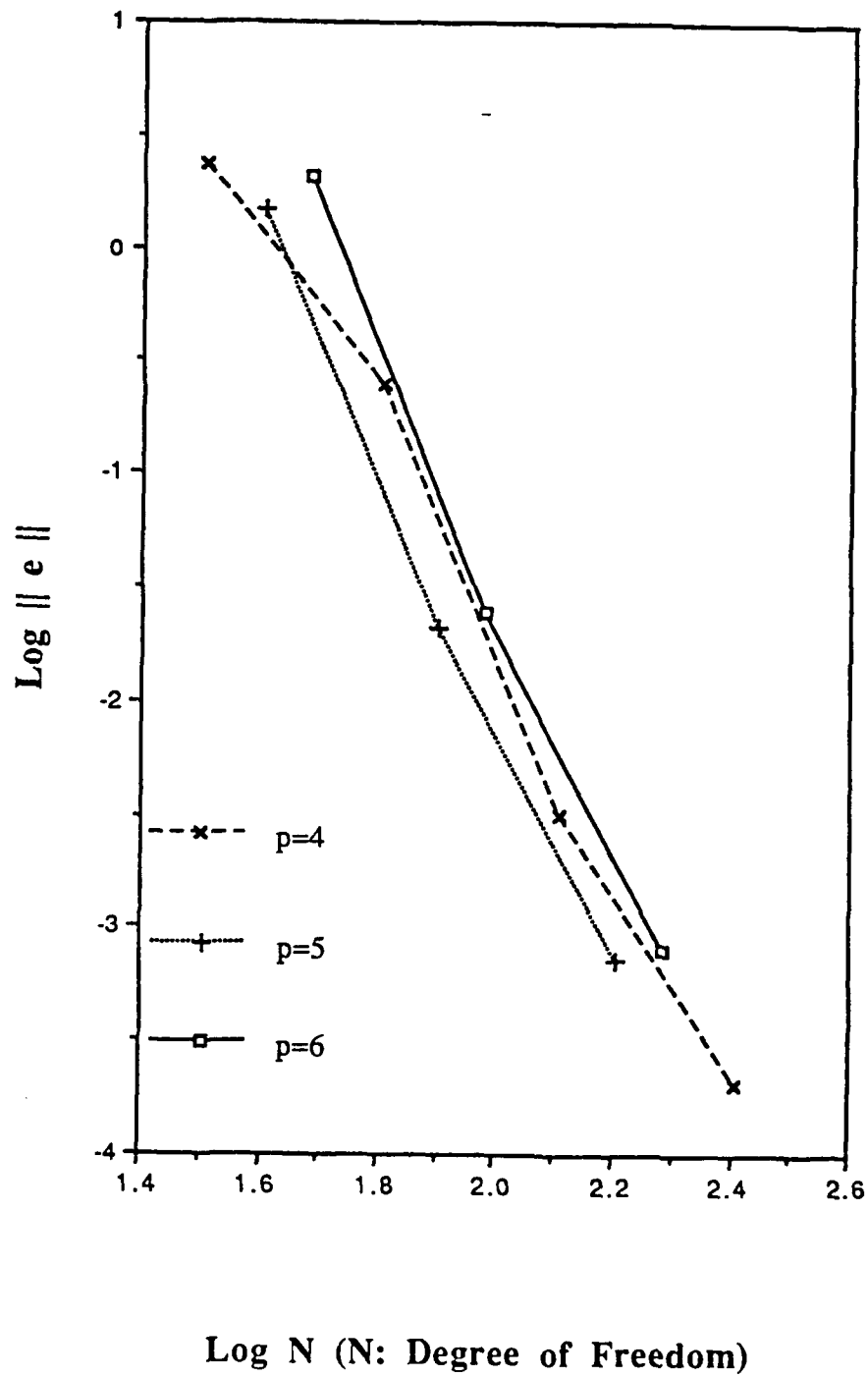Figure 18: Example 4. Experimental rates of convergence for uniform h-refinement ($p = 1$, 2, and 3).

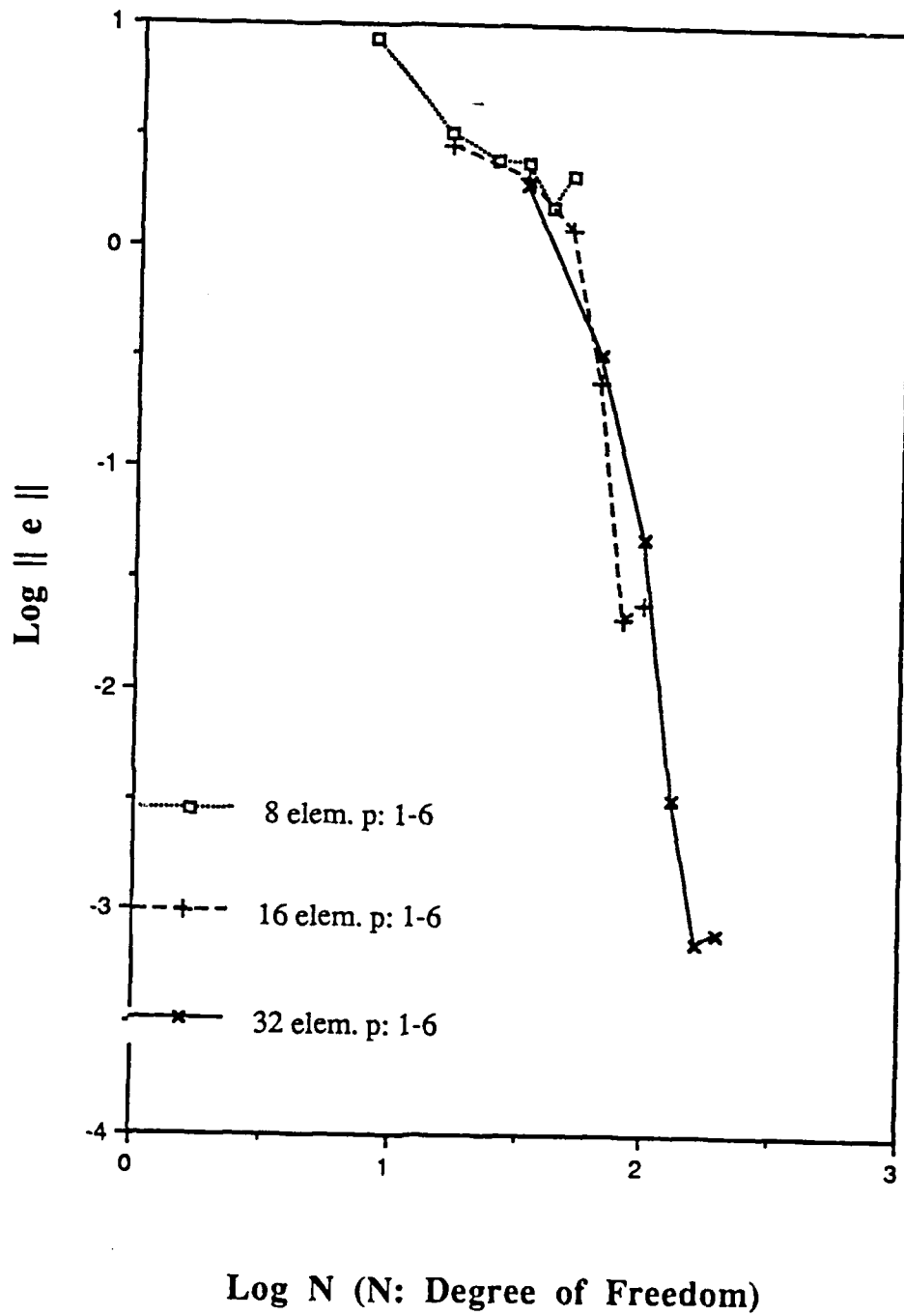Figure 19: Example 4. Experimental rates of convergence for uniform h-refinement ($p = 4$, 5, and 6).

Figure 20: Example 4. Experimental rates of convergence for uniform p-refinement.
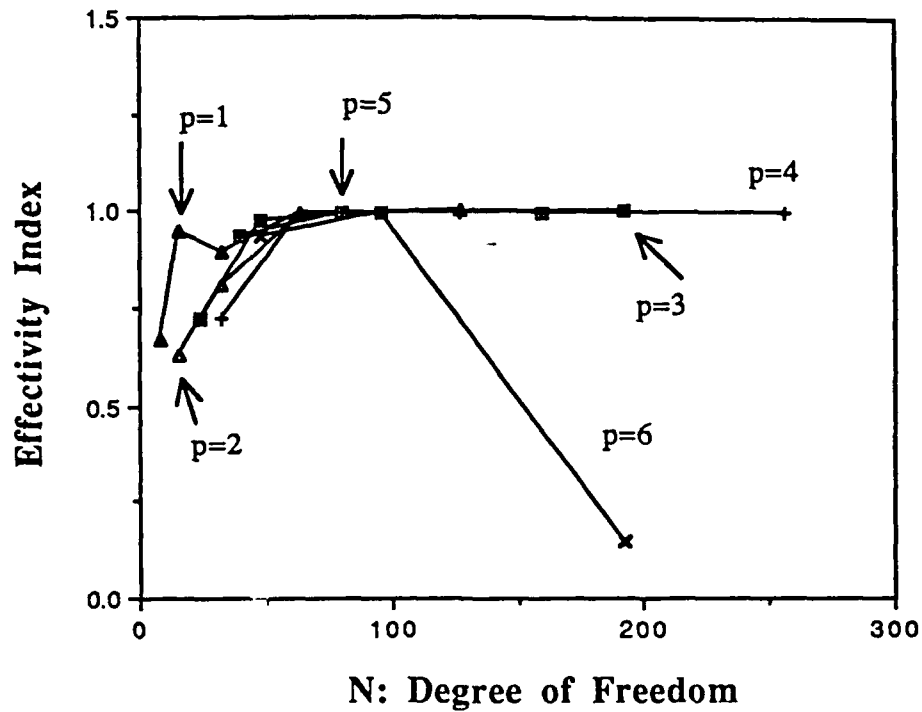
Figure 21: Example 5. Comparison of global L^2-errors with L^2-residual for the Helmholtz formulation ($k = 15$).
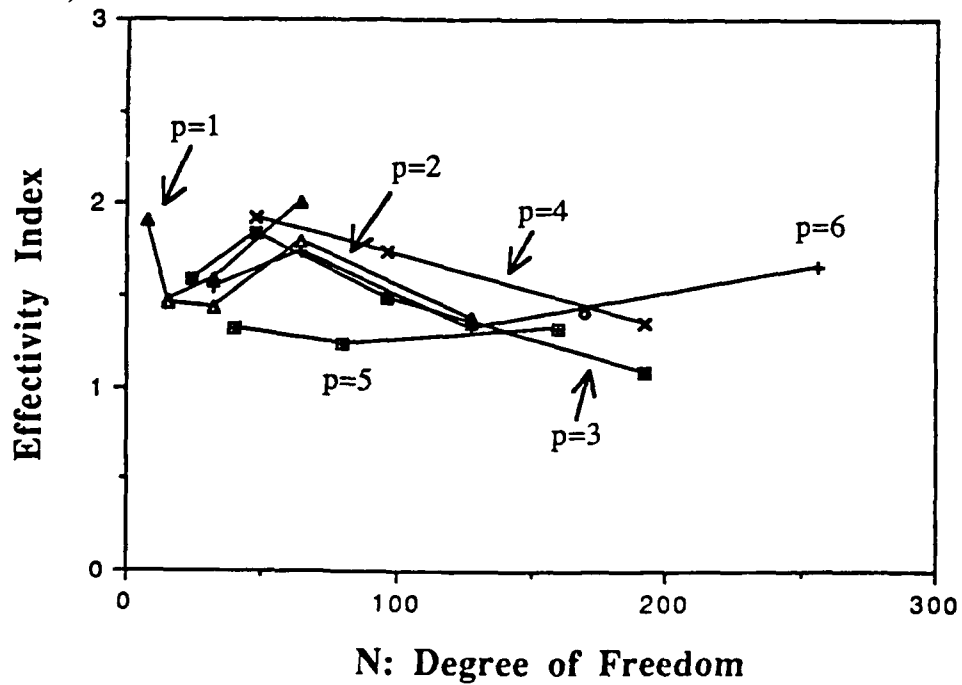

Figure 22: Example 5. Comparison of global L^2-errors with L^2-residual for the hypersingular formulation ($k = 15$).
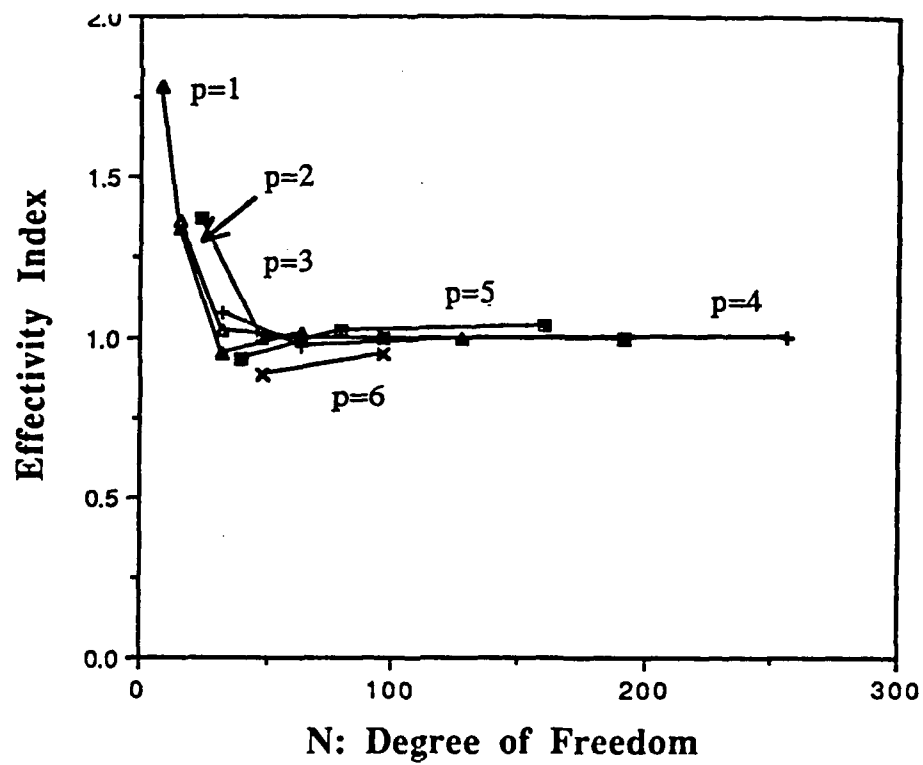
42

Figure 23: Example 5. Comparison of global L^2-errors with L^2-residual for the Burton-Miller formulation.
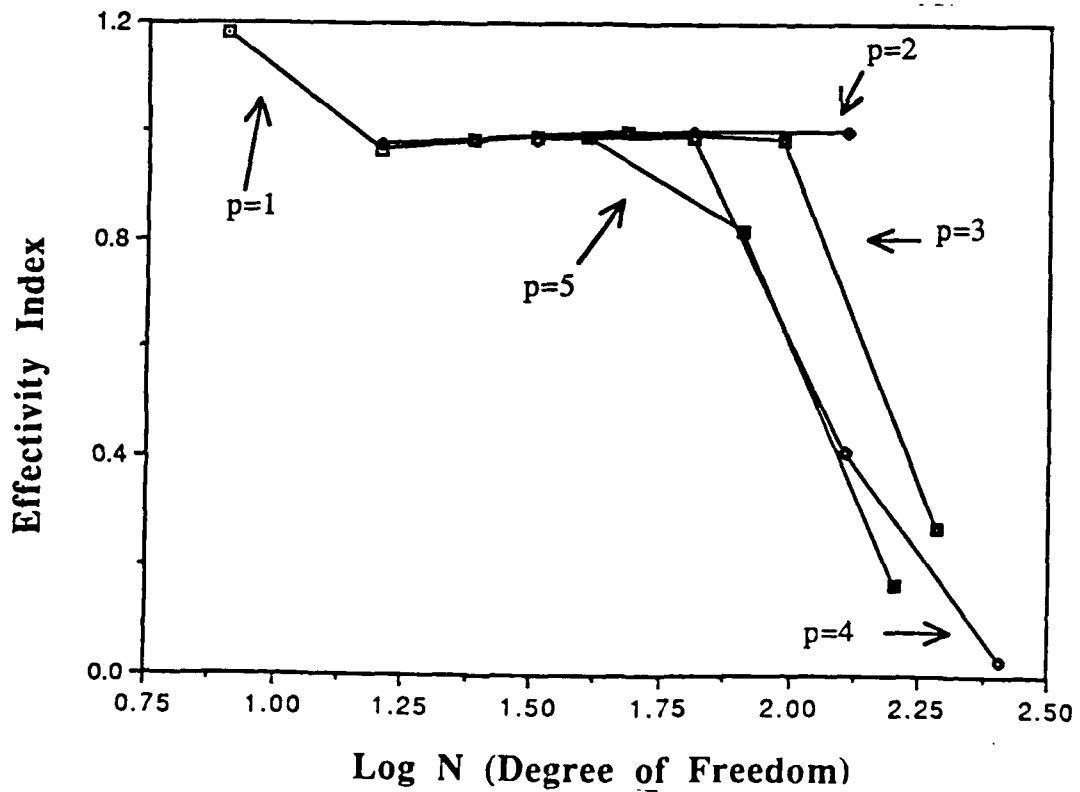
Figure 24: Example 5. Comparison of global L^2-errors with L^2-residual for the Burton-Miller formulation ($k = 15$).

43

Table 1: Example 6. Comparison of local L^2-errors and L^2-residuals for a mesh of 32 quadratic elements and Burton-Miller Formulation.

Elem. No.	$k = 5.1356$	$k = 15$
	Local Effectivity Index	
1	0.9928	1.0048
2	0.9991	0.9978
3	0.9976	1.0001
4	1.0017	0.9959
5	0.9974	1.0009
6	1.0004	0.9970
7	0.9999	0.9990
8	0.9968	1.0014
9	1.0035	0.9946
10	1.0104	0.9959
11	0.9996	1.0004
12	0.9905	0.9699
13	1.0118	0.9818
14	0.9820	1.0067
15	0.9890	0.9213
16	1.0138	1.0016
Global Effectivity Index		
0.9992	0.9963	

Appendix B

Adaptive Finite Element Methods For Hyperbolic Systems With Application to Transient Acoustics

Abstract

The solution of the hyperbolic systems of equations governing transient acoustics by adaptive finite elements and various finite difference time discretization schemes is addressed. Emphasis is placed on the use of a class of implicit Runge-Kutta methods for temporal approximations.

1 Introduction

This paper describes general high–order adaptive finite element methods for solving wave propagation problems characterized by hyperbolic systems of equations, with particular emphasis on problems of radiation and scattering in transient acoustics. Special features of the present analysis are numerated as follows:

1. We accept as a model of acoustic wave phenomena the full hyperbolic system of conservation laws derived from a perturbation analysis of the compressible Navier-Stokes equations. This is contrary to most approaches for acoustic modeling which are based on assumptions of a uniform background flow which renders these systems reducible to a problem in the frequency domain. The results for different frequencies must then be stored and then superimposed to solve the fully transient problem. In practice, this limits the application to cases in which, at most, a few hundred harmonics contribute to the solution.

   The use of the full transient formulation also provides a basis for considering the non-classical equations of acoustics resulting from the linearization of the compressible Euler equations around an *arbitrary* solution to the incompressible Euler equations. The resulting system of equations is still linear and hyperbolic but with variable coefficients depending on the back round, incompressible flow. The presence of space or time

varying coefficients renders inapplicable most of the classical methods (in particular, those designed for treating the reduction to the wave equation). Also, by generalizing the characterization of the flow that governed by the Navier-Stokes equations, viscous effects can be also included in this as well. Once the transient formulation is accepted, additional generalizations such as these can be easily incorporated into an existing code, making the whole approach very flexible.

2. We assume that the final discrete model is obtained by combining a time–discretization algorithm with an h-p FE discretization in space. In this sense the present work is a continuation of our study on h-p FE methods presented in [2,8,11]. Only *linear* time discretization schemes are considered, but both the method of lines and the method of discretization in time (see Section 3) are admitted in our formulation.

3. The study is directed towards designing fully automatic self-adaptive schemes with error control. The use of adaptive methods for wave propagation phenomens seems to be meaningful only for the class of problems with "short signal" propagation, where an initial disturbance moves throughout the domain but stays *local*, and therefore, requires only the addition of extra degrees of freedom locally. Several fundamental questions present themselves immediately:

   (a) *Space–Time Consistency:* For a given high–order h-p approximation, what particular time–discretization scheme should be selected? What are the desired properties of an optimal scheme, especially in the context of adaptive methods?

   (b) *Error Estimation:* Ideally, an error estimate should estimate errors resulting from discretization both in time and space variables. How can this be implemented into a practical analysis strategy?

   (c) *Adaptive Strategies:* What adaptive strategies are optimal? Should both h or p-refinements be used? Is there a need (and place) for h-p strategies?

   The study of hyperbolic systems using ideas of classical spectral theory, applied to acoustics, provides a general framework for addressing these questions and is used as a basis for the present investigation.

   The plan of the presentation is as follows. Following this introduction, we summarize the essential mathematical properties of the model in Section 2. Section 3 is devoted to a discussion of two main discretization concepts: the method of lines and the method of discretization in time. A study on implicit Runge-Kutta methods is presented in Section 4 and some preliminary results on adaptivity are given in Section 5.

2

2 Equations of Linear Acoustics—A Summary

We begin with a brief review of some fundamental mathematical results for the linear acoustics equations. For a detailed analysis of the subject, we refer to [6].

As a starting point, we record the conservation equations of isentropic, compressible inviscid flow in the form (see, e.g., [5, 7])

$$\left.\begin{aligned}
&\rho_{,t} + \left(\rho u_k\right)_{,k} = 0 \\[2mm]
&\rho\left(u_k + u_\ell u_{k,\ell}\right) + p_{,k} = 0 \\[2mm]
&p = A\rho^\gamma, \ A > 0, \ \gamma > 1, \ 1 \le k, \ \ell \le n = 2 \text{ or } 3
\end{aligned}\right\} \tag{2.1}$$

where ρ is the density, $\boldsymbol{u} = (u_k)$ the velocity vector (repeated indices are summed), p the pressure and the standard notation for differentiation is used ($\rho_{,t} = \partial\rho/\partial t$, $\rho_{,k} = \partial\rho/\partial x_k$, etc.).

Linearizing the equations around the equilibrium state

$$\rho = \rho_0 = \text{const}, \ \boldsymbol{u} = \boldsymbol{0} \tag{2.2}$$

and introducing the sound speed c_0 defined as

$$c_0^2 = \frac{dp}{d\rho}\left(\rho_0\right) \tag{2.3}$$

3

we arrive at the classical equations of linear acoustics in the form

$$\left.\begin{array}{rrll} \rho_{,t} & + & \rho_0 u_{k,k} & = & 0 \\[2mm] u_{k,t} & + & \dfrac{c_0^2}{\rho_0}\,\rho_{,k} & = & 0 \end{array}\right\}$$ (2.4)

where now ρ and u_k denote perburbations of density and velocity components from the equilibrium state. Introducing the perturbed pressure p defined by

$$p = c_0^2 \rho$$ (2.5)

we reformulate the equations in terms of pressure and velocity

$$\left.\begin{array}{rrll} p_{,t} & + & c_0^2\,\rho_0 u_{k,k} & = & 0 \\[2mm] u_{k,t} & + & \dfrac{1}{\rho_0}\,p_{,k} & = & 0 \end{array}\right\}$$ (2.6)

It is important to note that the entire linearization procedure can be performed around an arbitrary solution of the incompressible Euler equations resulting in the generalized equations of linear acoustics (see [7]).

Finally, introducing the nondimensional variables

$$x_k := \frac{x_k}{L}, \ t := \frac{tc_0}{L}, \ u_k := \frac{u_k}{c_0}, \ p := \frac{p}{c_0^2 \rho_0}$$ (2.7)

where L is a unit of length, we arrive at the nondimensional version of the equations in the form

$$\left\{\begin{array}{rrll} \boldsymbol{u}_{,t} & + & \mathbf{grad}\ p & = & \mathbf{0} \\[2mm] p_{,t} & + & div\ \boldsymbol{u} & = & 0 \end{array}\right.$$ (2.8)

Introducing the group variable $\boldsymbol{U} = (\boldsymbol{u}^T, p)^T$ and a (formal) operator A

$$A\boldsymbol{U} \stackrel{\text{def}}{=} -i \begin{pmatrix} \mathbf{0} & \mathbf{grad} \\[2mm] div & 0 \end{pmatrix} \begin{pmatrix} \boldsymbol{u} \\[2mm] p \end{pmatrix}$$ (2.9)

where i is the imaginary unit, we rewrite (2.8) in the abstract form,

$$\boldsymbol{U}_{,t} + iA\boldsymbol{U} = 0$$ (2.10)

Equations (2.10) are to be solved in a domain $\Omega \subset \mathbb{R}^n$, $n = 2, 3$. Typically, two particular cases are of interest:

4

- *interior* problems when Ω is bounded

- *exterior* problems when Ω is a complement of a bounded set

In both cases we restrict ourselves to two kinds of boundary conditions:

Case 1.   Kinematic boundary conditions (vibrating boundary)

$$u_n \stackrel{\text{def}}{=} \boldsymbol{u} \cdot \boldsymbol{n} = \hat{u}_n \qquad \text{on} \quad \Gamma_u \tag{2.11}$$

where $\boldsymbol{n}$ is the outward normal unit to the boundary and $\hat{u}_n$ is prescribed velocity of the vibrating boundary ("solid wall" if $\hat{u}_n = 0$).

Case 2.   Pressure boundary condition

$$p = \hat{p} \qquad \text{on} \quad \Gamma_p \tag{2.12}$$

where $\hat{p}$ is a prescribed pressure on Γ_p—part of the boundary ($\partial\Omega = \Gamma_u \cup \Gamma_p$, $\Gamma_u \cap \Gamma_p = \emptyset$). The initial boundary value problem is completed by specifying initial condition of the form

$$\boldsymbol{u} = \boldsymbol{u}_0 \text{ and } p = p_0 \quad \text{at} \quad t = 0 \tag{2.13}$$

or, equivalently,

$$\boldsymbol{U} = \boldsymbol{U}_0, \quad \text{where} \quad \boldsymbol{U}_0 = \left(\boldsymbol{u}_0^T, \ p_0\right)^T \tag{2.14}$$

In the case of homogeneous boundary conditions, the problem can be cast into the Hilbert space formulation as follows.

We introduce

- The Hilbert space

$$\boldsymbol{H} = \boldsymbol{L}^2(\Omega) \times L^2(\Omega) = \left(\prod_{j=1}^{n} L^2(\Omega)\right) \times L^2(\Omega)$$

- Operator $\boldsymbol{A} : \boldsymbol{H} \supset \boldsymbol{D(A)} \longrightarrow \boldsymbol{H}$

where the domain of $\boldsymbol{A}$, $\boldsymbol{D(A)}$, consists of all vectors $\boldsymbol{U} = (\boldsymbol{u}^T, p)^T$ such that

$$\begin{aligned} div \ \boldsymbol{u} \in L^2(\Omega) \quad &, \quad u_n = 0 \quad \text{on} \quad \Gamma_u \\ p \in H^1(\Omega) \quad &, \quad p = 0 \quad \text{on} \quad \Gamma_p \end{aligned} \tag{2.15}$$

Note that the boundary condition on p is satisfied in the sense of the trace theorem, whereas the boundary condition on $\boldsymbol{u}$ is interpreted in the sense of the generalized

Green's formula (comp., e.g., [13]). For that reason, the pressure boundary condition is classified as the *Dirichlet* boundary condition and the kinematic boundary condition as the *Neumann* boundary condition for operator A. Note also that the L^2-norm of the solution vector U can be interpreted as the total (mechanical) energy of the field.

Within the Hilbert space formalism, the initial boundary value problem can be reinterpreted as an abstract Cauchy problem for operator A:

$$
\begin{aligned}
U_{,t} + iAU &= 0 \quad t > 0 \\
U &= U_0 \quad t = 0
\end{aligned}
\tag{2.16}
$$

where $U_0 \in H$.

An H-valued function of time $U = U(t)$

$$
[0, \infty) \ni t \to U(t) \in H
$$

is called a *weak solution* to the Cauchy problem if $U(t)$ satisfies two conditions

(i) a regularity assumption

$$
U \in C([0, \infty) \; ; \; H)
\tag{2.17}
$$

(ii) a weak form of the equation given by

$$
\int_0^\infty \int_\Omega U^T \left(-\overline{\Phi}_{,t} + iA\overline{\Phi} \right) dx \, dt
$$
$$
- \int_\Omega U_0^T \overline{\Phi}(0, \cdot) dx = 0
\tag{2.18}
$$

for every test function

$$
\Phi \in C_0(\mathbb{R} \; ; \; D(A)) \cap C^1(\mathbb{R} \; ; \; H)
\tag{2.19}
$$

Note that this definition admits, in particular, solutions in the d'Alembert sense.

We record now some fundamental results concerning operator A and the existence and uniqueness of weak solutions U.

- Operator A is self–adjoint (in the complex sense) and therefore its spectrum lies on the real line and consists of a point spectrum (eigenvalues) and continuous spectrum (generalized eigenvalues) only.

6

- For the interior problems (Ω bounded), the spectrum of A consists only of eigenvalues symmetrically located on two parts of the real axis and "escaping" to infinity (A is unbounded)

$$\sigma(A) = \{0, \lambda_1, -\lambda_1, \lambda_2, -\lambda_2, \ldots\}$$
$$0 < \lambda_1 < \lambda_2 < \ldots < \lambda_n \to \infty$$

(2.20)

Except for the 0-eigenvalue, all eigenvalues are of finite multiplicity and the eigenvectors corresponding to λ_n and $-\lambda_n$ are complex conjugate to each other. All eigenspaces are orthogonal to each other.

- For the exterior problems, the discrete spectrum reduces to the single eigenvalue 0 while the rest of the real axis constitutes the continuous spectrum.

- In both cases, the eigenspace corresponding to zero eigenvalue, i.e., the null space of operator A, is of inifinite dimension and it contains all incompressible velocity fields. More precisely, it has the form

$$\mathcal{N}(A) = \left\{ \left(u^T, p\right)^T \in H : \, div \; u = 0 \right\}$$

(2.21)

where p is an arbitrary constant for Ω bounded and $\Gamma_p = \emptyset$ or $p = 0$ otherwise.

- In both cases, operator A admits a classical spectral decomposition. In the case of bounded Ω, it reduces to the series representation

$$AU = \sum_{i=-\infty}^{\infty} \lambda_i dP_i(U)$$

(2.22)

where dP_i is the orthogonal projection on the eigenspace corresponding to λ_i. For exterior problems,

$$AU = \int_{-\infty}^{\infty} \lambda dP_\lambda(U)$$

(2.23)

where the integral is understood in the Riemann-Stieltjes sense (see, e.g., [14]) and P_λ denotes the spectral family of A.

- A weak solution U exists and it is unique. Moreover, it is of the form

$$U(t) = e^{-iAt}U_0 \stackrel{\text{def}}{=} \int_{-\infty}^{\infty} e^{-i\lambda t} dP_\lambda(U_0)$$

(2.24)

where the integral reduces to the series representation for the interior problems and it is understood in the Riemann-Stieltjes sense for the exterior problems. From the form of the solution, it follows in particular that the energy is conserved

$$\|U(t)\| = \|U_0\| \qquad \forall \, t \geq 0$$

(2.25)

7

- If the initial condition function U_0 satisfies an additional regularity assumption

$$U_0 \in D(A) \tag{2.26}$$

then the solution $U \in C^1((0,\infty), H) \cap C((0,\infty), D(A))$. We say then that U is a *strict solution* to the problem.

3 Discretization

Any approximation of a transient problem must involve discretization both in time and space variables. Although a simultaneous discretization in all variables is possible (e.g., space–time finite elements), we will adopt the assumption here that the final approximation is obtained by using finite differences in time and finite elements in space variables.

Two different approaches are possible. In the classical *method of lines*, an approximation in space variables converts the original initial–boundary value problem into a system of ordinary differential equations (ODEs) which next is discretized in time using one of many time integration schemes for ODEs. An alternative procedure known as the *method of discretization in time* (also called the *Rothe's method*, see [12]), consists of the same two steps but done in the reverse order. By discretizing in time first, the initial–boundary value problem is converted into a sequence of boundary–value (–like) problems which, in turn, give a basis for a spatial approximation and, consequently, a fully discretized scheme.

Both procedures are symbolically depicted in Fig. 1. If A denotes the original operator, by A_h we mean its discrete counterpart obtained as a result of approximation in space performed first and $T(A_h)$ will denote a fully discrete transient operator resulting from the time discretization of the system of ODEs. In the notation we have restricted ourselves to one time step methods assuming that the approximate solution U_h^n at time level t_n is obtained using the solution U_h^{n-1}, from the previous time level, only. A more general situation is, of course, possible.

In Rothe's method the transient operator $T = T(A)$ is defined on the infinite-dimensional level and only an appropriate discretization in space, performed next, converts it into a fully discrete operator $T_h(A)$. Surprisingly enough, even if exactly the same approximation in time and space variables is used and even for linear equations like the acoustics problem, the two procedures *may* result in two *different* methods.

We proceed now with an example of such a situation. Assume that U is a strict solution to the problem. Taking (2.10) and multiplying both sides by the (complex conjugate of) a test function $V \in D(A)$ we arrive at the equivalent ($D(A)$ is dense in H) weak form of
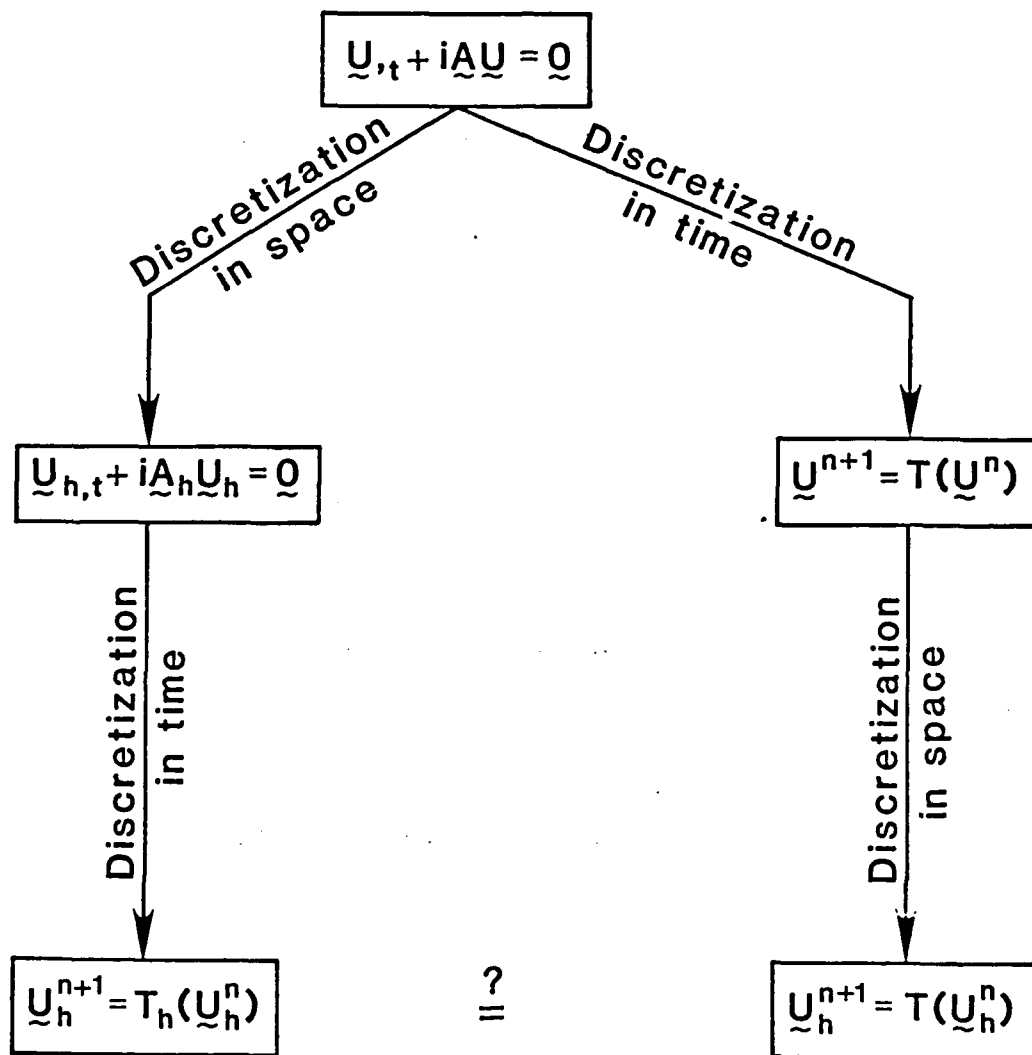
8

Figure 1: Method of lines and method of discretization in time—a comparison.

9

(2.10)

$$\frac{d}{dt}(U, V) + i(AU, V) = 0 \quad \forall \, V \in D(A) \tag{3.1}$$

Restricting ourselves now to a finite dimensional subspace X_h of $D(A)$, we can formulate the corresponding finite dimensional problem as

$$\frac{d}{dt}(U_h, V_h) + i(AU_h, V_h) = 0 \quad \forall \, V_h \in X_h \tag{3.2}$$

or equivalently

$$\frac{d}{dt}U_h + iA_hU_h = 0 \tag{3.3}$$

where the approximate operator $A_h : X_h \rightarrow X_h$ is defined as

$$A_h = P_h \circ A|_{X_h} \tag{3.4}$$

provided P_h denotes the orthogonal projection in H onto X_h. Note that the approximation A_h preserves the original properties of A, i.e., A_h is self–adjoint on the X_h,

$$(A_hU_h, V_h) = (U_h, A_hV_h) \quad \forall \, U_h, V_h \in X_h \tag{3.5}$$

The system of ODEs (3.3) has yet to be discretized in time. This can be done for instance by using the following finite difference formula of second order

$$U_h(t + \Delta t) - \alpha \, \frac{\Delta t^2}{2} \, U_{h,tt}(t + \Delta t)$$
$$= U_h(t) + \Delta t U_{h,t}(t) + (1 - \alpha)\frac{\Delta t^2}{2} \, U_{h,tt}(t) + 0(\Delta t^3) \tag{3.6}$$

Making use of (3.3) to replace the time derivatives with spatial derivatives and denoting by U_h^n the solution after n time steps Δt, we arrive at the final, fully discrete problem in the form

$$\left(I + \alpha \, \frac{\Delta t^2}{2} \, A_h^2\right) U_h^{n+1} = \left(I - i\Delta t A_h - (1 - \alpha) \, \frac{\Delta t^2}{2} \, A_h^2\right) U_h^n \tag{3.7}$$

Remarks:

1. Equation (3.7) does not require complex algebra computations. The complex setting is necessary to explore the self–adjointness of operators A, A_h in formal analysis, but does not enter the computations (contrary to frequency domain formulations, for instance).

10

2. Due to the self–adjointness of A_h, a stability analysis is immediately available. If $\lambda_1, \ldots, \lambda_N$ are the (real) eigenvalues of A_h and $\varphi_1, \ldots, \varphi_N$ are the corresponding eigenvectors (note that A_h has the same structure as operator A on bounded domains, i.e., the eigenvalues appear in pairs and the corresponding eigenvectors are complex conjugates of each other; see the discussion in the previous section) then (3.7) admits the usual orthogonal decomposition and for $U_h^n = \varphi_j$, we have $U_h^{n+1} = \mu_j \varphi_j$, where

$$\mu_j = \frac{1 - i(\Delta t \lambda_j) - \dfrac{1-\alpha}{2}(\Delta t \lambda_j)^2}{1 + \dfrac{\alpha}{2}(\Delta t \lambda_j)^2} \qquad (3.8)$$

Thus, even for an arbitrary FE mesh (particularly unstructured grids) it is possible to express the eigenvalues of the transient operator in terms of the eigenvalues of operator A_h.

3. A simple calculation reveals that

$$|\mu_j| \begin{cases} < 1 & \text{for} \quad \dfrac{1}{2} < \alpha \leq 1 \\[2ex] = 1 & \text{for} \quad \alpha = \dfrac{1}{2} \\[2ex] > 1 & \text{for} \quad 0 \leq \alpha < \dfrac{1}{2} \end{cases} \qquad (3.9)$$

Thus the method is *unconditionally stable* but dissipative for $\alpha > \frac{1}{2}$, stable and energy conserving (like the exact solution) for $\alpha = \frac{1}{2}$ and *unconditionally unstable* for $\alpha < \frac{1}{2}$.

4. Note finally that

$$\begin{aligned} \left(A_h^2 U_h, V_h\right) &= (P_h A P_h A U_h, V_h) \\ &= (A P_h A U_h, V_h) \\ &= (P_h A U_h, A V_h) \\ &\neq (A U_h, A V_h) \end{aligned} \qquad (3.10)$$

which implies that the solution of (3.7) in just one step would result in a fully populated stiffness matrix (due to the presence of the projection). A practical way to avoid such a situation is to use the decomposition

$$I + \alpha \, \frac{\Delta t^2}{2} \, A_h^2 = \left(I + i\,\sqrt{\frac{\alpha}{2}}\,\Delta t A_h\right)\left(I - i\,\sqrt{\frac{\alpha}{2}}\,\Delta t A_h\right) \qquad (3.11)$$

11

and obtain U_h^{n+1} in two steps:

$$U_h^{n+\frac{1}{2}} = \left(I - i\sqrt{\frac{\alpha}{2}}\,\Delta t A_h\right)^{-1}\left(I - i\Delta t A_h - (1-\alpha)\frac{\Delta t^2}{2}\,A_h^2\right)U_h^n$$

$$U_h^{n+1} = \left(I + i\sqrt{\frac{\alpha}{2}}\,\Delta t A_h\right)^{-1} U_h^{n+\frac{1}{2}}$$

(3.12)

A different situation arises when the method of discretization in time is used. Using the same discretization in time, we arrive first at the infinite–dimensional counterpart of (3.7),

$$\left(I + \alpha\,\frac{\Delta t^2}{2}\,A^2\right)U^{n+1} = \left(I - i\Delta t A - (1-\alpha)\,\frac{\Delta t^2}{2}\,A^2\right)U^n$$

(3.13)

Note that the use of (3.13) requires increased regularity of the initial data U^0 and consecutive step solutions U^n, as they must be elements of $D(A^2)$. This stringent assumption is avoided if we replace (3.13) with the *relaxed* variational version of the form

$$\left(U^{n+1}, V\right) + \alpha\,\frac{\Delta t^2}{2}\,\left(A U^{n+1}, A V\right)$$

$$= (U^n, V) - i\Delta t\,(A U^n, V) - (1-\alpha)\,\frac{\Delta t^2}{2}\,(A U^n, A V)$$

(3.14)

$$\forall\,V \in D(A)$$

as U^0 and U^n now must belong only to $D(A)$.

If this *relaxed* formulation (3.14) is adopted now as a basis for spatial approximation, we replace simply U and V with their finite dimensional counterparts U_h, $V_h \in X_h$ arriving at

$$\left(U_h^{n+1}, V_h\right) + \alpha\,\frac{\Delta t^2}{2}\,\left(A U_h^{n+1}, A V_h\right)$$

$$= (U_h^n, V_h) - i\Delta t\,(A U_h^n, V_h) - (1-\alpha)\,\frac{\Delta t^2}{2}\,(A U_h^n, A V_h)$$

(3.15)

$$\forall\,V_h \in X_h$$

One easily recognizes this as the well known Taylor-Galerkin method (see, e.g., [3]).

Obviously, equations (3.15) and (3.7), or equivalently (3.12), are different. The key point is the relaxation procedure performed at the infinite–dimensional level in the Taylor-Galerkin method formulation. Let us mention in particular (see [3] for proof) that (3.15) is unconditionally stable for $\alpha \geq \frac{1}{2}$ and conditionally stable $\alpha < \frac{1}{2}$. For *none* of these cases

12

is the method energy conserving. At the infinite–dimensional level the energy conservation takes place for $\alpha = \frac{1}{2}$. But even for this value of α, the relaxed formulation combined with the spatial approximation results in extra "diffusion" and eigenvalues decay in modulus as the "wave number" increases.

Finally, we emphasize that while in the method of lines the eigenvalues of the discrete transient operator were directly related to the eigenvalues of the discrete operator A_h, the eigenvalues of the transient operator resulting from (3.15) can only be related to the spectrum of transient operator corresponding to (3.14) which in turn can be represented in terms of spectrum of the orginal operator A.

This example suggests that as long as no relaxation predure is involved in the method of discretization in time, both procedures lead to the same discrete scheme. The class of implicit Runge-Kutta methods we address in the next section satisfies this assumption.

As a final remark, we note that when using the method of lines, other approximations of operator A are possible. In particular, upwinded methods will result in composing A with other, different projection operators. We do not address this subject in this paper.

4 Implicit Runge-Kutta Methods. Rational Approximations of the Exponential Function

Consider a general system of ordinary differential equations of the form

$$\dot{y} = f(y) \tag{4.1}$$

where y is a $1 \times N$ vector of unknowns and f is, in general, a nonlinear function of y. The implicit Runge-Kutta methods for solving (4.1) can be classified as one–step methods taking an n-th step solution y^n into y^{n+1} through s auxiliary stages Z_j, $j = 1, 2, \ldots, s$, called the *internal approximations*, in the following way

$$\begin{cases} Z_i & = & y^n + \Delta t \sum_{j=1}^{s} a_{ij} f(Z_j), \ i = 1, 2, \ldots, s \\ \\ y^{n+1} & = & y^n + \Delta t \sum_{j=1}^{s} b_j f(Z_j) \end{cases} \tag{4.2}$$

where $a_{ij}, b_j \in \mathbb{R}, i, j = 1, \ldots, s$. In general, determining y^{n+1} thus reduces to the solution of $N \times s$ nonlinear (or linear if the original system is linear) simultaneous algebraic equations. There are several good reasons for paying such a price, and high accuracy and good stability properties represent at least two of them. A complete discussion of the method in the context of ODEs can be found in [1].

13

Special cases are of interest. If $a_{ij} = 0$ for $j > i$, system (4.2) can be decoupled and reduces to the solution of s consecutive single equations for internal approximations $Z_1, \ldots, Z_s$. Schemes belonging to this subclass are known as *semi–implicit* methods.

Another closely related subclass of implicit Runge-Kutta methods of interest are the so–called *singly–implicit* methods, where the matrix of coefficients a_{ij} is *similar* to a lower triangular one. Reference to this class of schemes as singly–implicit refers to the fact that the coefficient matrix a_{ij} has only a single real s-fold eigenvalue. In implementation, methods of this type are as economical as the semi–implicit schemes.

Applying the approximation (4.2) to the Cauchy problem of linear acoustics, we arrive at the one–step calculations in the form

$$Z_k - \Delta t \sum_{j=1}^{s} a_{kj} i A Z_j = U^n, \quad k = 1, 2, \ldots, s$$

$$U^{n+1} = U^n + \Delta t \sum_{j=1}^{s} b_j i A Z_j$$

$$(4.3)$$

where Z_j, $j = 1, 2, \ldots, s$ are the intermediate internal approximations. As the variational formulation of (4.3) does not involve relaxation, both the classical method of lines and the method of discretization in time produce the same result and the spectral decomposition of the evolution operator is available both at infinite– and finite–dimensional levels. Substituting for U^n an eigenvector Φ of A and denoting by λ a corresponding eigenvalue of operator A, we arrive at the following system of equations for coefficients $d_j, j = 1, \ldots, s$

$$d_k - i(\lambda \Delta t) \sum_{j=1}^{s} a_{kj} d_j = 1 \quad k = 1, 2, \ldots, s \tag{4.4}$$

where $Z_k = d_k \Phi$, resulting in the formula for the growth factor E in the form

$$E = 1 + i(\lambda \Delta t) \sum_{j=1}^{s} b_j d_j \tag{4.5}$$

Solving (4.4) for $d_j, j = 1, \ldots, s$, we can represent them as rational functions of $(-i\lambda \Delta t)$ with coefficients depending upon the choice of matrix a_{kj}.

Consequently, the growth factor E can be represented as a rational function of $\lambda \Delta t$, too

$$E(-i\lambda t) = \frac{N(-i\lambda \Delta t)}{D(-i\lambda \Delta t)} \tag{4.6}$$

where N and D are polynomials. Note that in the case of *explicit* Runge-Kutta methods, (4.6) reduces to a polynomial representation.

14

Thus, all implicit Runge-Kutta methods, when applied to the acoustics equations, fall into the category of one–step methods corresponding to (4.6), resulting in the transient operator of the form

$$U^{n+1} = D(-i\Delta t A)^{-1} N(-i\Delta t A)U^n \qquad (4.7)$$

As polynomial D can always be decomposed into a product of linear factors (possibly with complex coefficients) the solution of (4.7) can always be reduced to the solution of s decoupled single equations. Thus, for the problems of interest, with the proper factorization of polynomial D, all implicit Runge-Kutta schemes can be reduced to the solution of s consecutive systems.

Finally, we note that combining some linear factors in D into quadratic terms and using the method of discretization in time, one can arrive at various relaxed schemes of the Taylor-Galerkin type discussed in the previous section.

We proceed now with the discussion of some particular cases.

Padé Approximations

Figure 2 reproduces (from [1]) a partial list of Padé polynomial approximations to the exponential function $\exp(x)$. Each of the approximations may correspond to a particular time discretization scheme of type (4.7). We can classify them into three groups:

(a) Schemes corresponding to the terms above the main diagonal (Gauss-Legendre methods). They are at most conditionally stable.

(b) Schemes corresponding to the main diagonal. They are all *unconditionally stable* and *energy conserving* as the fractions are all in modulus equal one. In particular, the second term on the diagonal corresponds to the Crank-Nicolson method of second order and the third to the two–stage Gauss-Legendre method of fourth order.

(c) Schemes corresponding to the terms below the diagonal. It can be shown ([1], p. 243) that all terms from the first two subdiagonals are bounded in modulus by one for all x for $Re\ x \le 0$. Schemes of this type are called A-stable. (Those corresponding to the first subdiagonal are known as Gauss-Radau and to the second one as Gauss-Lobatto schemes, respectively.) In our case, x is purely imaginary and, therefore, all these schemes are unconditionally stable. They are only slightly dissipative. Schemes corresponding to the third and further subdiagonals are not unconditionally stable ([1], p. 245).

Note that for all these schemes relaxes versions are possible.

15

Restricted Padé Approximations

The function

$$r(z) = \frac{P(z/\gamma)}{(1 - z/\gamma)^s} \qquad (4.8)$$

where P is a polynomial of degree m, is called a *restricted Padé approximation* to the exponential function if

$$|r(z) - \exp(z)| = 0(z^{m+1}) \qquad (4.9)$$

In practice, $m = s - 1$, s, $s + 1$. Schemes corresponding to (4.8) are called *singly–implicit*. They are especially attractive as the solution of one step requires only one matrix inversion and $s - 1$ resolutions. It can be proved ([1], p. 247) that

$$r(\gamma z) = \frac{(-1)^s \sum_{j=0}^{m} L_s^{(s-j)}(\gamma) z^j}{(1 - z)^s} \qquad (4.10)$$

where L_s are the Laguerre polynomials of order s. The choice of pole γ is somehow arbitrary. One can show, for example, that for $m = s$ and $s = 1, 2, \ldots, 6$ and 8 the pole γ can be selected in such a way as to render the unconditional stability (equivalent to A stability in this case); for $s = 7, 9, 10, \ldots$, such a choice is impossible. For a summary of results, we refer once again to [1].

Numerical Examples

We conclude this section with a series of experiments comparing the behavior of various time discretization schemes falling into the categories discussed on a model problem depicted in Fig. 3.

Each of the time–integration schemes is combined with a particular uniform h-p approximation in space variables (see [2] for details). For each of the cases, the calculated pressure component is plotted at time $t = 2.0$. Additional graphs provide an insight into dissipative properties of a scheme, showing the variation of the growth factor and phase as functions of $\lambda \Delta t$ (the range from 0 to π, corresponding to the classical von Neumann analysis, is assumed). For comparison, the exact pressure component solution is shown in Fig. 4.

The following abbreviations are used throughout the text

16

1	$\dfrac{1+x}{1}$	$\dfrac{2+2x+x^2}{2}$	$\dfrac{6+6x+3x^2+x^3}{6}$
$\dfrac{1}{1-x}$	$\dfrac{2+x}{2-x}$	$\dfrac{6+4x+x^2}{6-2x}$	$\dfrac{24+18x+6x^2+x^3}{24-6x}$
$\dfrac{2}{2-2x+x^2}$	$\dfrac{6+2x}{6-4x+x^2}$	$\dfrac{12+6x+x^2}{12-6x+x^2}$	$\dfrac{60+36x+9x^2+x^3}{60-24x+3x^2}$
$\dfrac{6}{6-6x+3x^2-x^3}$	$\dfrac{24+6x}{24-18x+6x^2-x^3}$	$\dfrac{60+24x+3x^2}{60-36x+9x^2-x^3}$	$\dfrac{120+60x+12x^2+x^3}{120-60x+12x^2-x^3}$
$\dfrac{24}{24-24x+12x^2-4x^3+x^4}$	$\dfrac{120+24x}{120-96x+36x^2-8x^3+x^4}$	$\dfrac{360+120x+12x^2}{360-240x+72x^2-12x^3+x^4}$	$\dfrac{840+360x+60x^2+4x^3}{840-480x+120x^2-16x^3+x^4}$
$\dfrac{120}{120-120x+60x^2-20x^3+5x^4-x^5}$	$\dfrac{720+120x}{720-600x+240x^2-60x^3+10x^4-x^5}$	$\dfrac{2520+720x+60x^2}{2520-1800x+600x^2-120x^3+15x^4-x^5}$	$\dfrac{6720+2520x+360x^2+20x^3}{6720-4200x+1200x^2-200x^3+20x^4-x^5}$
$\dfrac{720}{720-720x+360x^2-120x^3+30x^4-6x^5+x^6}$	$\dfrac{5040+720x}{5040-4320x+1800x^2-480x^3+90x^4-12x^5+x^6}$	$\dfrac{20160+5040x+360x^2}{20160-15120x+5400x^2-1200x^3+180x^4-18x^5+x^6}$	$\dfrac{60480+20160x+2520x^2+120x^3}{60480-40320x+12600x^2-2400x^3+300x^4-24x^5+x^6}$

Figure 2: Padé approximations to $\exp(x)$.
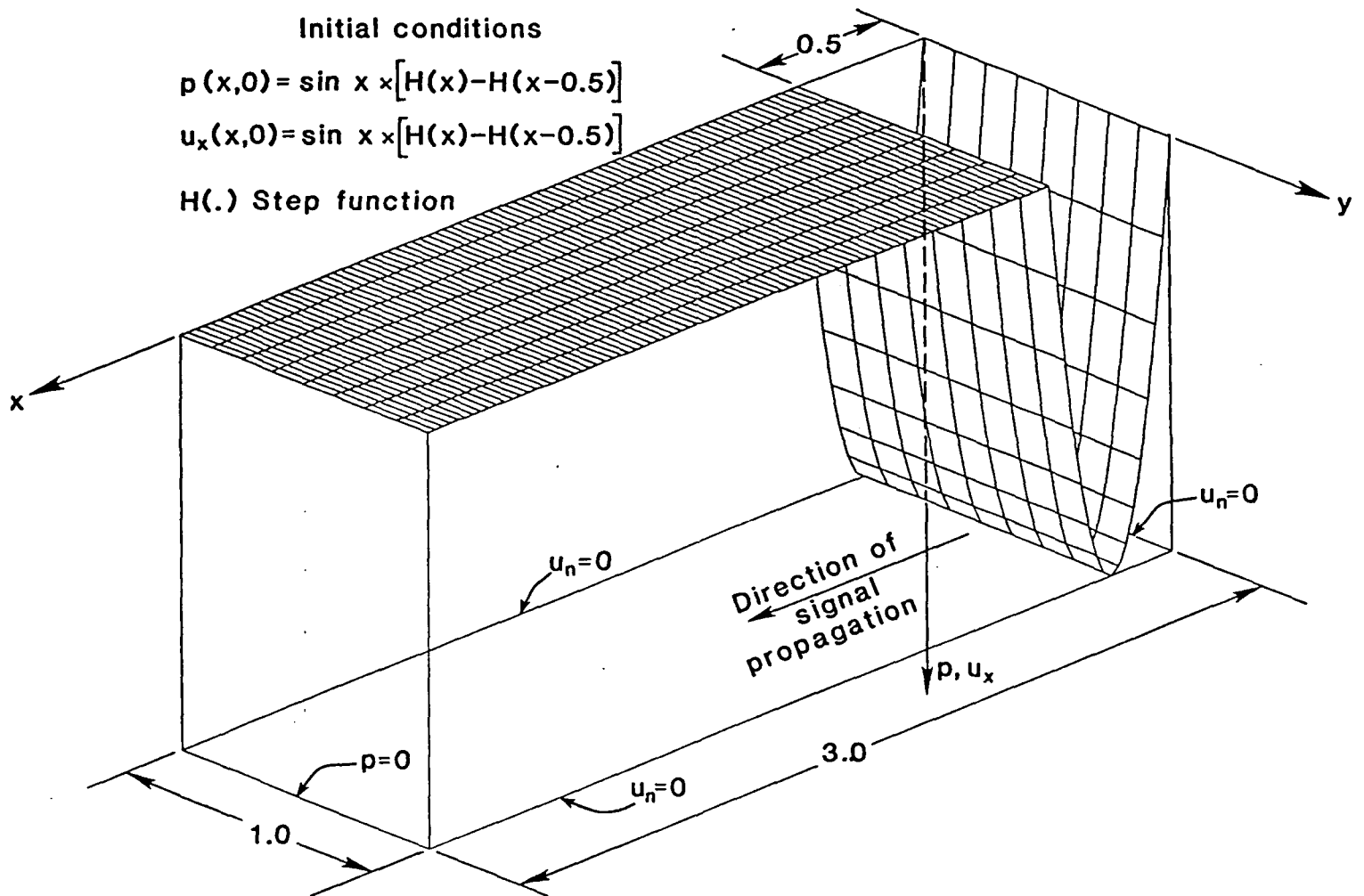
Figure 3: Test problem definition (geometry, boundary, and initial conditions).

18

SIRK (s, m)	=	s-stage, m-th order Singly Implicit Runge-Kutta Method;
GAUSS-LEGENDRE (s, m)	=	s-stage, m-th order Implicit Runge-Kutta Method based on Gauss-Legendre quadrature;
RADAU (s, m)	=	s-stage, m-th order Implicit Runge-Kutta Method based on Gauss-Radau quadrature (designated as Radau IA in [1]);
LOBATTO (s, m)	=	s-stage, m-th order Implicit Runge-Kutta Method based on Gauss-Lobatto quadrature (designated as Lobatto IIIC in [1]).

Test 1—comparison of various schemes on a uniform mesh of quadratic elements.

The first test compares performance of various time stepping schemes with a fixed time step $\Delta t = 0.0625$ combined with a fixed uniform mesh of quadratic elements shown in Fig. 5. (Element size $h = 0.125$, order of approximation $p = 2$.) Note that the combination $\Delta t - h$ corresponds to two time steps per element

Several schemes, including CRANK-NICHOLSON, TAYLOR-GALERKIN and different versions of SIRK, GAUSS-LEGENDRE, RADAU and LOBATTO were investigated. Some of the results are depicted in Figs. 6–13.

The following observations can be made:

1. Energy dissipating schemes (RADAU, LOBATTO, SIRK, TAYLOR-GALERKIN) give less oscillatory results than the energy conserving schemes (CRANK-NICHOLSON, GAUSS-LEGENDRE), and, therefore, should be preferred.

2. The energy dissipating schemes tested (RADAU, LOBATTO, SIRK) give comparable results. Consequently, SIRK schemes should be preferred because of their low cost compared with the RADAU and LOBATTO schemes.

3. As expected, it is inappropriate to combine high order time stepping schemes with low order spatial approximation. Increasing the order of approximation in time does not improve the results and, e.g., SIRK (5,5) gives even more oscillatory results than SIRK (4,4).

Finally, we mention that several schemes belonging to the class of *Linear Multistep Methods* have also been tested, including the *Method Based on Five–Eight Rules*, the *Adams-Moulton Method*, and *Gear's Backward Difference Schemes* (see [1] for details). Of those, all schemes of order greater than 2 proved to be unstable when applied to the test problem.

19
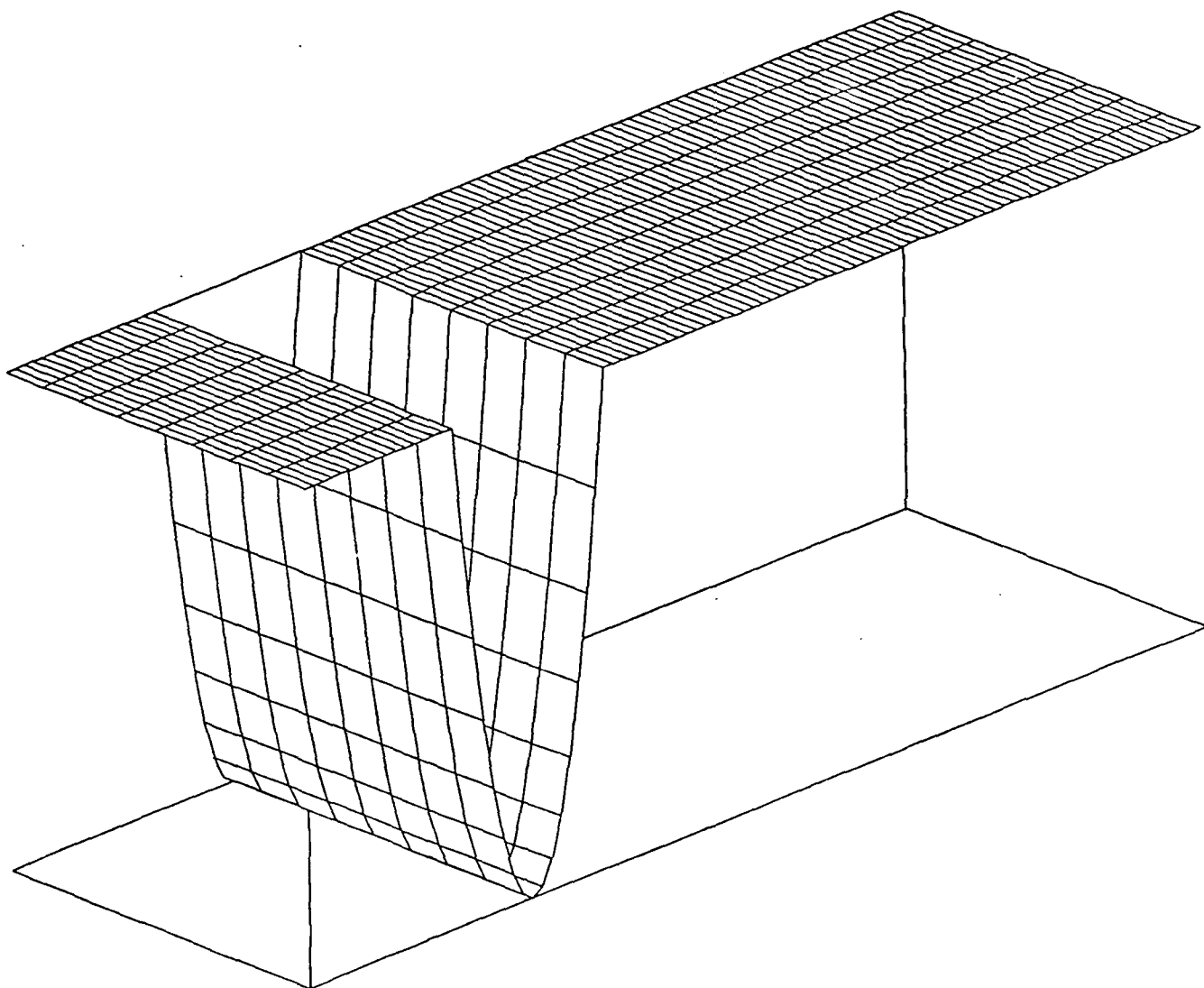
Figure 4: Test problem. Exact solution at $t = 2.0$.
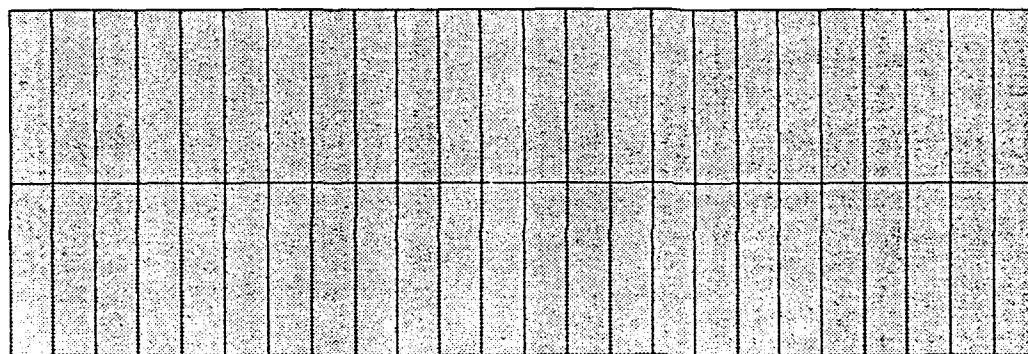
Figure 5: Test 1. An h-p FE mesh, $h = 0.125$. $p = 2$.
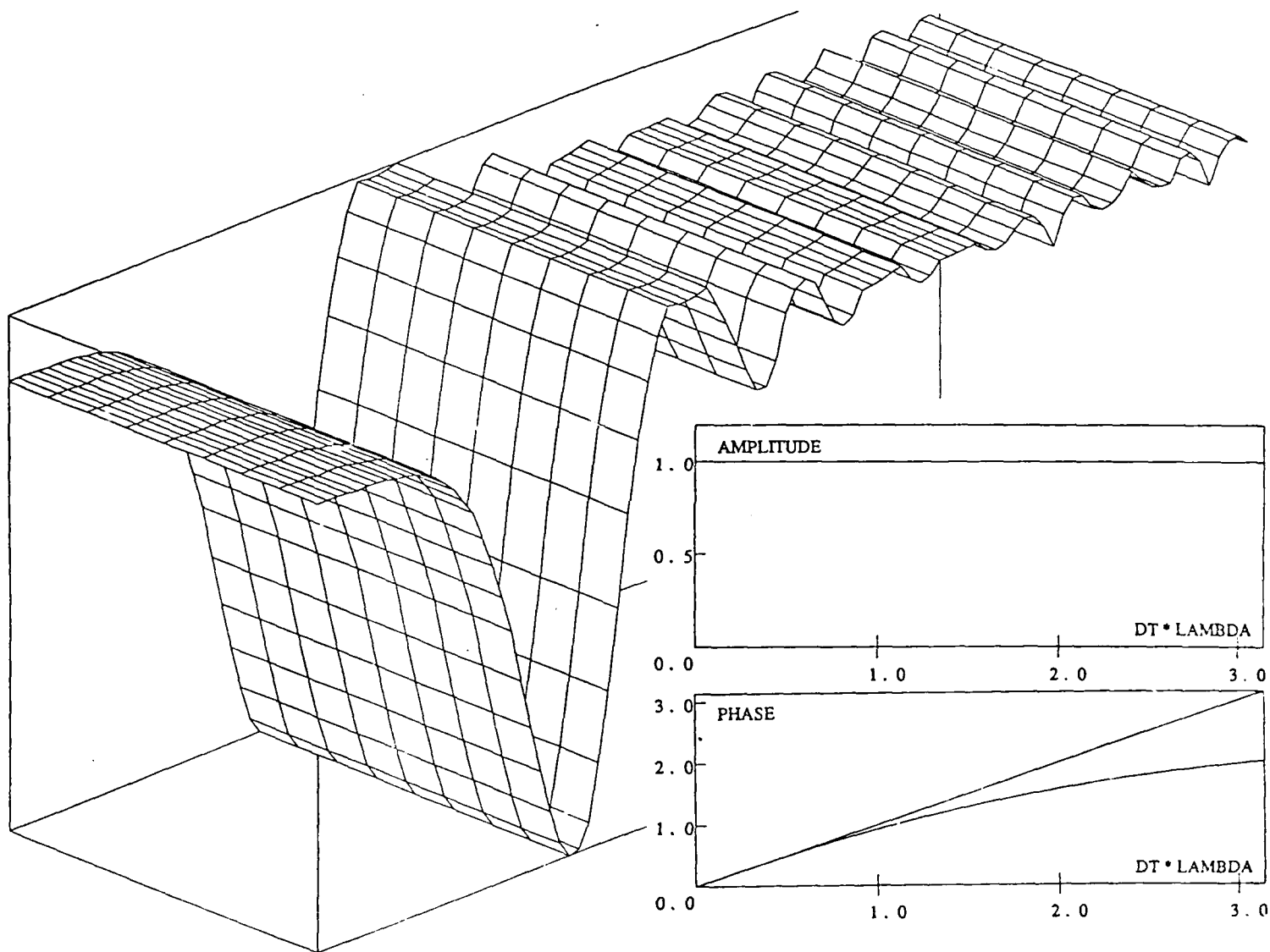
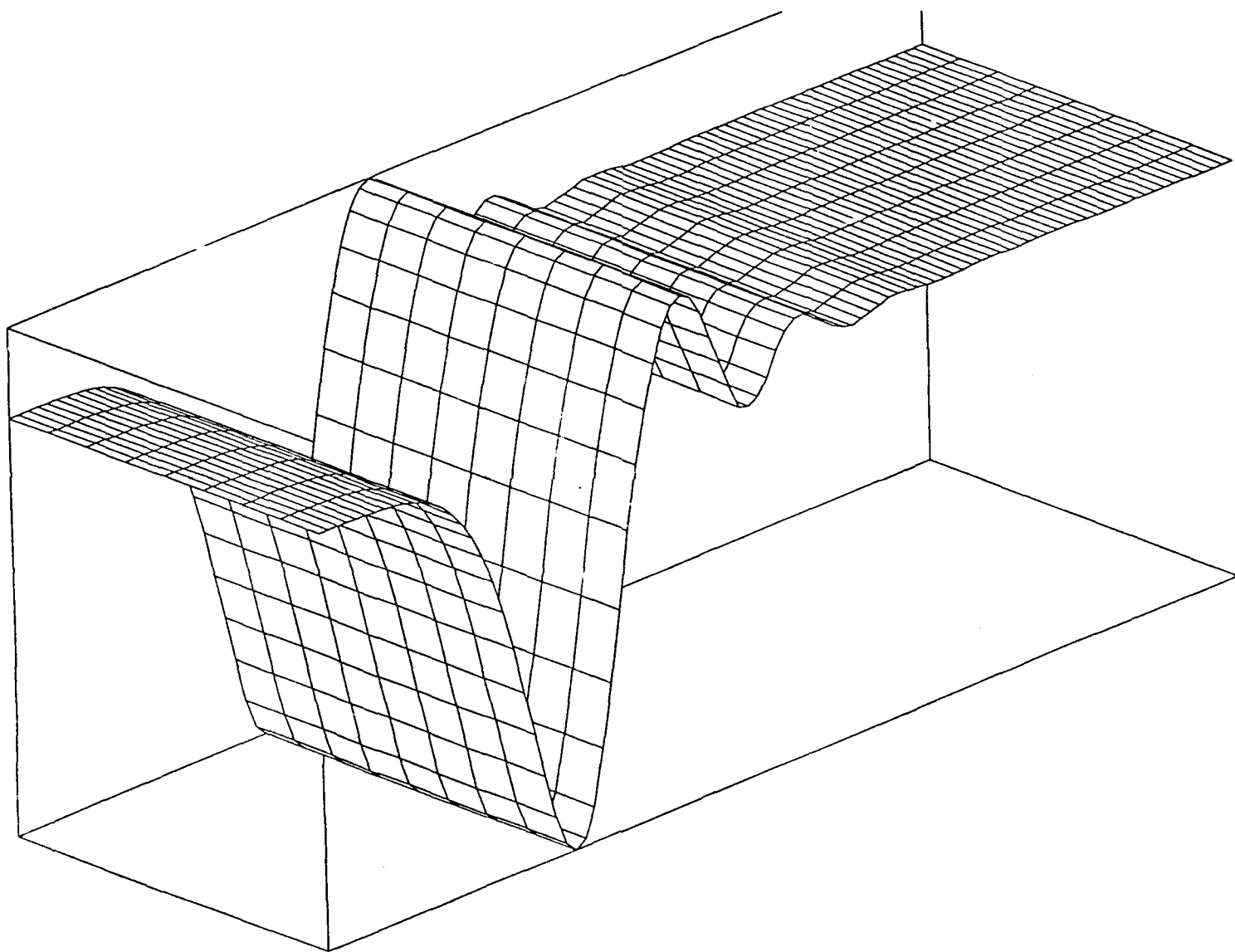Figure 6: Test 1. CRANK-NICHOLSON scheme, $\Delta t = 0.0625$, $h = 0.125$, $p = 2$.

Figure 7: TAYLOR-GALERKIN scheme, $\alpha = \frac{1}{2}$, $\Delta t = 0.0625$, $h = 0.125$, $p = 2$.
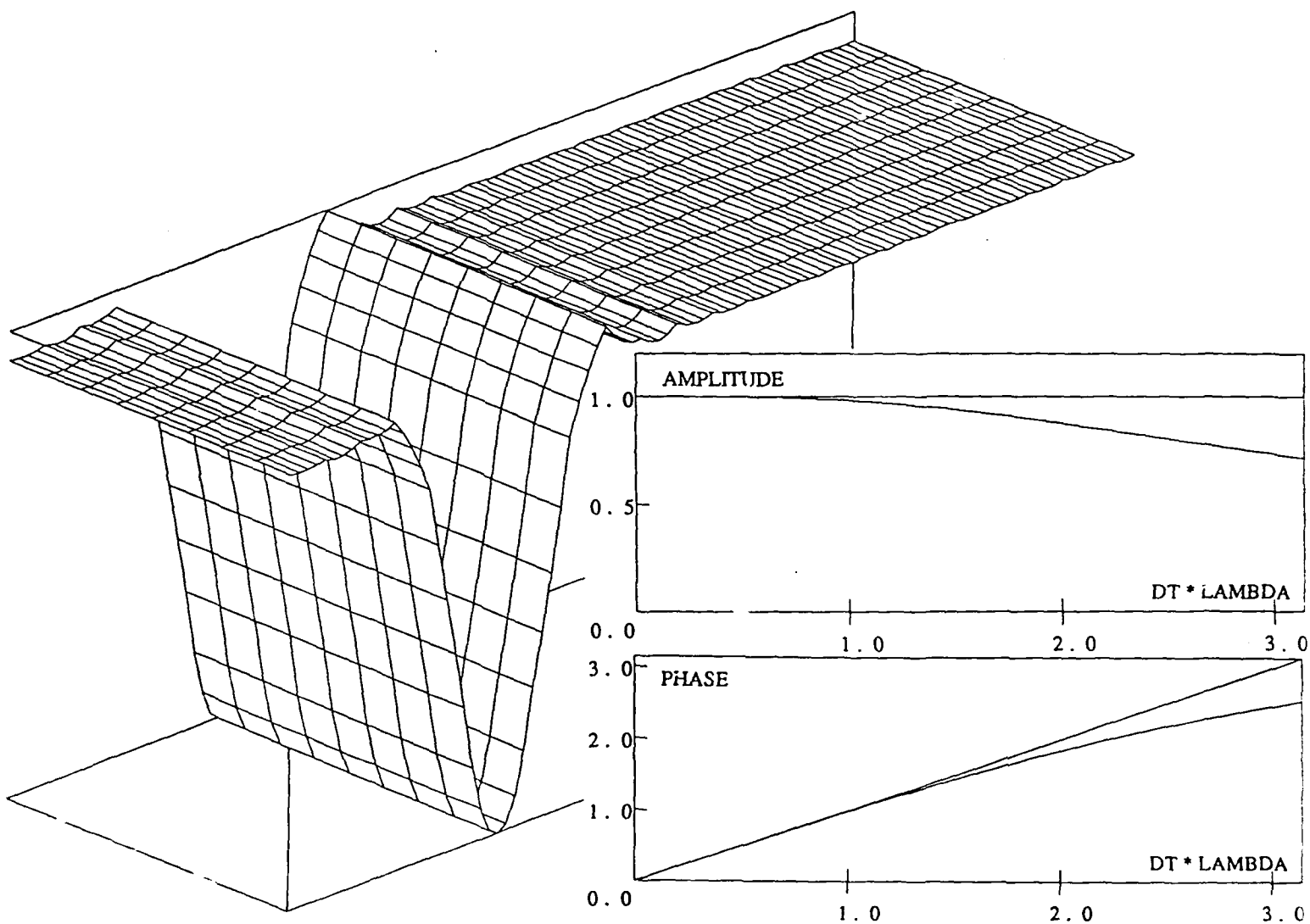
23

AMPLITUDE

1. 0

0. 5

0. 0

DT * LAMBDA

1. 0   2. 0   3. 0

3. 0   PHASE

2. 0

1. 0

0. 0

DT * LAMBDA

1. 0   2. 0   3. 0

Figure 8: Test 1. SIRK (3,3) scheme, $\Delta = 0.0625$, $h = 0.125$, $p = 2$.

24
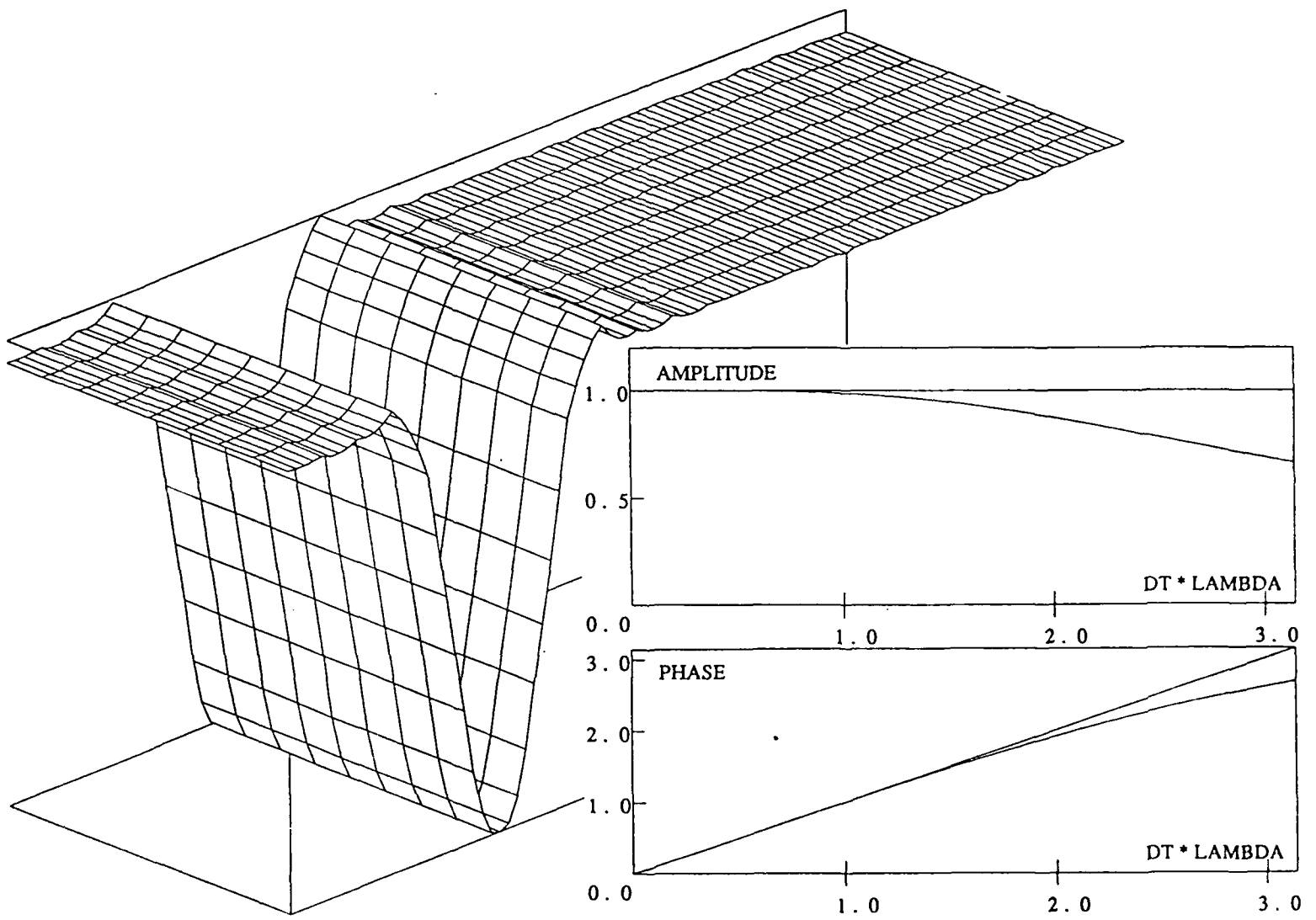
Figure 9: Test 1. RADAU (2,3) scheme. $\Delta t = 0.0625$, $h = 0.125$, $p = 2$.
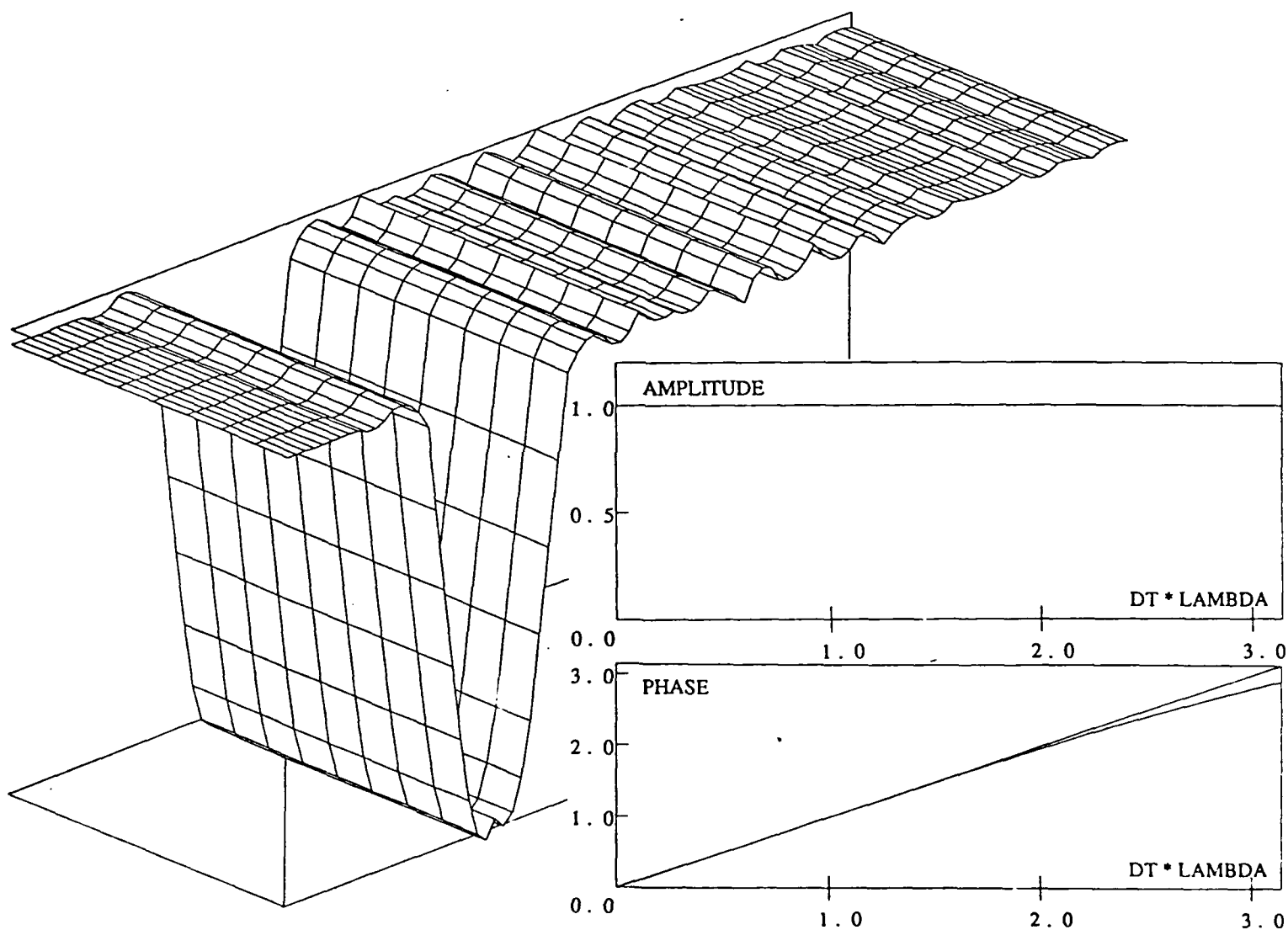
Figure 10: Test 1. GAUSS-LEGENDRE (2.4) scheme, $\Delta t = 0.0625$, $h = 0.125$, $p = 2$.
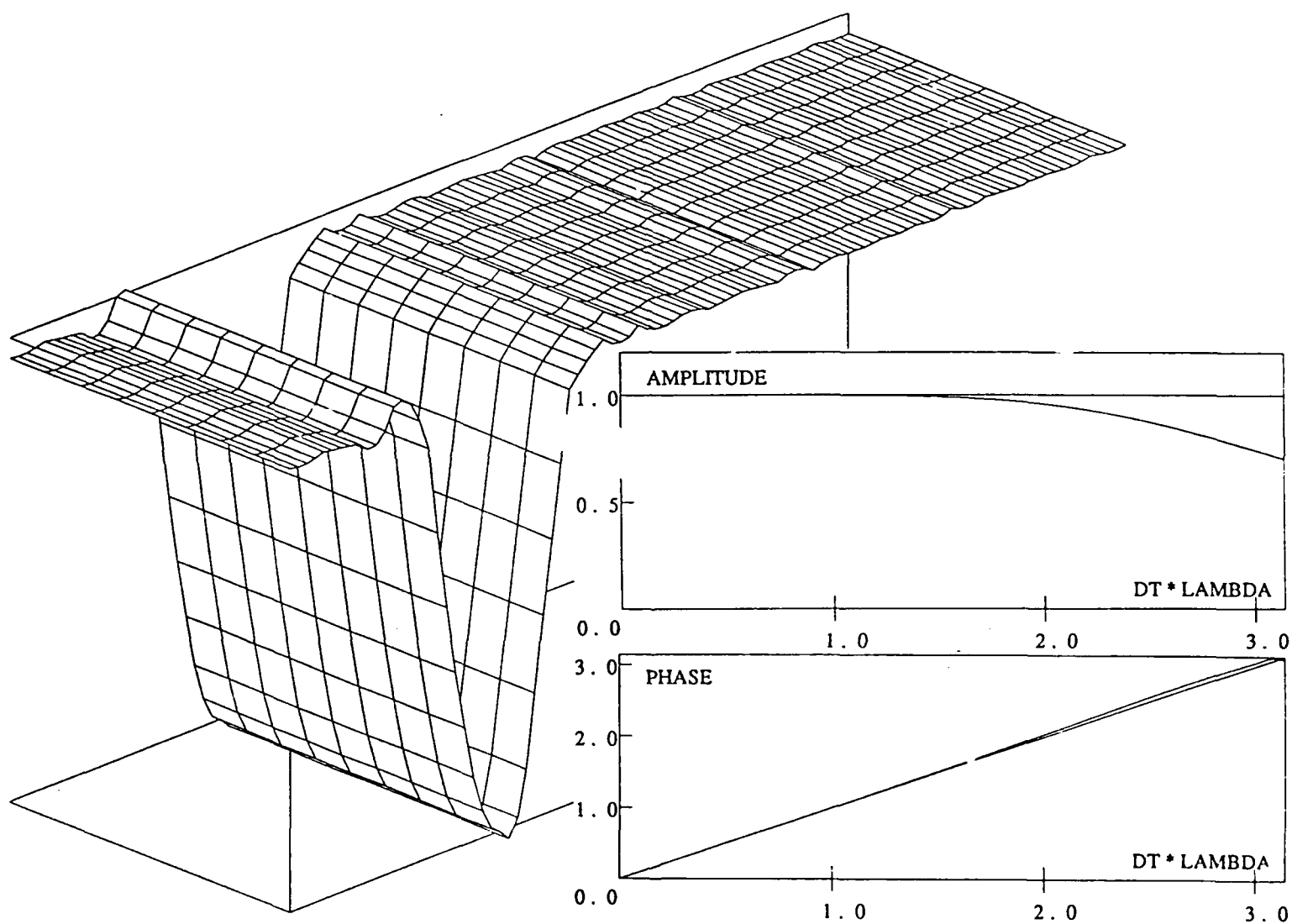
Figure 11: Test 1. LOBATTO (3,4) scheme. $\Delta t = 0.0625$, $h = 0.125$, $p = 2$.
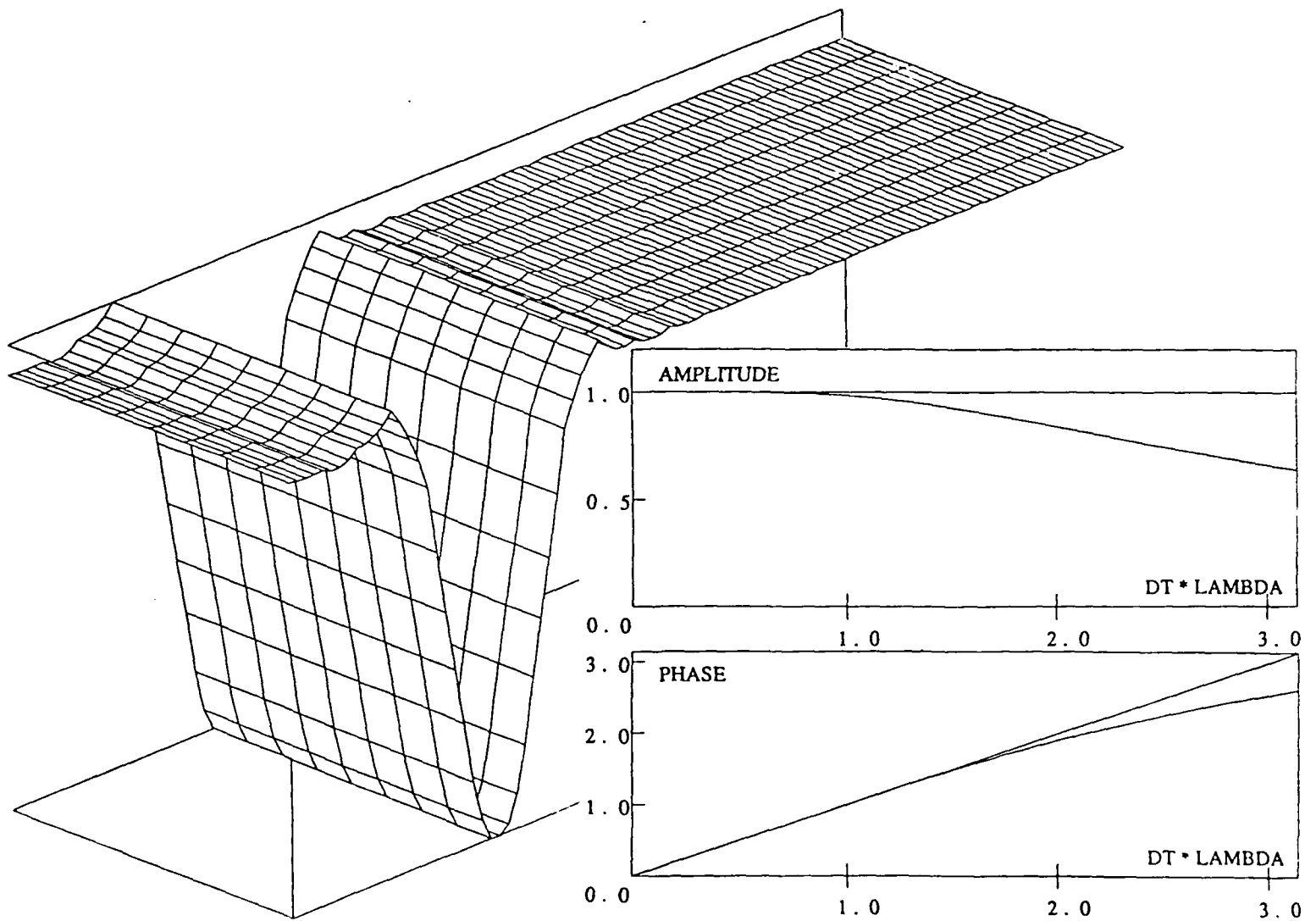
Figure 12: Test 1. SIRK (4,4) scheme, $\Delta t = 0.0625$, $h = 0.125$, $p = 2$.

Test 2-Comparison of SIRK schemes.

As the *SIRK* schemes were judged to yield the most promising results in the first test. the objective of the second test was to compare the performance of SIRK $(s, s+1)$ with that of SIRK (s, s). This time a uniform FE mesh of cubic elements, shown in Fig. 14. was used. The results for SIRK (3,4) and SIRK (4,4) are shown in Fig. 15 and Fig. 16. respectively. As can be seen, SIRK (4,4) produces better results than SIRK (3.4).

Test 3—Comparison of SIRK (s, s) schemes combined with different p-order FE meshes.

In the last test, an attempt was made to find an optimal combination of the order of time stepping SIRK (s, s) scheme and the spectral order p of spatial FE approximation. A uniform FE mesh with $h = 0.125$ and various orders of approximation $p = 4, 5, 6, 7$ was used. The results for various combinations of SIRK (s, s) schemes and different p's are shown in Figs. 17 to 25. It seems that for the optimal combination one should select $p = s - 1$. As expected, the test results are obtained with the highest order of approximation, namely for SIRK (8,8) combined with $p = 7$.

5   Adaptivity

We conclude this paper with some initial results on adaptivity using the Taylor-Galerkin scheme with $\alpha = \frac{1}{2}$ discussed in Section 3.

Error Estimation

The temporal discretization error has been neglected whereas the error due to the spatial approximation is estimated using the element residual method in the form (comp. [8, 9,])

$$\|U_{h,p} - U_{h,p+1}\|_{E,\Omega} \le \left(\sum_K \eta_K^2\right)^{\frac{1}{2}} \tag{5.1}$$

where

- $U_{h,p}$ is the approximate solution at some time level corresponding to elements of order p.

- $\| \cdot \|_{E,\Omega}$ is the global "energy" norm defined as

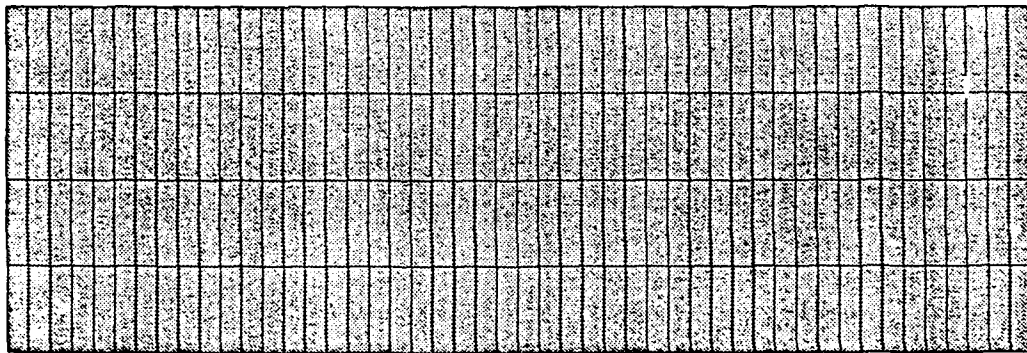$$\|U\|_{E,\Omega}^2 = B(U, U) \tag{5.2}$$
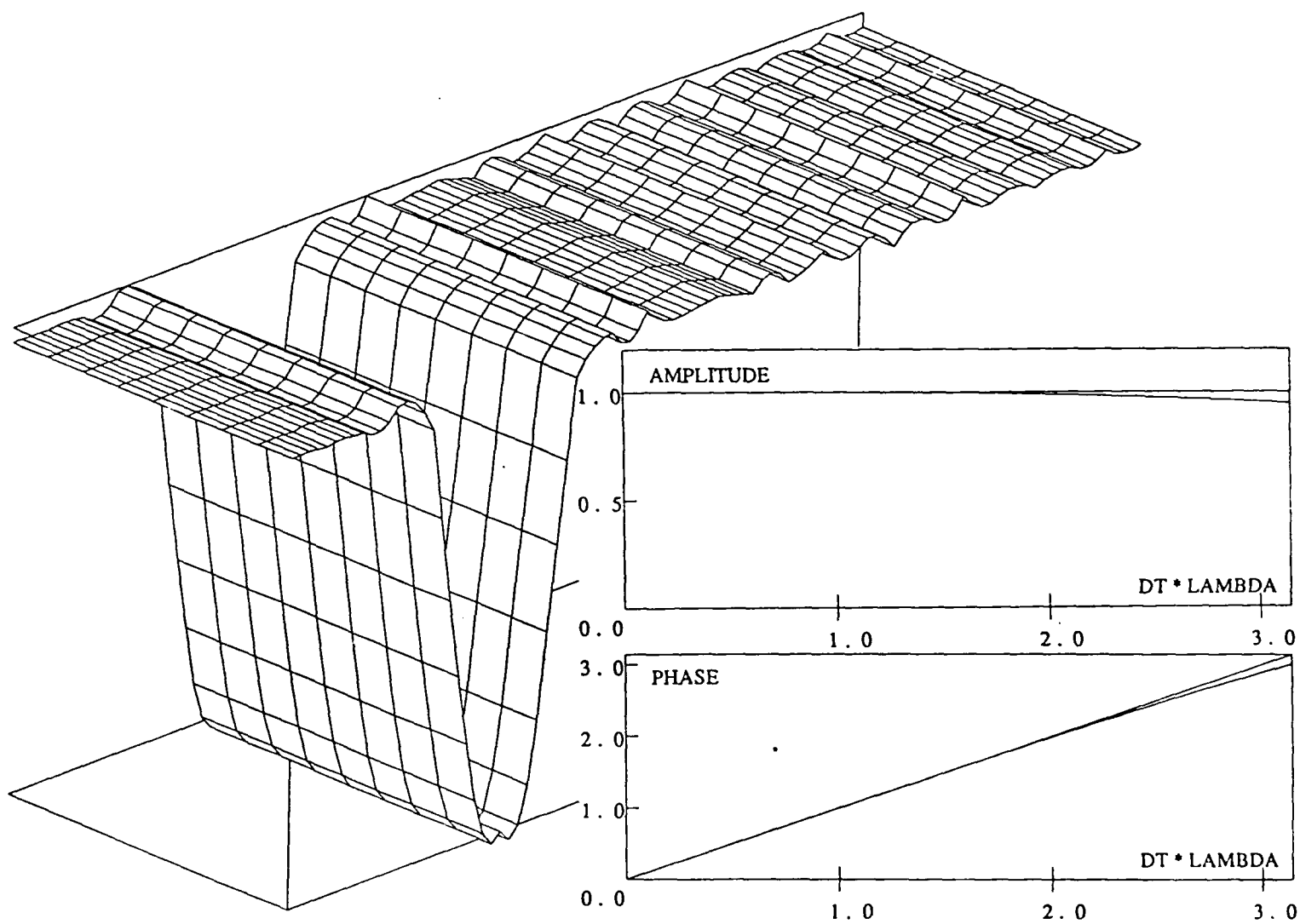
Figure 13: SIRK (5,5) scheme, $\Delta t = 0.0625$, $h = 0.125$, $p = 2$.

D.O.F= 1885

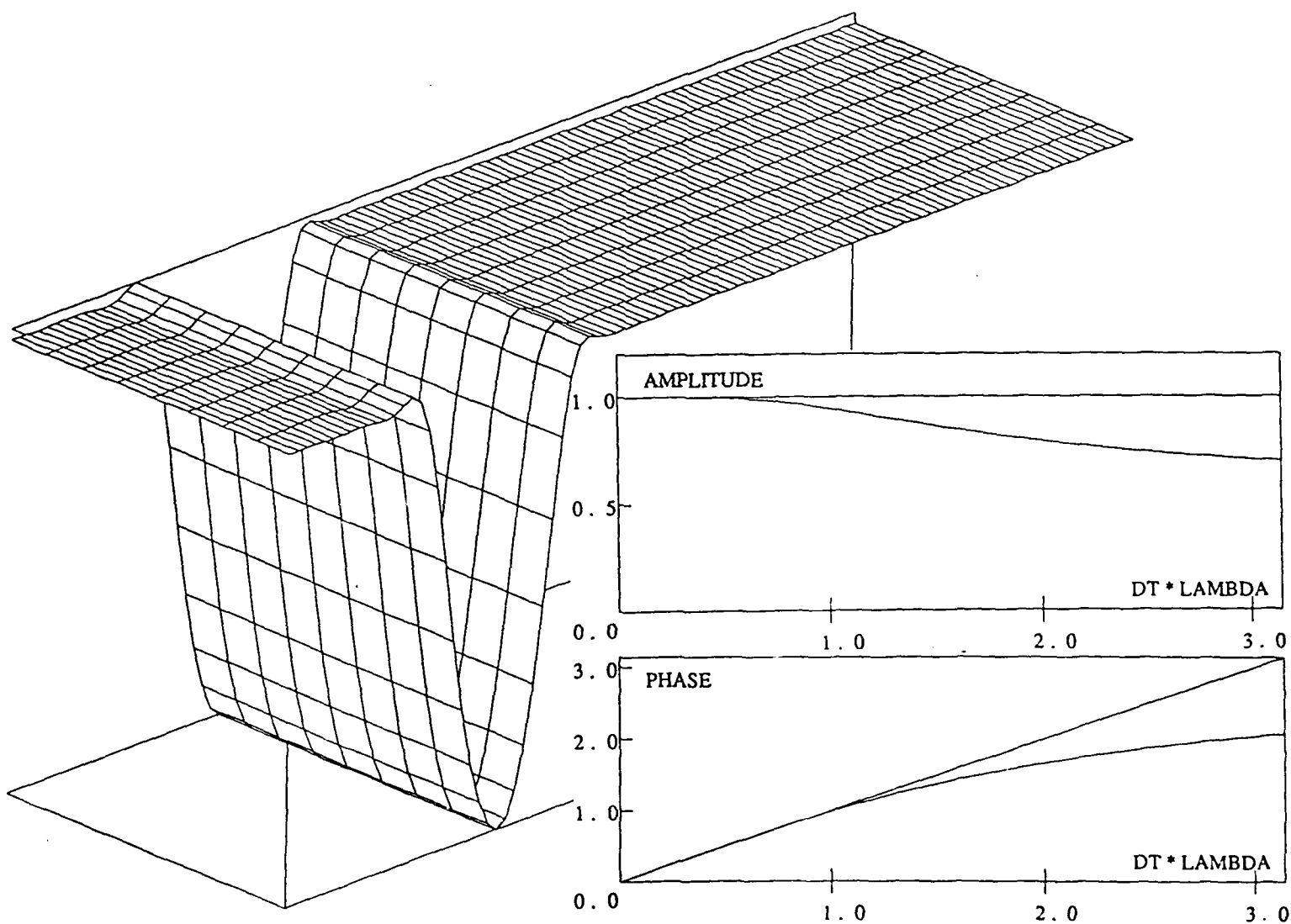Figure 14: Test 2. An h-p FE mesh. $h = 0.0625$, $p = 3$.

Figure 15: Test 2. SIRK (3,4) scheme, $\Delta t = 0.015625$, $h = 0.0625$, $p = 3$.
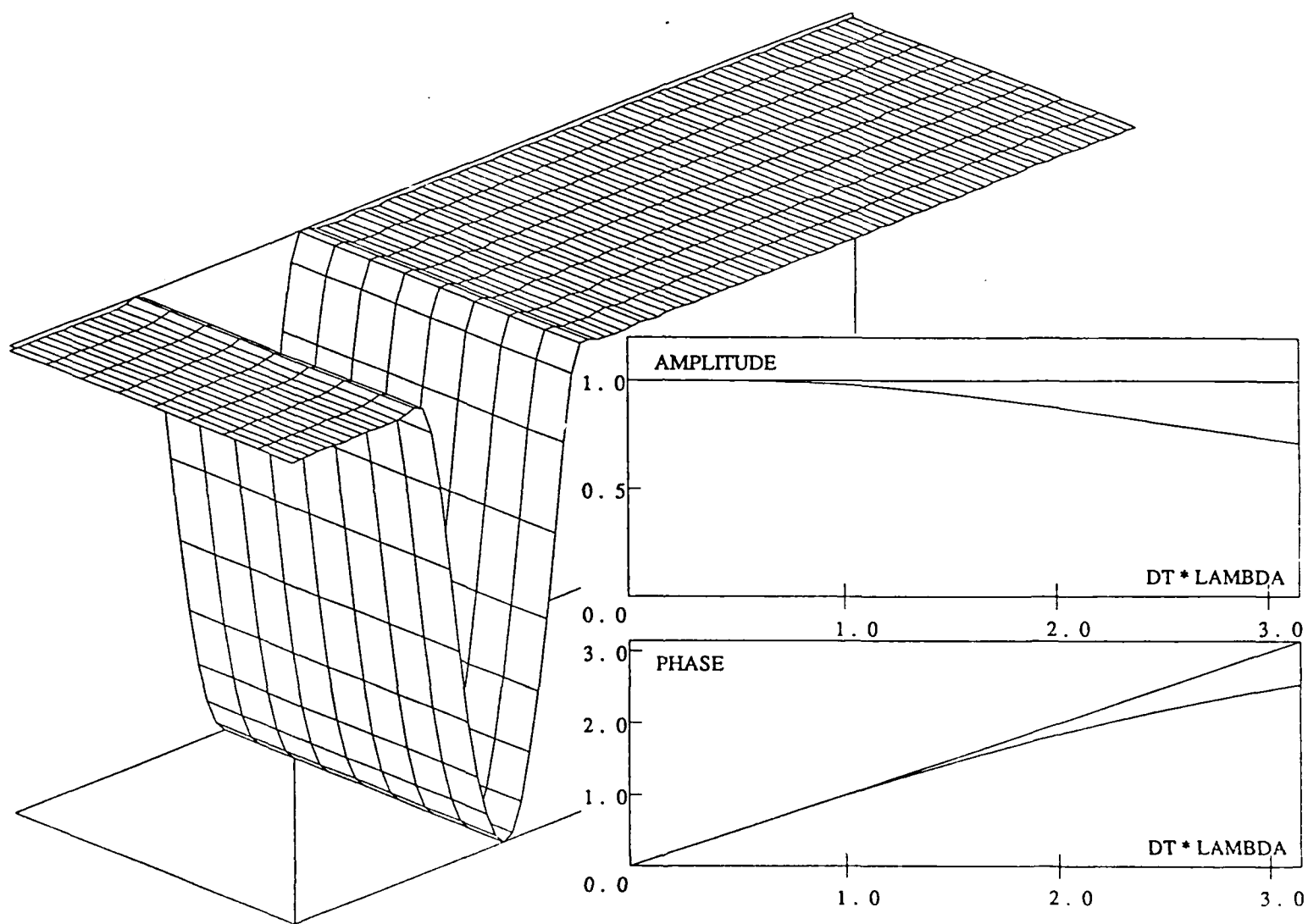
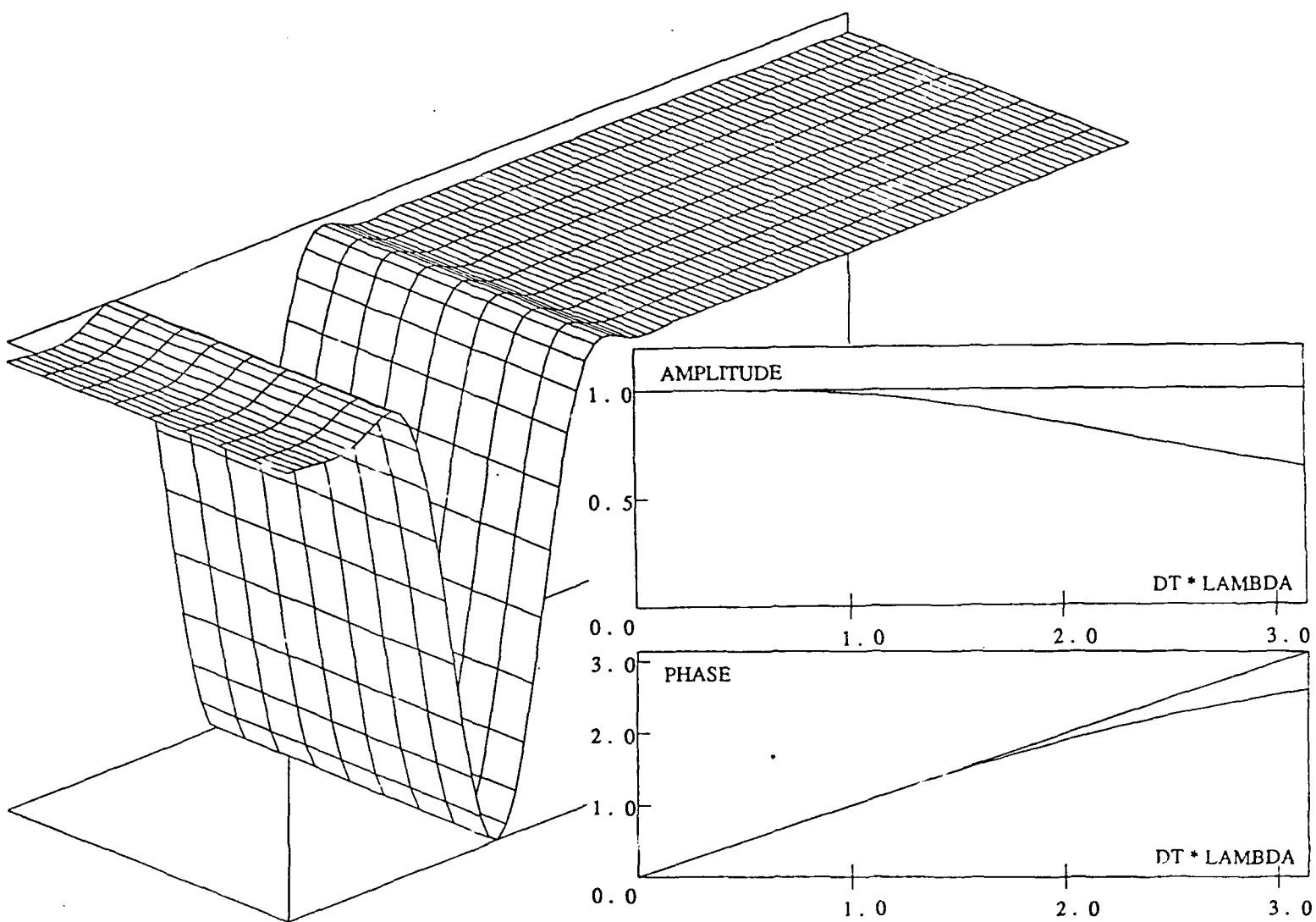Figure 16: Test 2. SIRK (4,4) scheme, $\Delta t = 0.015625$, $h = 0.0625$, $p = 3$.

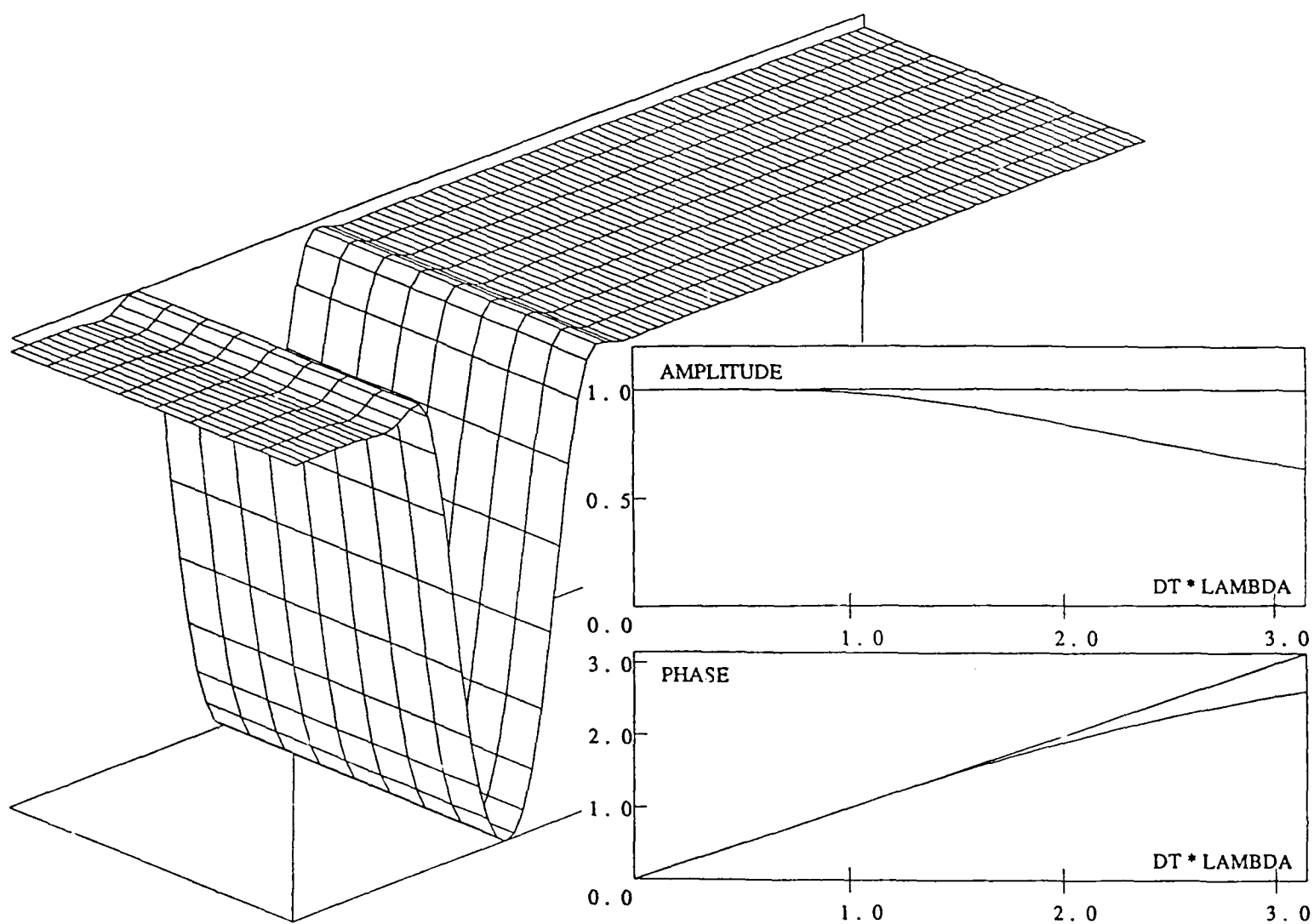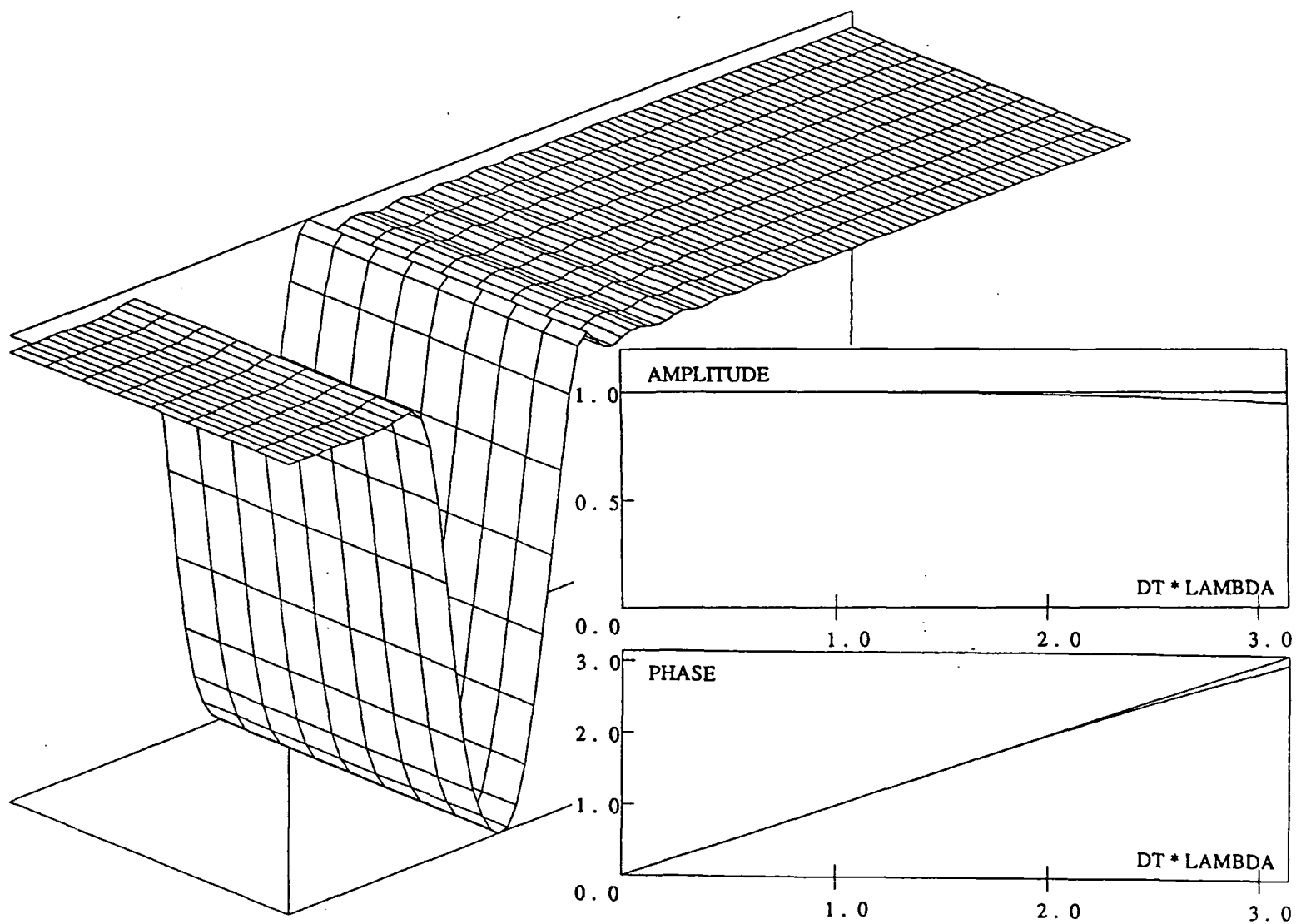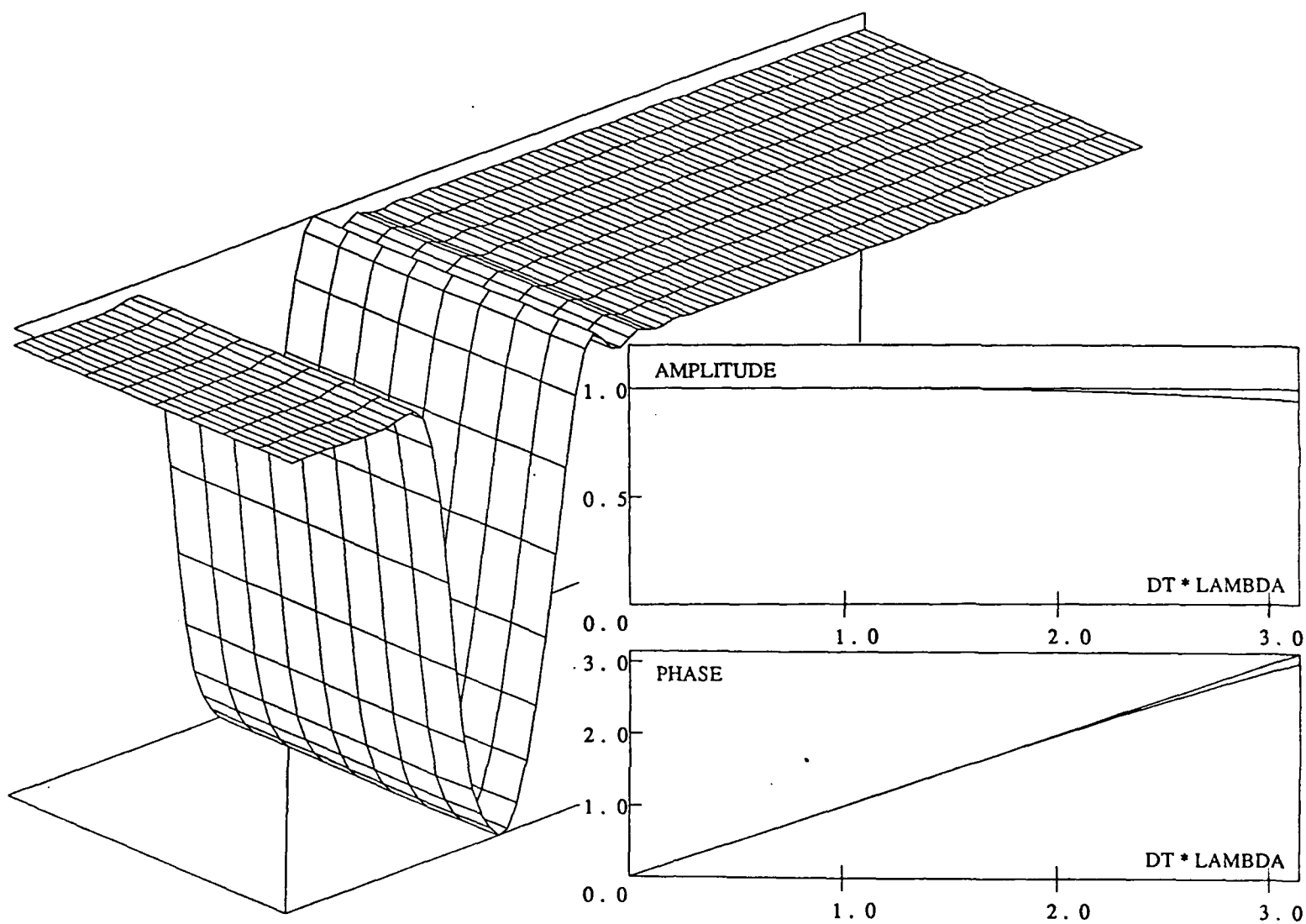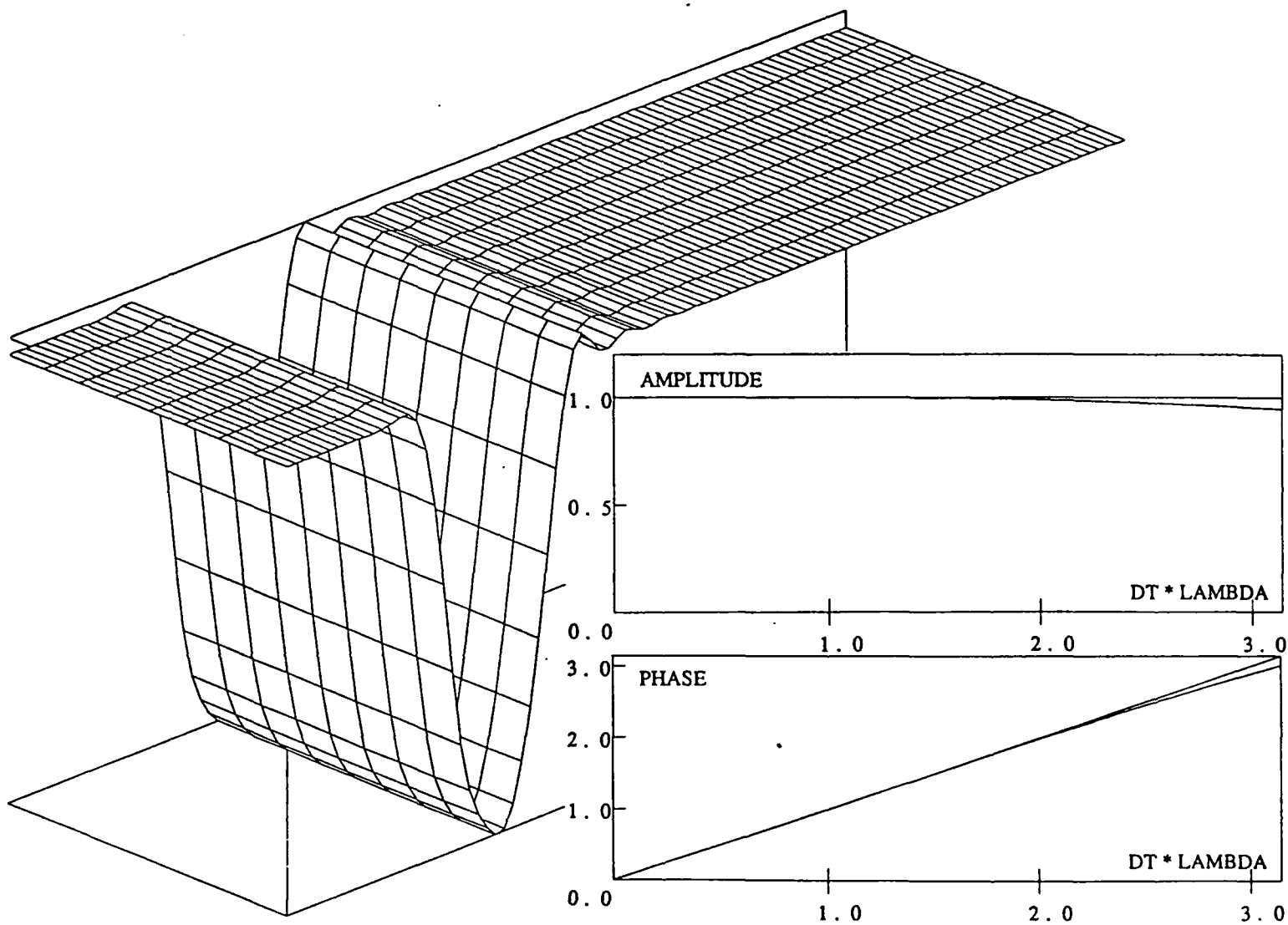Figure 17: Test 3, SIRK (4,4) scheme, $\Delta t = 0.0625$, $h = 0.125$, $p = 5$.

Figure 18: Test 3. SIRK (4,4) scheme. $\Delta t = 0.03125$, $h = 0.125$, $p = 5$.

Figure 19: Test 3. SIRK (5,5) scheme, $\Delta t = 0.0625$, $h = 0.125$, $p = 4$.

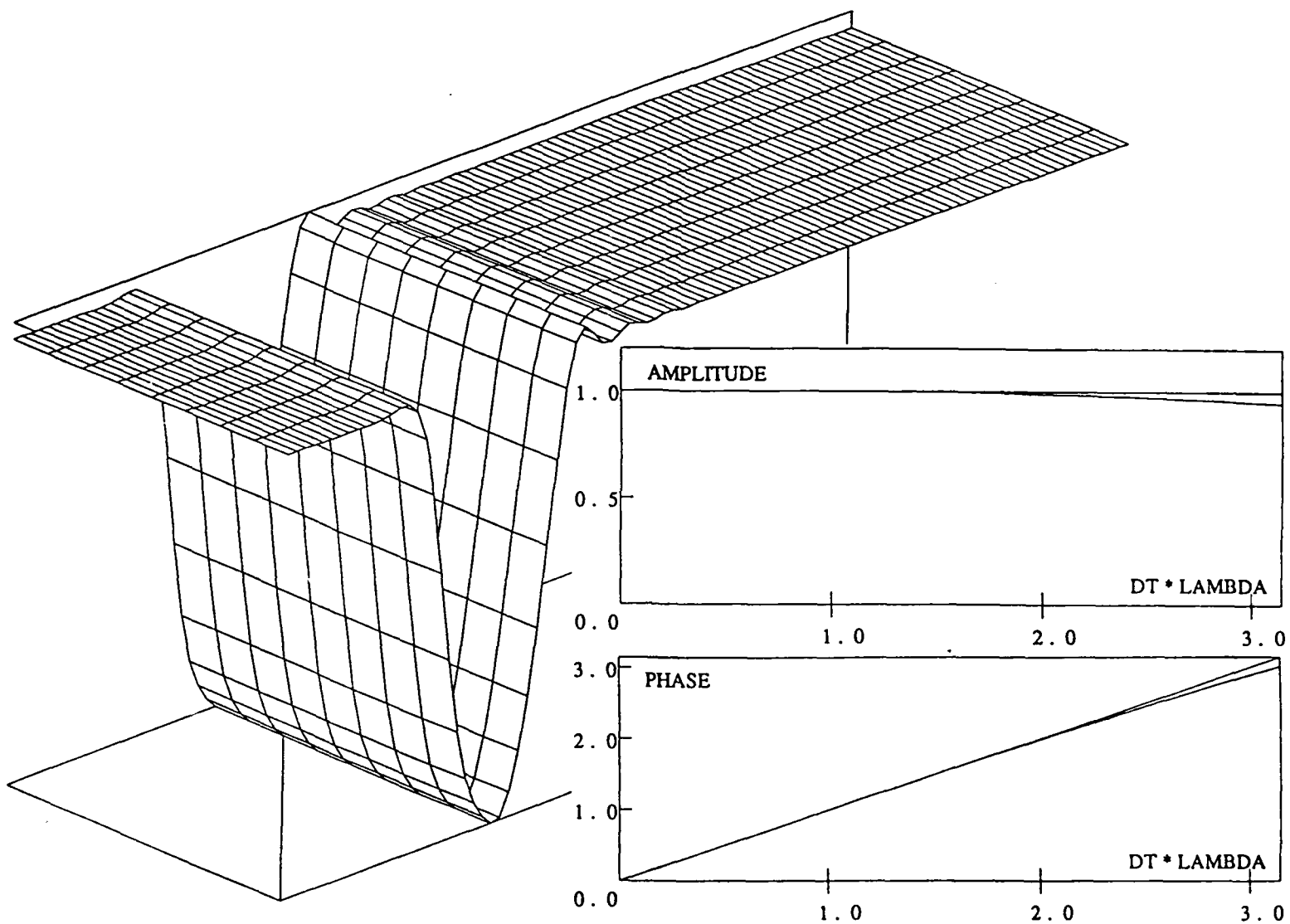Figure 20: Test 3. SIRK (5,5) scheme, $\Delta t = 0.0625$, $h = 0.125$, $p = 5$.

Figure 21: Test 3. SIRK (5,5) scheme, $\Delta t = 0.0625$, $h = 0.125$, $p = 6$.

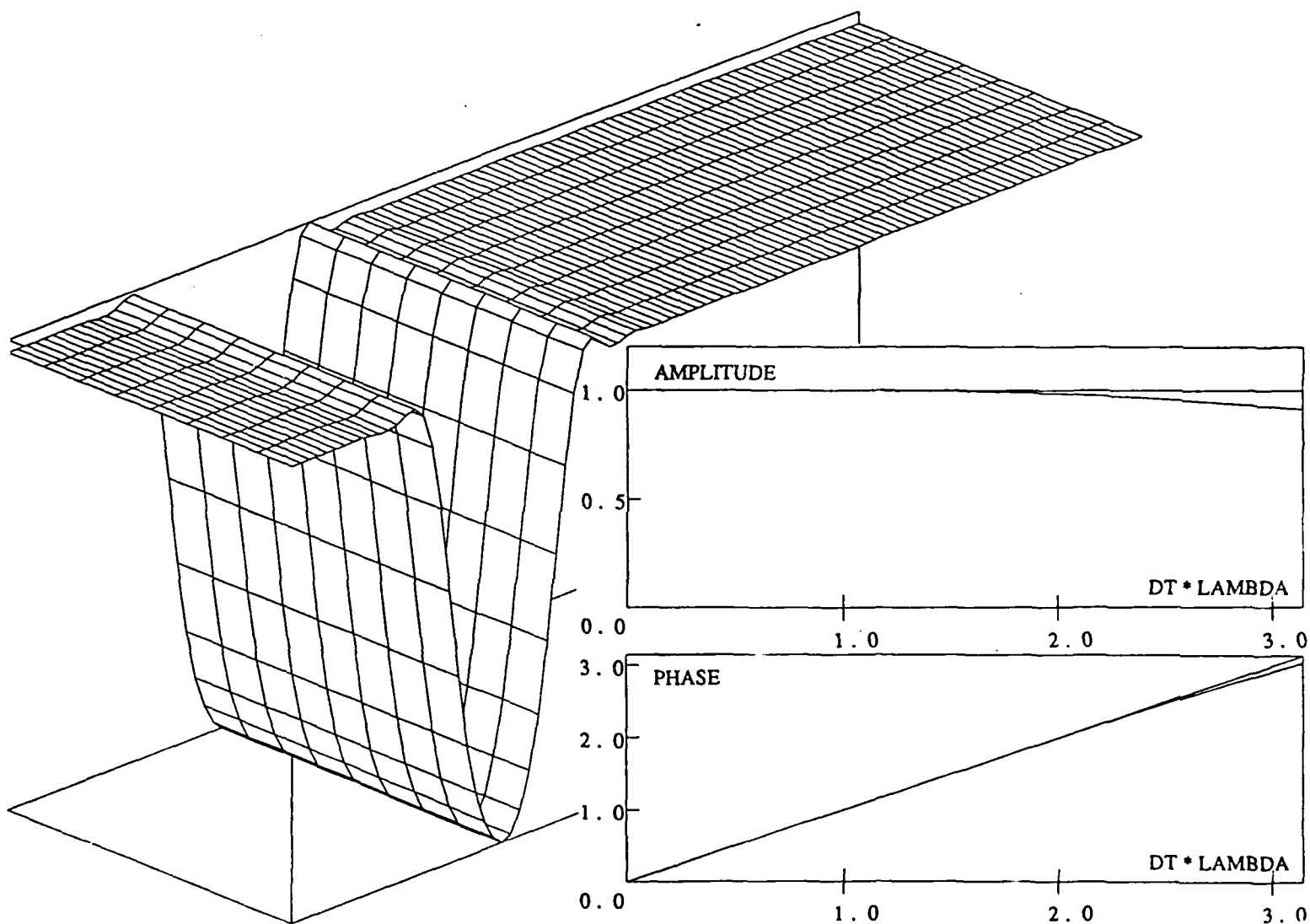Figure 22: Test 3. SIRK (5,5) scheme, $\Delta t = 0.0625$, $h = 0.125$, $p = 7$.

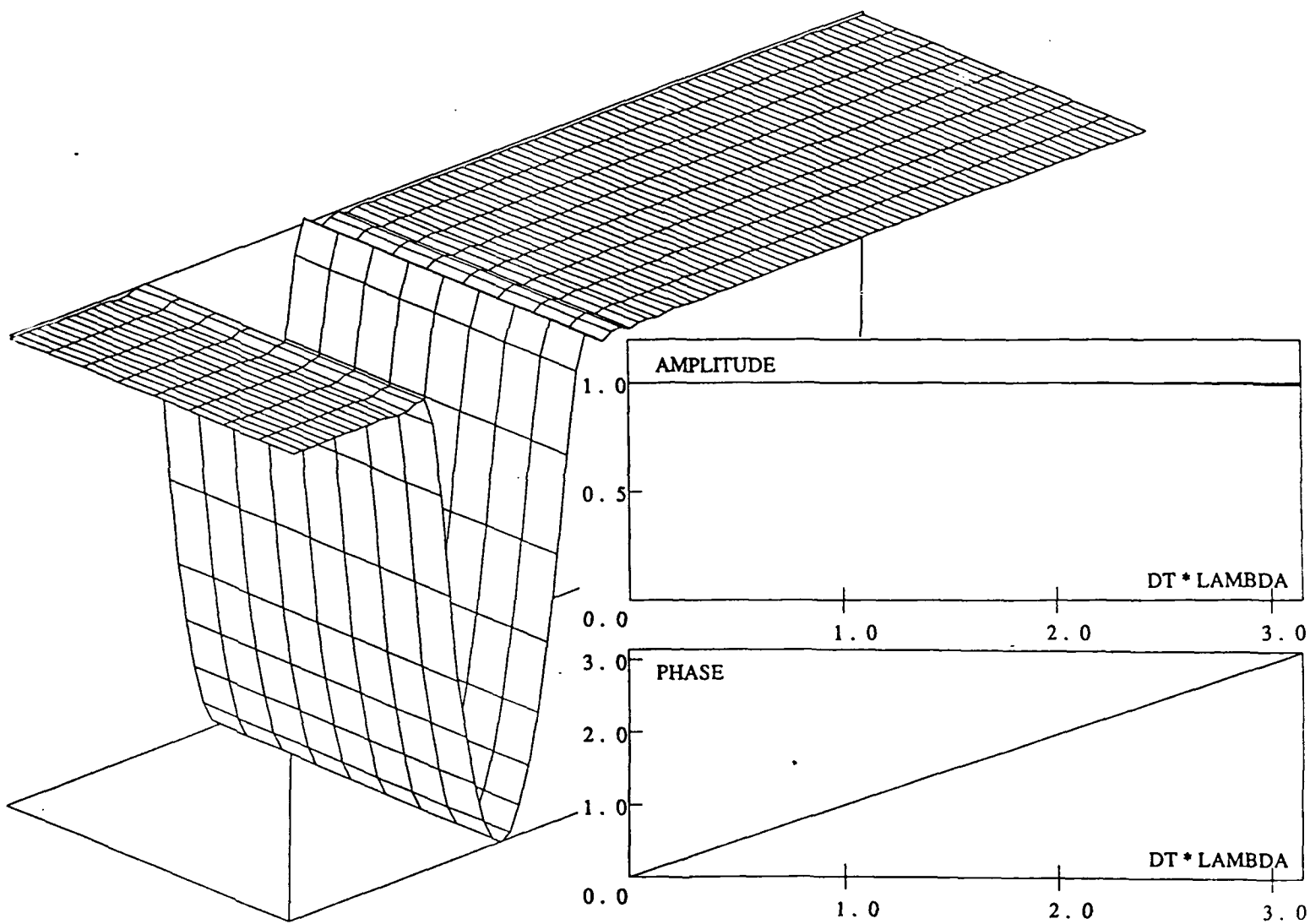Figure 23: Test 3. SIRK (6,6) scheme, $\Delta t = 0.0625$, $h = 0.125$, $p = 6$.

Figure 24: Test 3. SIRK (8,8) scheme, $\Delta t = 0.0625$, $h = 0.125$, $p = 6$.

where B is a bilinear form defining the left–hand side of a variational formulation corresponding to a particular time–discretization scheme.

- η_K is the element error indicator function evaluated as

$$\eta_K^2 = B_K(\varphi_K, \varphi_K) \tag{5.3}$$

with B_K the element contribution to the global bilinear form and the φ_K the element indicator function which is the solution to the local problem

$$\begin{cases} \text{Find } \varphi_K \in X_{h,p+1}^0(K) \text{ such that} \\ B_K(\varphi_K, W) = R(W) \; \forall \; W \in X_{h,p+1}^0(K) \end{cases} \tag{5.4}$$

where R is an appropriate residual corresponding to element K and $X_{h,p+1}^0(K)$ the space of "bubble" functions.

For all details we refer to [].

While the mesh refinements are done on the basis of the element residual method, the unrefinements are based on elements contribution to the global, "physical" energy, i.e., simply the L^2-norm

$$\xi_K^2 = \int_K U^T U \; dx \tag{5.5}$$

Adaptive Strategy

In the following η and ξ denote the maximum values of elements error and energy indicators

$$\eta = \max_K \eta_K \;, \; \xi = \max_K \xi_K \tag{5.6}$$

and η_{ad}, ξ_{ad} some fixed parameters. The following adaptive strategy has been used when solving for a typical next step solution U^{n+1}.

1. Solve for U^{n+1}

   mesh refinements

2. Estimate error

3. Check if $\eta_K \le \eta_{ad}$ for every element K

   if "yes" then

   go to step 4

42

```
    else
            refine all elements $K$ for which $\eta_K > \eta_{ad}$
            go to step 1
    endif
```

mesh unrefinements

4. Unrefine all elements for which $\xi_K < \xi_{ad}$

5. Set $U^n = U^{n+1}$ and go to step 1

Numerical Experiments—The Vibrating Cylinder Problem

The problem is defined as follows (see Fig. 26).

1. Governing equations (2.6) are to be solved in the domain

$$\Omega = I\!\!R^2 \setminus \{(r,\theta) : r \le a\} \tag{5.7}$$

2. Boundary condition

$$u_n = A \, \sin \, \omega t[H(t) - H(t - T/2)] \tag{5.8}$$

where A, ω, T are constants and $H(\cdot)$ is the Heaviside function.

3. Sommerfeld radiation condition at $r = \infty$

4. Initial condition

$$\boldsymbol{U_0 = 0} \tag{5.9}$$

For computations we accept the computational domain

$$\Omega = \{(r,\theta) : a < r < r_\infty \, , \, -\alpha < \theta < \alpha\} \tag{5.10}$$

The problem was solved using the Taylor-Galerkin method with $\alpha = 0.5$ and a constant time step $\Delta t = 0.015625$. The following boundary conditions were used in one time–step calculations: Boundary condition (5.8) at $r = a$, $-\alpha < \theta < \alpha$ and

$$u_n = 0 \quad \text{at} \quad a < r < r_\infty \, , \, \theta = \pm\alpha$$

$$\frac{\partial U}{\partial n} = 0 \quad \text{at} \quad r = r_\infty \, , \, -\alpha < \theta < \alpha$$

The adaptive strategy was based on h-refinements. Figure 27 shows an initial FE mesh of quadratic elements and the consecutive figures 28, 29, and 30 present the evolution of FE mesh at time stages $t = 0.5$, 1.0 and $t = 1.5$, respectively. Finally, Fig. 31 shows the computed pressure distribution at time $t = 1.5$.
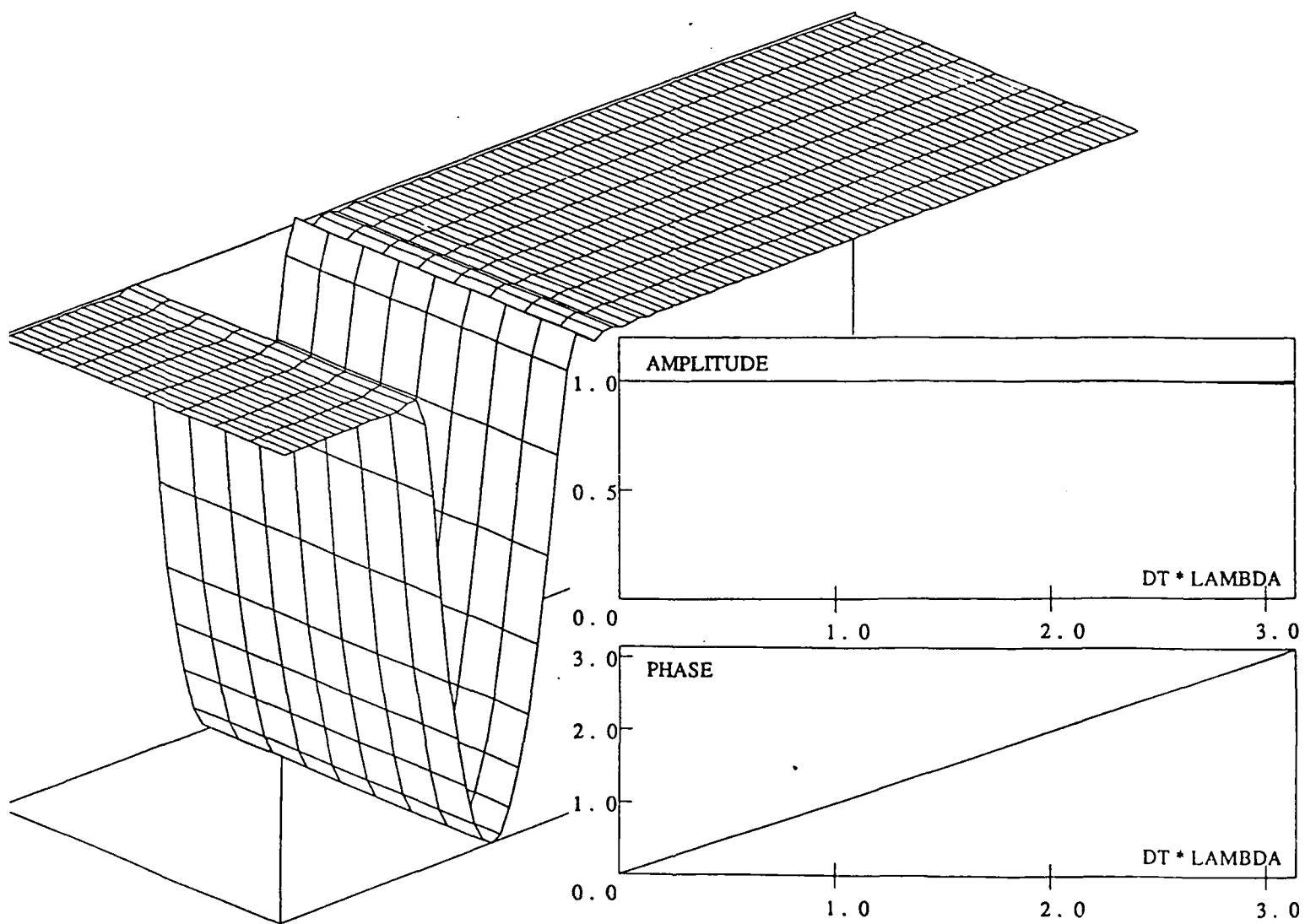
43

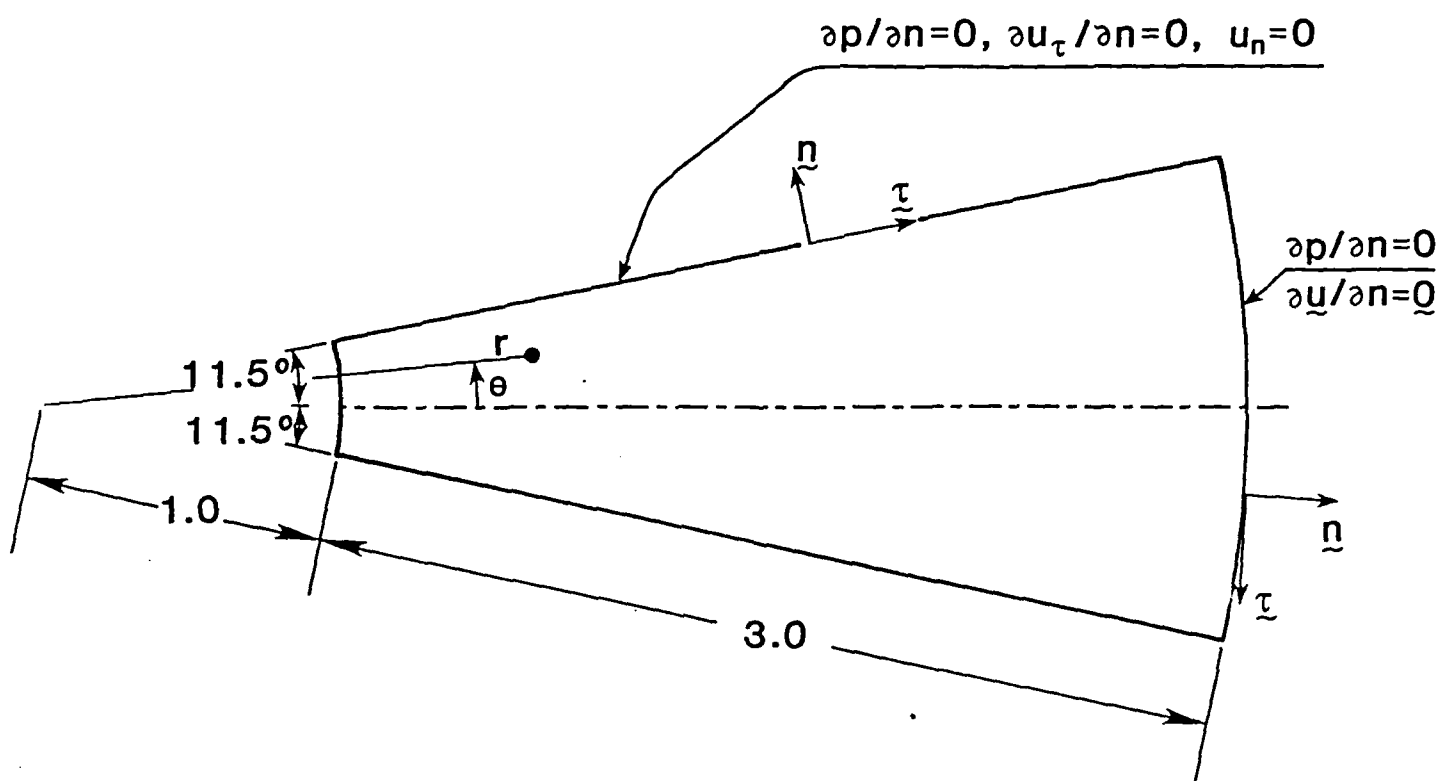Figure 25: Test 3. SIRK (8,8) scheme, $\Delta t = 0.0625$, $h = 0.125$, $p = 7$.

Figure 26: The Vibrating Cylinder Problem.

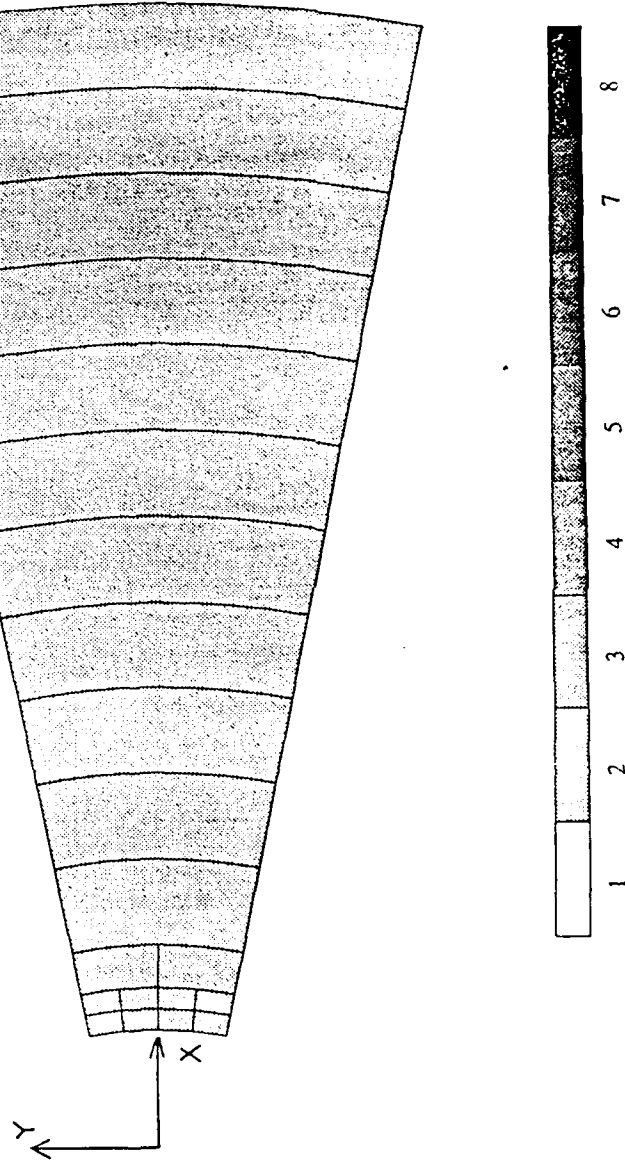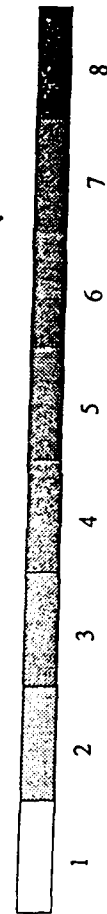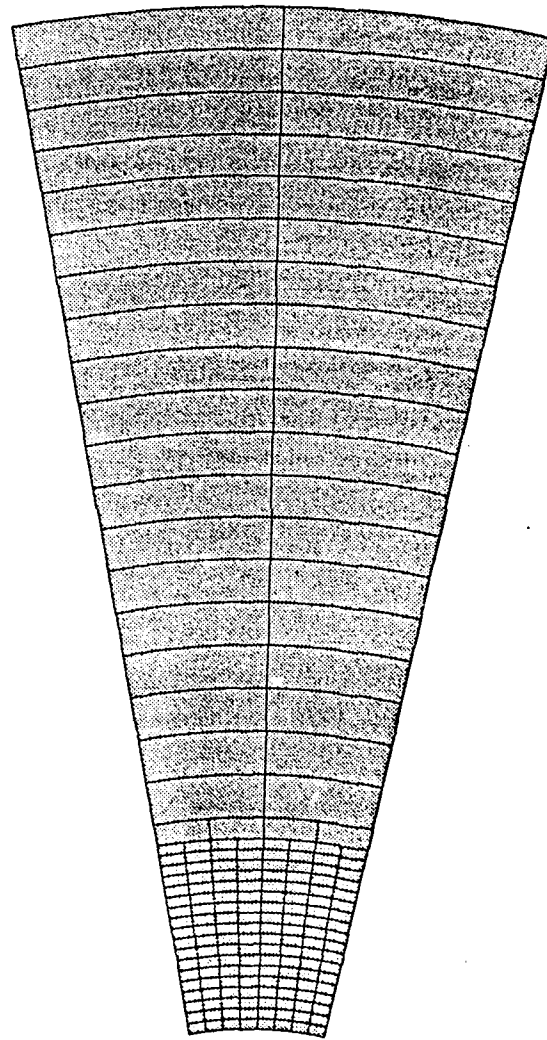project: deck   MESH   adapt h-p/2d

D.O.F= 115

Figure 27: The Vibrating Cylinder Problem. Initial mesh of elements of second order.

project: deck

MESH

adapt h-p/2d

D.O.F= 825

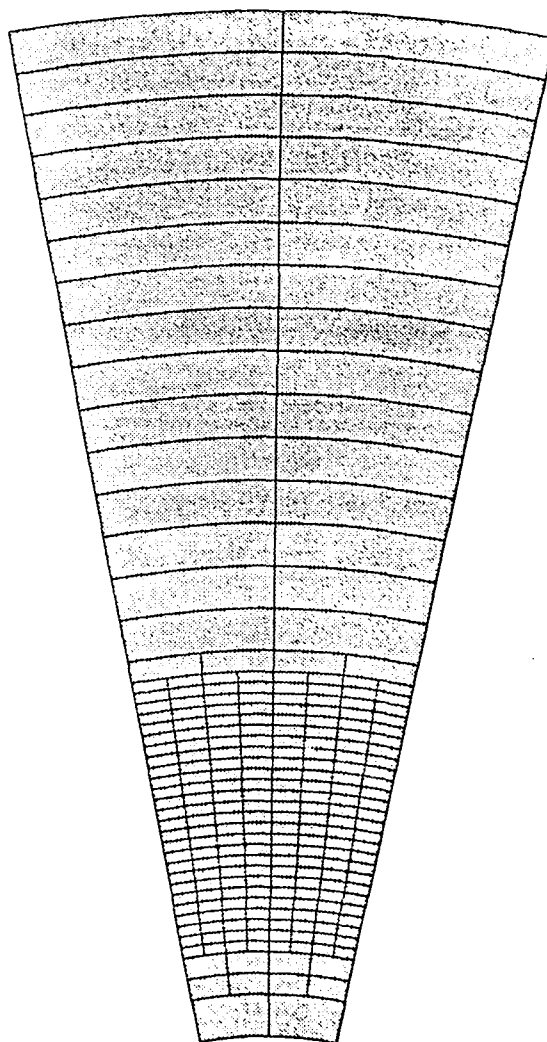Figure 28: The Vibrating Cylinder Problem. *h-refined/unrefined* mesh at time = 0.5.

Figure 29: The Vibrating Cylinder Problem. *h*-refined/unrefined mesh at time = 1.0.
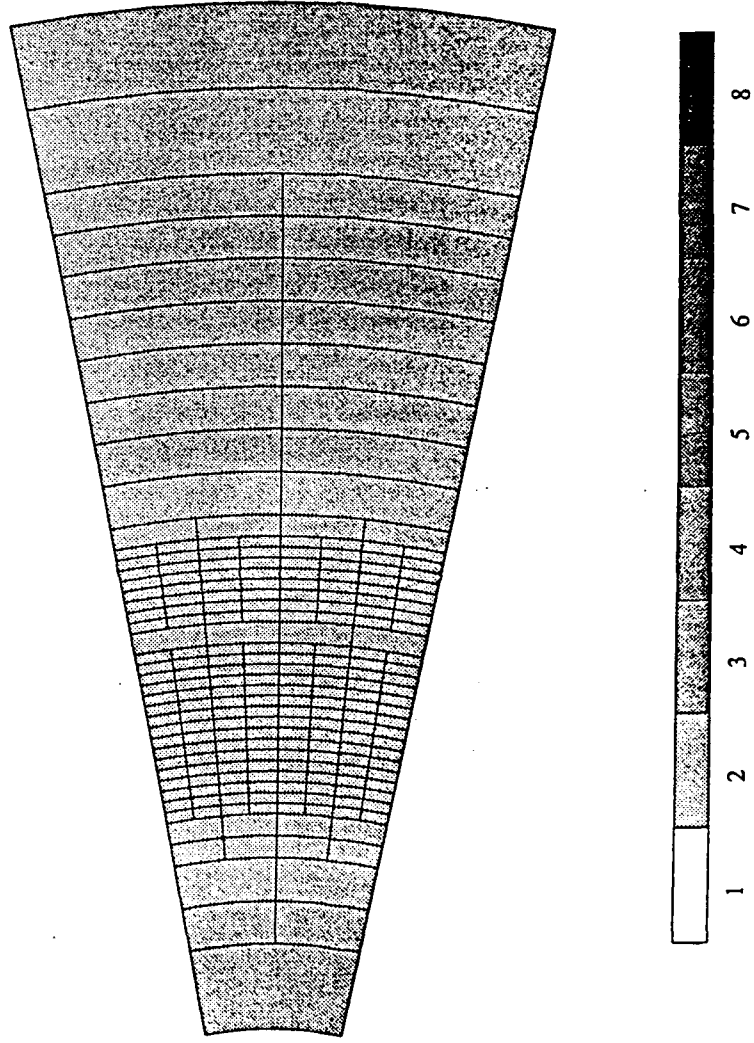
D.O.F= 987

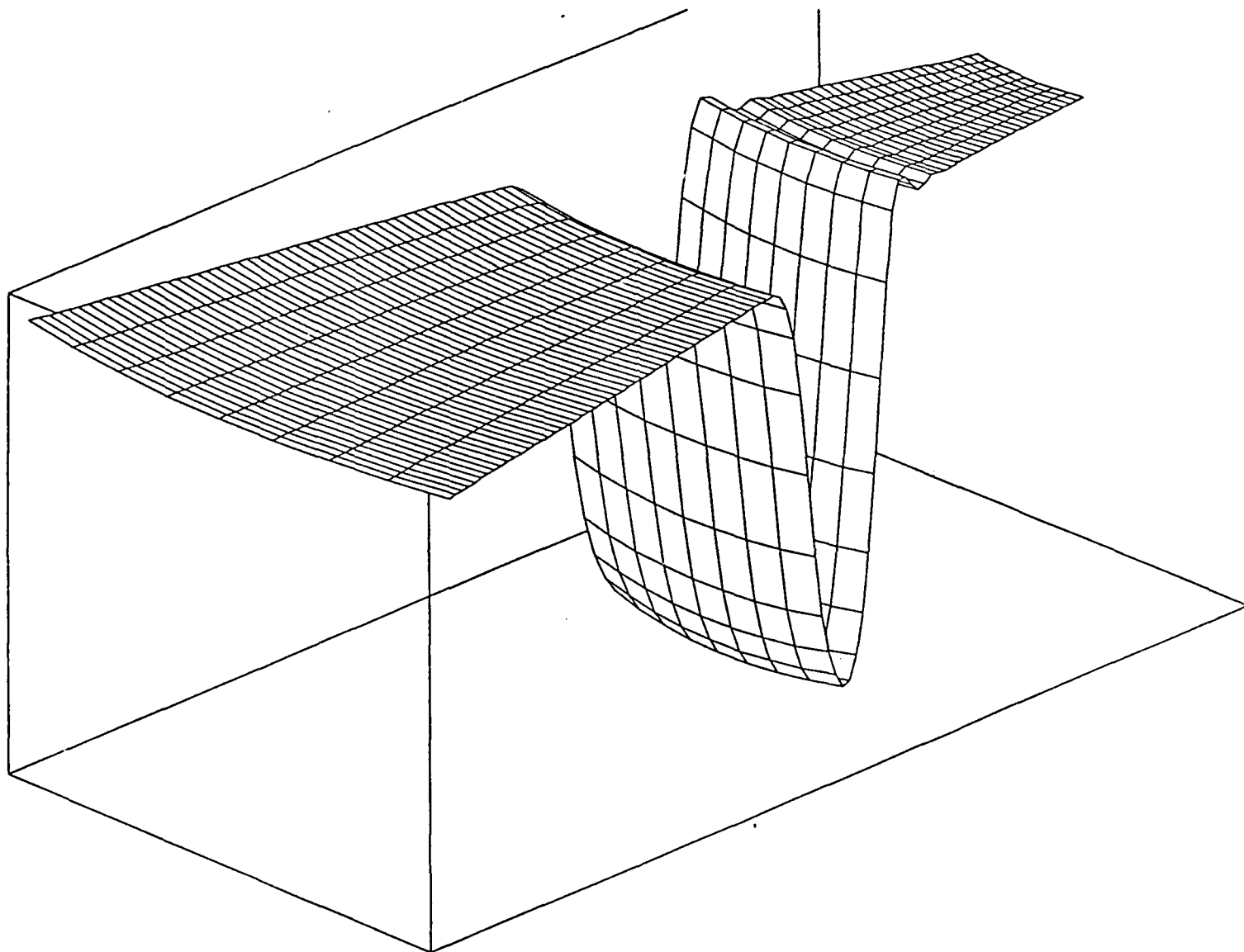Figure 30: The Vibrating Cylinder Problem. *h*-refined/unrefined mesh at time = 1.5.

Figure 31: The Vibrating Cylinder Problem. Pressure distribution at time = 1.5.

6 Conclusions. Further Research

The paper presents some preliminary results toward designing fully automated self-adaptive methods for solving transient problems of type (2.10) with applications to linear acoustics. Two concepts of discretization have been presented and discussed: the method of lines and the method of discretization of time. While the latter one provides a natural basis for every step mesh refinements/unrefinements, the first allows for an explicit representation of spectrum of the transient operator in terms of the eigenvalues of the approximation operator A_h, including the case of arbitrary, unstructured meshes. Consequently, all diffusive and dispersive properties of the transient operator are known (in particular the stability analysis is easily available) and the whole analysis reduces to the investigation of the spectrum of operator A_h as a function of adapting meshes.

The implicit Runge-Kutta schemes are shown to belong to the class of methods for which both discretization concepts yield the same result and seem to be a natural candidate for constructing approximations to the considered problem.

Several questions remain unresolved and are under current investigation. To mention a few:

- Dependence of the spectrum of the approximate operator A_h on spatial approximation, including h-p meshes. For regular, uniform grids, eigenvalues of A_h are uniformly distributed and often are available in a closed form (that is why the von Neumann stability analysis is available). Their structure for non-uniform meshes is not known. Does the adaptivity, in particular that causing local transitions in element size (h) and order (p), affect strongly the shape of the corresponding eigenvalues?

- If the mesh is refined/unrefined, the spectral representation of A_h changes and the corresponding solution has to be represented using different eigenfunctions (transfer of energy between different modes). Can the spectral properties of A_h be controlled? control it? What effect does it have on the error?

- A combined *a posteriori* error estimate including both time and space discretization. Some of the SIRK schemes allow for an error control, provided one extra iteration is performed (comp. [1]). It may be possible to combine those techniques with residual-type estimates with respect to the space variables.

- Is it possible, by using adaptive methods, to obtain exponential convergence for the transient hyperbolic equations?

We hope to answer some of these questions in a forthcoming work.

51

References

1. Butcher, J. C., **The Numerical Analysis of Ordinary Differential Equations**, John Wiley and Sons, New York, 1987.

2. Demkowicz, L., Oden, J. T., Rachowicz, W., and Hardy, O., "Toward a Universal h-p Adaptive Finite Element Strategy. Part 1: Constrained Approximation and Data Structure," *Comp. Meth. in Appl. Mech. and Engrg.*, **77**, pp. 79–112, 1989.

3. Demkowicz, L., Oden, J. T., Rachowicz, W., and Hardy, O., "An h-p Taylor-Galerkin Finite Element Method for Compressible Euler Equations" (in preparation).

4. Demkowicz, L., Oden, J. T., and Rachowicz, W., "A New Finite Element Method for Solving Compressible Navier-Stokes Equations Based on an Operator Splitting Method and h-p Adaptivity," *Comp. Meth. in Appl. Mech. and Engrg.* (to appear).

5. Junger, M. C., and Feit, D., **Sound, Structures and Their Interaction**, The MIT Press, Cambridge, 1986 (second edition).

6. Leis, R., **Initial Boundary Value Problems in Mathematical Physics**, John Wiley and Sons, New York, 1986.

7. Majda, A., **Compressible Fluid Flow and Systems of Conservation Laws in Several Space Variables**, Springer-Verlag, New York, 1984.

8. Oden, J. T., Demkowicz, L., Rachowicz, W., and Westrmann, T. A., "Toward a Universal h-p Adaptive Finite Element Strategy. Part 2: *A Posteriori* Error Estimation," *Comp. Meth. in Appl. Mech. and Engrg.*, **77**, pp. 113–180, 1989.

9. Oden, J. T., Demkowicz, L., Rachowicz, W., and Westermann, T. A., "*A Posteriori* Error Analysis in Finite Elements: The Element Residual Method for Symmetrizable Problems with Applications to Compressible Euler and Navier-Stokes Equations," *Comp. Meth. in Appl. Mech. and Engrg.* (to appear).

10. Oden, J. T., Liszka, T., and Wu, W., "An h-p Adaptive Finite Element Method for Incompressible Viscous Flows," **The Mathematics of Finite Elements with Applications**, Ed. by J. R. Whiteman, Academic Press, London (to appear).

11. Rachowicz, W., Oden, J. T., and Demkowicz, L., "Toward a Universal h-p Adaptive Finite Element Strategy. Part 3: Design of h-p Meshes," *Comp. Meth. in Appl. Mech. and Engrg.*, **77**, pp. 181–212, 1989.

12. Rectory, S. K., **The Method of Discretization in Time and Partial Differential Equations**, D. Reidel Publishing Company, Boston 1982.

13. Showalter, R., **Hilbert Space Methods for Partial Differential Equations**, Pitman, London 1977.

14. Riesz, F., and Nagy, B., **Functional Analysis**, Dover, New York 1990.